

# Metallurgical Characteristics of High Strength Structural Materials

[Ninth Quarterly Report]

R. J. GOODE, R. W. HUBER, D. G. HOWE,  
R. W. JUDY, JR., P. P. PUZAK, K. B. LLOYD, T. W. CROOKER,  
R. E. MOREY, E. A. LANGE, AND C. N. FREED

*Metallurgy Division*

November 1965

APPROVED FOR PUBLIC  
RELEASE - DISTRIBUTION  
UNLIMITED



**U.S. NAVAL RESEARCH LABORATORY**  
Washington, D.C.

DISTRIBUTION OF THIS DOCUMENT IS UNLIMITED

#### PREVIOUS REPORTS IN THIS SERIES

First Quarterly Report - "Metallurgical Characteristics of High Strength Structural Materials," P.P. Puzak, K.B. Lloyd, E.A. Lange, R.J. Goode, R.W. Hubert, E.P. Dahlberg and C.D. Beachem, NRL Memo. Rept. 1438, June 30, 1963

Second Quarterly Report - "Metallurgical Characteristics of high Strength Structural Materials," P.P. Puzak, K.B. Lloyd, E.A. Lange, R.J. Goode, and R.W. Huber, NRL Memo. Rept. 1461, Sept. 1963

Third Quarterly Report - "Metallurgical Characteristics of High Strength Structural Materials," P.P. Puzak, K.B. Lloyd, R.J. Goode, R.W. Huber, D.G. Howe, T.W. Crooker, E.A. Lange, and W.S. Pellini, NRL Report 6086, Jan. 1964

Fourth Quarterly Report - "Metallurgical Characteristics of High Strength Structural Materials," R.J. Goode, R.W. Huber, D.G. Howe, R.W. Judy, Jr., T.W. Crooker, R.E. Morey, E.A. Lange, P.P. Puzak, and K.B. Lloyd, NRL Report 6137, June 1964

Fifth Quarterly Report - "Metallurgical Characteristics of High Strength Structural Materials," T.W. Crooker, R.E. Morey, E.A. Lange, R.W. Judy, Jr., C.N. Freed, R.J. Goode, P.P. Puzak, K.B. Lloyd, R.W. Huber, D.G. Howe, and W.S. Pellini, NRL Report 6196, Sept. 1964

Sixth Quarterly Report - "Metallurgical Characteristics of High Strength Structural Materials," W.S. Pellini, R.J. Goode, R.W. Huber, D.G. Howe, R.W. Judy, Jr., P.P. Puzak, K.B. Lloyd, E.A. Lange, E.A. DeFelice, T.W. Crooker, R.E. Morey E.J. Chapin, and L.J. McGeady, NRL Report 6258, Dec. 1964

Seventh Quarterly Report - "Metallurgical Characteristics of High Strength Structural Materials," R.J. Goode, D.G. Howe, R.W. Huber, P.P. Puzak, K.B. Lloyd, T.W. Crooker, R.E. Morey, E.A. Lange, R.W. Judy, Jr., and C.N. Freed, NRL Report 6327, May 1965

Eight Quarterly Report - "Metallurgical Characteristics of High Strength Structural Materials," P.P. Puzak, K.B. Lloyd, R.J. Goode, R.W. Huber, D.G. Howe, R.W. Judy, Jr., T.W. Crooker, R.E. Morey, E.A. Lange, and C.N. Freed, NRL Report 6364, Aug. 1965

## CONTENTS

Abstract. . . . .	iii
Problem Status. . . . .	iii
Authorization . . . . .	iii
INTRODUCTION. . . . .	1
TITANIUM ALLOYS . . . . .	4
The Titanium Fracture Toughness Index Diagram. . . . .	4
Mechanical Properties of Some New Titanium Alloy Plates. . . . .	6
Welding Studies. . . . .	8
Heat-Treatment Studies . . . . .	10
STRESS-CORROSION-CRACKING OF TITANIUM ALLOYS. . . . .	23
Results. . . . .	24
HIGH STRENGTH STEELS. . . . .	34
Drop-Weight Tear Tests of Special Melt Practice HY-80 Steels . . . . .	34
Drop-Weight Tear Tests of "Old" Alloy High Strength Steels . . . . .	42
Fracture Toughness Index Diagram For Steels . . . . .	51
ALUMINUM ALLOYS . . . . .	57
Small Laboratory Tests . . . . .	57
Explosion Tear Tests . . . . .	60
Fracture Toughness Index Diagram . . . . .	60
THE EFFECT OF MEAN STRAIN ON LOW-CYCLE FATIGUE CRACK PROPAGATION IN 5Ni-Cr-Mo-V STEEL AND 7079-T6 ALUMINUM. . . . .	66
Materials and Experimental Procedure . . . . .	67

CONTENTS - Continued

Discussion of Test Results. . . . . .71

Summary . . . . . .73

DEVELOPMENT OF A LOW-CYCLE FATIGUE CRACK . . . . . .74  
PROPAGATION TEST EMPLOYING FRACTURE  
MECHANICS PARAMETERS

Test Specimen Design and Materials. . . . . .75

Experimental Procedure. . . . . .79

Preliminary Test Results. . . . . .80

Discussion. . . . . .83

EFFECT OF SIDE-GROOVES ON PLANE-STRAIN  
FRACTURE TOUGHNESS MEASUREMENTS. . . . . .86

Experimental Details and Materials. . . . . .87

Results and Discussion. . . . . .89

REFERENCES . . . . . .95

## ABSTRACT

A progress report covering research studies in high strength structural materials, conducted in the period August 1965 to November 1965, is presented. This report includes fracture toughness studies on high strength steels, titanium alloys, and aluminum alloys. Fracture Toughness Index Diagrams, modified to include the latest information, are presented for these materials; the effects of melting practice and processing variables are reflected in the Fracture Toughness Index Diagram for steels by the addition of a new optimum materials trend line for consumable-electrode-vacuum melting of steels. Results are presented for studies concerning (1) the use of side-grooved plane-strain fracture mechanics specimens for valid determination of fracture toughness, (2) heat-treatment effects on fracture toughness of several titanium alloys, (3) the effect of vacuum heat treatment on stress-corrosion-cracking sensitivity of titanium, and (4) the screening of a variety of titanium alloy plates for sensitivity to stress-corrosion-cracking. The effects of mean strain on low-cycle fatigue crack propagation in 5Ni-Cr-Mo-V steel and 7079-T6 aluminum are presented. Also described is a newly-developed low-cycle fatigue crack propagation test employing fracture mechanics parameters. Results are given for D6AC steels studied in this new test.

## PROBLEM STATUS

This is a progress report; work is continuing.

## AUTHORIZATION

NRL Problem F01-17; Project SP-01426  
NRL Problem M01-05; Projects SF-020-01-01-0724,  
RR-007-01-46-5405, and SP-01426  
NRL Problem M01-18; Projects SF-020-01-05-0731,  
RR-007-01-46-5420, SP-01426, and  
MIPR-ENG-NAV 66-2  
NRL Problem M03-01; Projects SF-020-01-01-0850,  
SP-01426, and RR-007-01-46-5414

Manuscript submitted March 7, 1966.

METALLURGICAL CHARACTERISTICS OF  
HIGH STRENGTH STRUCTURAL MATERIALS  
[NINTH QUARTERLY REPORT]

INTRODUCTION

This is the ninth status report covering the U.S. Naval Research Laboratory Metallurgy Division's long-range program of determining the performance characteristics of high strength materials. The program is primarily aimed at determining the fracture toughness characteristics of these materials, using standard and recently-developed laboratory test methods and is directed towards establishing the significance of the laboratory tests for predicting the service performance of the materials in large complex structures. Although the program is aimed at Navy requirements, the information that is developed is pertinent to all structural uses of these high strength materials. Quenched and tempered (Q&T) steels, maraging steels, titanium alloys, and aluminum alloys are the principle high strength structural metals currently under investigation.

The fracture toughness index diagrams for steels, titanium and aluminum have been modified to reflect the latest test results. A further "breakout" on the effects of melting practice has been made for high strength steels. This has resulted in the establishment of an additional optimum materials trend line for two-slag consumable electrode vacuum melt practice with one-to-one cross-roll. The effects of process variables on the purity level, gas and inclusions, and fracture toughness characteristics of high strength steels are discussed in relation to the fracture toughness index diagram for steels.

The results of recently-initiated studies on the stress-corrosion-cracking sensitivity of titanium alloys are presented for the first time in this Quarterly Report series. Screening studies are being conducted on all those previously reported, as well as recently processed, alloys for which material is available. Also described

in this report are the results to date on a brief study of the effects of vacuum annealing compared to gas annealing on stress-corrosion-cracking sensitivity for several alloys. The results at present indicate that interstitial hydrogen may be a contributing factor, not the sole factor, to stress-corrosion-cracking sensitivity in titanium.

Drop-weight tear test results are reported for several titanium weldments submitted to NRL for evaluation. Also, the effects of heat treatment on the strength and fracture toughness properties of Ti-6Al-4V-2Sn and Ti-7Al-2.5Mo are presented.

Tensile, Charpy-V, drop-weight tear, and explosion tear test results are reported for the aluminum alloys 7075-T7351, 2219-T851, 7005-T63, and 7106-T63. The 7075 and 2219 alloys exhibited very low fracture toughness properties for the indicated temper conditions, whereas the 7005 and 7106 alloys demonstrated high drop-weight tear test energy values and correspondingly high plastic overload capabilities in the explosion tear test.

The effects of mean strain on low-cycle fatigue crack propagation in 5Ni-Cr-Mo-V steel and 7079-T6 aluminum are presented. The effects of mean strain on the growth rate of fatigue cracks in both materials is dependent upon mean strain level and cyclic total strain range level. For elastic strain amplitudes, mean strain acts as an additive increase in strain range for tension mean strains and a similar decrease in strain range for compressive mean strains. For the high strength steels and aluminum alloys, mean strain can have a 10x and 100x effect, respectively, on the structural life of high performance structures of these materials.

A very interesting low-cycle fatigue crack propagation test for high strength materials, employing fracture mechanics parameters, is being developed. The test uses an edge-notched and side-grooved cantilever specimen which is fatigued in a slightly modified version of the fatigue machine designed for the "Lehigh" plate bend specimen. Preliminary test results obtained on a D6AC steel are presented and discussed. Also, the results obtained in the new test are compared to those obtained for the "Lehigh" type specimen of D6AC steel in the regular low-cycle fatigue test.

The limits to which linear-elastic fracture mechanics can be used to determine valid fracture toughness properties of high strength materials are being investigated. The use of side-grooved specimens has extended the capability of determining crack-instability to the tougher high strength materials. With the accepted type of specimens (non-side-grooved) crack instability is not sharp, if evident at all, and accurate measurements are not possible with this type of material. The final section in this report describes the preliminary comparative results obtained with side-grooved and smooth-sided specimens of several high strength, low toughness titanium and aluminum alloys.

## TITANIUM ALLOYS

(R.J. Goode, R.W. Huber, and D.G. Howe)

Fracture toughness studies of a wide variety of titanium alloys in the form of 1-in.-thick plate have provided the only reliable means of referencing the fracture toughness characteristics of the spectrum of high strength titanium alloys in thick sections. A preliminary Fracture Toughness Index Diagram (FTID) has been developed for titanium which has aided in the development of new alloys and in the modification of existing alloys, through chemistry and processing, that have shown improved combinations of strength and toughness over alloys that were available several years ago. This diagram correlates the fracture toughness characteristics of the material as measured by the drop-weight tear test, a laboratory test, with the performance of the material in the explosion tear test, a structural prototype element test, over a wide yield strength range. These tests have been described for titanium in an earlier report (1). The correlation of the results of these two tests have provided for the first time the necessary information for establishing meaningful fracture toughness specifications for titanium alloys (2).

### THE TITANIUM FRACTURE TOUGHNESS INDEX DIAGRAM

The FTID for 1-in.-thick titanium is shown in Fig. 1. New test results obtained during the reporting period have been incorporated in the diagram to keep it current. The "fracture index" aspects of the diagram are illustrated by the correlation of explosion tear test (ETT) performance with drop-weight tear test (DWTT) energy for fracture below yield and for the level of plastic strain required for fracture propagation above yield. For example, in the ETT all materials having less than 1500 ft-lb DWTT energy will "break flat" -- elastic strains are sufficient to cause catastrophic propagation of fractures. For those materials having DWTT energies above 1500 ft-lb ~~plastic~~ plastic strains are required to cause propagation of fractures and the level of plastic strain in the ETT necessary to cause failure is proportional to the DWTT energy. DWTT energies of 2000-2500 ft-lb indicate that a capability of 1 - 2% plastic strain without failure is assured and 3 - 5% plastic strain is generally expected. Above 2500 ft-lb plastic strains in the order of 5-- 7% would be expected. The optimum materials trend line (OMTL) indicates the highest DWTT

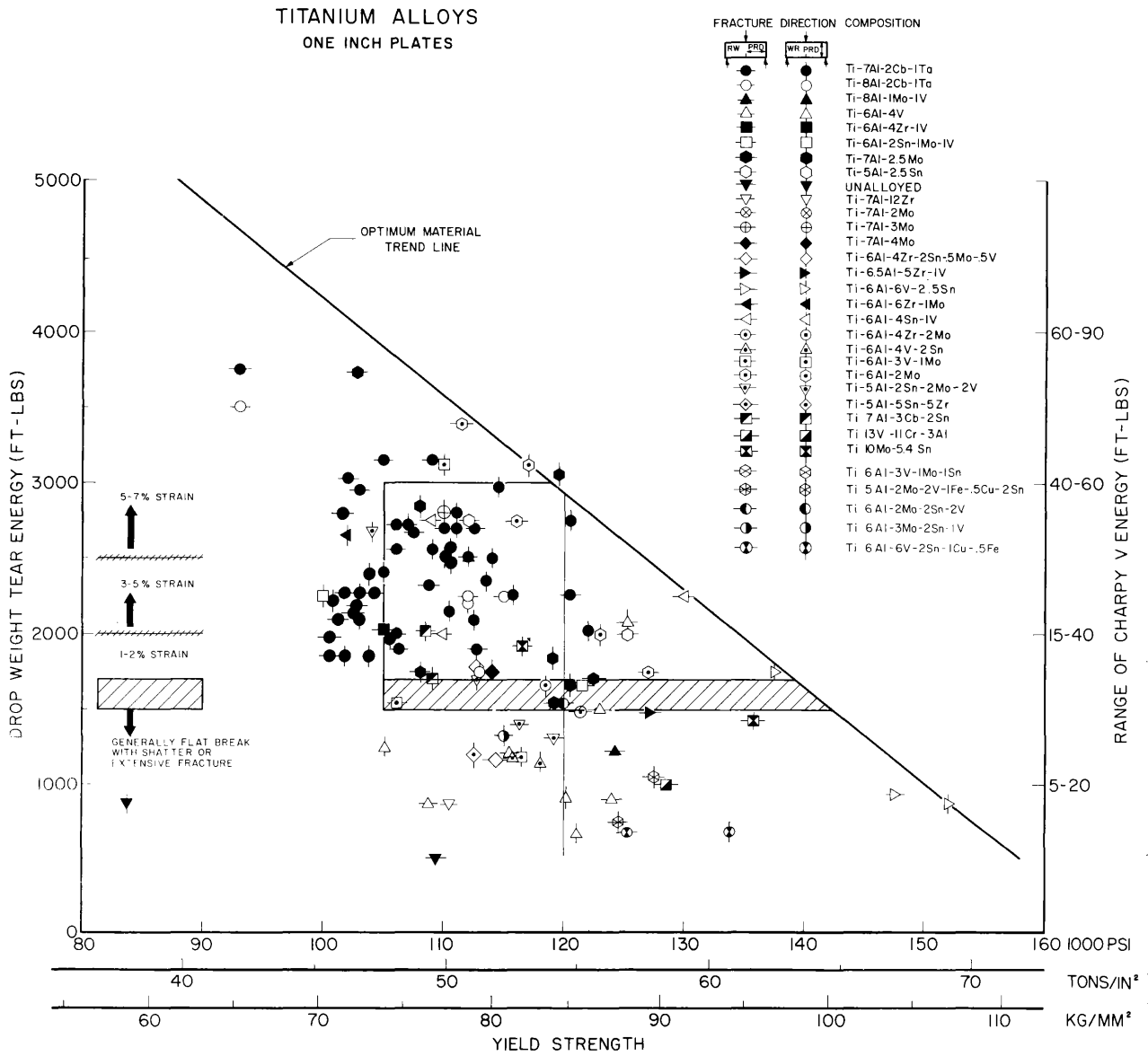


Fig. 1 - FTID for titanium alloys. One-inch-thick titanium alloys showing correlation of DWTT, ETT,  $C_V$ , and YS. The OMTL indicates the highest level of strength for any given level of toughness.

energy values obtained as a function of yield strength (YS) for the WR ("weak") fracture direction (3). Contrasted to the FTID for steels (discussed in another section), where a series of OMTL's corresponding to different melting and rolling practices are established, the single titanium OMTL represents the only melting process used in the titanium industry--consumable electrode, double vacuum arc remelts. This would correspond to the special melt CEVM process for steels. The effects of different processing variables, such as degree of cross-rolling, are unknown for titanium at the present time. The effects of interstitial elements, especially oxygen, hydrogen, and strong beta stabilizing elements as impurities in thick titanium plates, are to decrease the level of fracture toughness and generally increase the yield strength. Most of our work has been concerned with material of very low interstitial content (0.08% oxygen maximum) and beta stabilizing impurity elements, therefore the single OMTL on the titanium FTID represents the "best" that can be produced by industry at the present time. The impingement of the ETT elastic-plastic transition band at 1500-1700 ft-lb DWTT energy on the OMTL indicates that above about 140-ksi YS even the "best" of the titanium materials would be expected to propagate fracture in the ETT at elastic stress levels. Fracture mechanics techniques will be required to determine the fracture toughness characteristics of these materials. Unless the utmost care is exercised with regards to maintaining the lowest possible interstitial impurity levels in the starting materials and during melting and, at the same time, optimum processing procedures are developed and closely followed, commercially-produced plate material will generally fall below the OMTL that has been established. The rectangular box on the FTID indicates that above about 120-ksi YS, most of the plate material produced at the present time can be expected to propagate fractures at levels of stress below the yield strength of the material. Below 120-ksi YS, a large variety of alloys should be expected to require large plastic overloads for fracture and should not be analyzable by presently accepted fracture mechanics techniques.

#### MECHANICAL PROPERTIES OF SOME NEW TITANIUM ALLOY PLATES

The discovery by B.F. Brown (4) that the Ti-7Al-2Cb-1Ta

(7-2-1) alloy was susceptible to stress-corrosion-cracking (SCC) has resulted in an intensive effort by the U.S. Bureau of Ships laboratories and industry to minimize or eliminate this problem by chemistry modification or processing. The addition of a small amount of molybdenum to the alloy has been reported to decrease the stress-corrosion-cracking sensitivity considerably. Also, decreasing the aluminum content slightly would tend to minimize the "ordering" reaction on consequent embrittlement that is thought by some to be responsible for the environmental sensitivity of the alloy. Specimens have been furnished to NRL from the U.S. Bureau of Ships program for DWTT evaluation.

A DWTT specimen of a Ti-7Al-3Cb-.8Mo (T-87) alloy, made from a small laboratory heat and reported to be insensitive to the aqueous environment, was supplied by the U.S. Navy Marine Engineering Laboratory. The DWTT energy value obtained for this material was 810 ft-lbs. Two SCC specimens were obtained from a section of the broken DWTT specimen and tested in a 3.5% salt water solution using the techniques described in the titanium stress-corrosion-cracking section of this report. Using the step-loading technique, the air and salt water  $K_I$  values were essentially the same value, 130 ksi $\sqrt{\text{in}}$ . The yield strength of this material was not determined.

A Ti-6Al-2Cb-1Ta-.8Mo alloy, also a product of a 100-lb laboratory heat and reported as being immune to salt water stress-corrosion-cracking, had DWTT energy values above 2000 ft-lb at reported yield strength levels of 106 to 109-ksi. A large commercial heat of this alloy has been made and from it 1-in. and 2-in.-thick plates are to be distributed to Navy laboratories for evaluation.

A quantity of 1-in., 2-1/2-in., and 4-in. Ti-7Al-2Cb-1Ta plate (T-89), purchased by MEL from Titanium Metals Corporation of America and processed at the Sparrows Point Mill of Bethlehem Steel Corporation, was recently received. This material was water-spray quenched after rolling from above the beta transus temperature. The DWTT energy values of the as-received 1-in. plate are 1900 and 2140 ft-lb in the WR and RW fracture directions, respectively, with the corresponding measured yield strengths of 109.5 and 112.8-ksi.

A low interstitial, commercial heat of Ti-7Al-1Mo-1V (T-88), ordered the first quarter of 1965, was received in October as 1/2-in. and 1-in.-thick plate. This plate was rolled from 1800°F with water quenching after the last pass. The as-received 1/2-in.-thick plate had the following properties as reported by the producer: 146-150-ksi UTS, 138-143-ksi YS, 10-15% elongation (1-in.) and Charpy V ( $C_v$ ) notch energy values of 19 and 26.5 ft-lb at 32°F. Solution annealing at 1800°F for one hour and air cooling gave a minimum yield strength of 112-ksi and  $C_v$  energy value of 45 ft-lb at 32°F. Aging for two hours at 1200°F increased the yield strength to about 120-ksi while the  $C_v$  energy decreased to 40 ft-lb. Incomplete tests indicate that the 1/2-in.-thick plate in the as-received condition is immune to salt water stress-corrosion-cracking.

The 1-in.-thick plate of the same material in the as-received condition has DWTT energy values of 1326 and 1540 ft-lb in the WR and RW fracture directions, respectively, at a reported yield strength level of 126-ksi. Annealing for one hour at 1800°F in a cold wall vacuum furnace, followed by helium gas cooling (equivalent to air cooling), gave DWTT values of 2000 and 2100 ft-lb at 110-114-ksi YS.

Five titanium alloys, also ordered early in 1965, have been received as 1-in., 2-in., and 3-in.-thick circular-rolled plates. The nominal compositions of these alloys are shown in Table 1 along with the DWTT values and tensile properties for the 1-in.-thick as-received plates. The effects of preliminary vacuum annealing treatments on DWTT properties are also listed. The DWTT values have not been corrected for variations in thickness in the nominally 1-in.-thick plate which varied from 1-in. to 1.25-in. for the different alloys. Test specimens (1-1/8-in. and 1-in. thick) will be prepared by machining equal amounts from both surfaces of the 1.25-in. T-94 plate and this data will be used to determine the corrections to be applied to off-gage plate. These alloys will be used quite extensively for weldment studies. Evaluation of the weldments will be performed by the Metallurgy Division and the Mechanics Division of NRL.

#### WELDING STUDIES

Drop-weight tear tests of a Ti-6Al-4V and a Ti-7Al-2.5Mo

TABLE 1  
MECHANICAL PROPERTIES FOR ONE-INCH THICK TITANIUM ALLOY PLATE

Alloy No.	Nominal Composition*	As-Received Properties						Annealed Properties					
		YS (ksi)		Tensile UTS (ksi)		RA (%)		Elong. (%)		Heat Treatment		DWT (ft-lb)	
		Long.	Trans.	Long.	Trans.	Long.	Trans.	Long.	Trans.	Long.	Trans.	Long.	Trans.
T-90	Ti-5Al-2V-2Mo-2Sn	116.3	112.7	134.0	132.1	26.6	23.1	9.7	9.3	1723	1418	1660°F/1 hr (He cooled)	1723
T-91	Ti-6Al-4V	109.0	104.9	124.8	123.1	35.1	35.8	10.8	11.8	1228	870		
T-92	Ti-6Al-6V-2Sn-1Cu-.5Fe	126.2	133.7	148.8	149.7	21.1	18.2	8.6	6.8	680	680	1660°F/1 hr (He cooled)	811
T-93	Ti-6Al-3Mo-1V	109.8	116.5	124.6	128.4	21.5	27.5	8.9	10.7	1540	1173	1800°F/1 hr (He cooled)	1662
T-94	Ti-7Al-2.5Mo	119.1	120.5	133.2	134.9	24.1	20.2	8.6	8.6	1662 <sup>†</sup>	1540 <sup>‡</sup>	1800°F/1 hr (He cooled)	4380 <sup>‡</sup>

† Average of 2 specimens  
 \* With .08 wt-% maximum oxygen content  
 ‡ Specimen 1.25-in.-thick

specimen, MIG welded at Titanium Metals Corporation of America, have been completed. The specimens were 3-in.-wide as supplied, whereas the standard DWTT specimen has a 5-in.-width. This necessitated welding a crack-starter strip along the side of each specimen, thus leaving a net fracture test section of only 2.8-in. as compared to the usual 3.5-in. in the standard specimen.

The DWTT energy required to fracture the Ti-6Al-4V weld was 1200 ft-lb and for the Ti-7Al-2.5Mo weld, 1000 ft-lb. The fracture surface of the Ti-6Al-4V weld sample showed a lack of fusion of 1/8-in. all along the root face of the plate. Assuming a linear correction of the DWTT on a cross-sectional area basis, this would increase the DWTT energy value for the Ti-6Al-4V specimen to 1500 ft-lb and the Ti-7Al-2.5Mo to 1250 ft-lb. These corrected values for the Ti-6Al-4V MIG welded specimen are comparable to similar NRL MIG welds. However, the corrected DWTT energy value for the Ti-7Al-2.5Mo MIG weld is considerably less than the 1400-1500 ft-lb usually obtained on as-welded samples prepared at NRL. Annealing an NRL MIG weld in Ti-7Al-2.5Mo alloy at 1800°F for one hour and gas cooling further increases the DWTT energy value to 2200 ft-lb.

#### HEAT-TREATMENT STUDIES

Heat-treatment studies on a number of titanium alloys have been continued in order to develop information on the stability of the alloys and to determine the heat treatments which will produce an optimum combination of strength and toughness.

The effects of heat treatments on the mechanical properties of the alloys Ti-6Al-4V-2Sn (T-67) and Ti-7Al-2.5Mo (T-71) are shown in Tables 2 and 3 respectively. The alloy Ti-6Al-4V-2Sn (T-67) shows poor fracture toughness as measured by the Charpy V ( $C_V$ ) test, even at the lowest yield strength levels, regardless of the heat treatments that were given it. However, as shown in Fig. 2, the variation of heat treatments did produce a significant change in the yield strength of the material. A solution annealing treatment at a temperature just below the beta transus of the alloy increased the yield strength to over 150,000 psi.

**TABLE 2**  
**TEST DATA FOR SOLUTION ANNEALING AND AGING TREATMENTS ON THE ALLOY Ti-6Al-4V-2Sn (T-67)**

Alloy No. and Nominal Composition	Solution Heat Treatment	Aging Heat Treatment	C <sub>v</sub> Notch Energy (ft-lbs)				.2% YS (ksi)	UTS (ksi)	Elong. (%)	RA (%)
			RW -80°F	WR -80°F	RW +32°F	WR +32°F				
Ti-6Al-4V-2Sn (T-67)	As received condition	As received condition	17.5	18.5	21.0	20.5	115.8(L) 123.4(T)	127.6(L) 133.2(T)	13.1 12.1	35.3 24.6
	1750°F/1 hr/WQ		16.0	14.5	17.0	16.0	129.8(L) 129.3(T)	154.5(L) 153.5(T)	9.3 7.1	25.7 25.7
	1750°F/1 hr/WQ	1100°F/2 hr/AC	13.0	14.0	15.0	16.0	150.5(L) 153.8(T)	161.1(L) 161.5(T)	5.0 5.7	11.8 13.0
	1750°F/1 hr/WQ	1200°F/2 hr/AC	16.0	17.5	19.0	17.5	143.9(L) 140.9(T)	152.2(L) 150.5(T)	6.4 6.4	13.6 14.9
	1700°F/1 hr/WQ		20.0	17.5	23.0	19.5	125.2(L) 123.3(T)	154.2(L) 151.5(T)	10.0 10.0	23.6 28.5
	1700°F/1 hr/WQ	1100°F/2 hr/AC	16.5	16.0	19.5	20.0	152.2(L) 148.2(T)	161.8(L) 159.2(T)	7.1 6.4	19.0 15.0
	1700°F/1 hr/WQ	1200°F/2 hr/AC	19.0	18.0	21.0	23.0	142.6(L) 145.9(T)	154.2(L) 156.2(T)	10.0 9.3	25.7 19.6
	1650°F/1 hr/WQ		17.5	18.0	20.0	18.5	99.8(L) 108.4(T)	135.8(L) 138.3(T)	13.6 12.9	36.6 36.4
	1650°F/1 hr/WQ	1100°F/2 hr/AC	15.5	14.0	17.5	16.0	134.8(L) 138.6(T)	145.6(L) 148.5(T)	7.9 7.9	20.0 14.2
	1650°F/1 hr/WQ	1200°F/2 hr/AC	17.5	16.0	19.0	19.0	130.3(L) 130.6(T)	139.6(L) 139.9(T)	12.1 10.0	22.4 22.9
	1550°F/1 hr/WQ						93.5(L) 92.1(T)	135.5(L) 136.5(T)	13.6 14.3	36.0 39.7
	1550°F/1 hr/WQ	1100°F/2 hr/AC	18.0	15.5	23.0	19.0	134.8(L) 133.8(T)	143.5(L) 141.9(T)	10.0 12.1	11.2 23.1
	1550°F/1 hr/WQ	1200°F/2 hr/AC	21.0	16.0	22.0	20.0	125.7(L) 131.2(T)	134.6(L) 139.5(T)	11.4 12.9	30.6 28.6
	1750°F/1 hr/AC		19.5	18.5	25.0	26.5	113.7(L) 112.7(T)	130.0(L) 128.6(T)	10.7 10.0	24.7 26.8
	1750°F/1 hr/AC	1100°F/2 hr/WQ	19.00	18.5	24.5	24.5	119.5(L) 120.6(T)	129.5(L) 130.4(T)	10.7 11.4	34.4 31.6
	1750°F/1 hr/AC	1200°F/2 hr/WQ	17.5	17.0	24.5	23.0	118.6(L) 125.0(T)	126.5(L) 131.0(T)	10.7 11.4	26.7 24.3
	1700°F/1 hr/AC		20.0	19.5	25.0	24.5	110.1(L) 115.4(T)	128.0(L) 131.3(T)	12.1 12.1	30.2 27.5
	1700°F/1 hr/AC	1100°F/2 hr/WQ	23.0	22.0	26.5	24.5	119.2(L) 121.4(T)	129.5(L) 130.3(T)	12.1 11.4	33.5 28.0
	1700°F/1 hr/AC	1200°F/2 hr/WQ	17.5	17.0	22.5	21.5	120.2(L) 121.7(T)	128.2(L) 129.0(T)	14.3 11.4	34.6 39.7
	1650°F/1 hr/AC		22.0	20.0	28.5	25.0	109.4(L) 113.1(T)	127.1(L) 130.0(T)	12.9 12.0	31.8 32.9
	1650°F/1 hr/AC	1100°F/2 hr/WQ	23.0	21.0	26.5	24.5	117.8(L) 123.7(T)	128.5(L) 132.3(T)	10.7 11.4	24.2 33.4
	1650°F/1 hr/AC	1200°F/2 hr/WQ	19.5	17.5	23.0	21.0	121.4(L) 121.8(T)	129.0(L) 130.5(T)	12.1 12.1	28.0 33.5
	1550°F/1 hr/AC		17.5	19.5	23.0	23.0	111.8(L) 116.4(T)	127.5(L) 130.0(T)	14.3 11.4	26.4 32.4
	1550°F/1 hr/AC	1100°F/2 hr/WQ	20.0	18.5	23.0	23.0	123.3(L) 127.2(T)	131.0(L) 134.8(T)	14.3 11.4	39.7 30.3
	1550°F/1 hr/AC	1200°F/2 hr/WQ	16.0	16.0	21.5	21.0	123.8(L) 125.7(T)	130.8(L) 132.0(T)	11.4 10.0	25.9 29.7

TABLE 3

## TEST DATA FOR SOLUTION ANNEALING AND AGING TREATMENTS ON THE ALLOY Ti-7Al-2.5Mo (T-71)

Alloy No. and Nominal Composition	Solution Heat Treatment	Aging Heat Treatment	Cv Notch Energy RW +32°F	WR +32°F	Energy (ft-lbs)	.2% YS (ksi)	UTS (ksi)	Elong. (%)	RA (%)
Ti-7Al-2.5Mo (T-71)	As received condition	As received condition	37.5	37.5		122.4(L) 119.0(T)	134.8(L) 132.3(T)	9.3 8.6	19.5 21.7
	1850°F/1 hr/AC	1100°F/2 hr/WQ	28.0	28.5		123.7(L) 122.0(T)	136.3(L) 138.6(T)	10.7 10.0	19.0 17.8
	1850°F/1 hr/AC	1200°F/2 hr/WQ	26.5			120.0(L) 123.3(T)	131.3(L) 132.3(T)	8.6 10.7	21.8 21.2
	1800°F/1 hr/AC	1100°F/2 hr/WQ	52.5	47.5					
	1800°F/1 hr/AC	1200°F/2 hr/WQ	44.0						
	1750°F/1 hr/AC	1100°F/2 hr/WQ	51.0			123.4(L)	138.1(L)	11.4	24.6
	1750°F/1 hr/AC	1200°F/2 hr/WQ	49.0						
	1700°F/1 hr/AC	1100°F/2 hr/WQ	42.5	43.5		123.2(L) 120.7(T)	137.9(L) 135.3(T)	11.4 10.7	16.0 22.3
	1700°F/1 hr/AC	1200°F/2 hr/WQ	38.0			122.8(L)	134.5(L)	10.0	16.0
	1850°F/1 hr/WQ	1100°F/2 hr/AC	16.0	20.5		151.2(L) 151.5(T)	167.4(L) 165.0(T)	3.6 2.1	4.4 3.7
	1850°F/1 hr/WQ	1200°F/2 hr/AC	21.0			155.2(L) 153.8(T)	166.8(L) 165.1(T)	3.6 2.1	5.6 5.0
	1800°F/1 hr/WQ	1100°F/2 hr/AC	21.0			143.2(L)	160.5(L)	3.6	5.0
	1800°F/1 hr/WQ	1200°F/2 hr/AC	21.0			138.7(L)	152.8(L)	5.0	9.9
	1750°F/1 hr/WQ	1100°F/2 hr/AC	30.0			138.3(L)	157.8(L)	5.0	6.2
	1750°F/1 hr/WQ	1200°F/2 hr/AC	41.5	38.5		136.4(L)	149.9(L)	7.1	9.4
	1700°F/1 hr/WQ	1100°F/2 hr/AC	40.0			138.3(L)	156.5(L)	5.7	9.4
1700°F/1 hr/WQ	1200°F/2 hr/AC	40.0			137.8(L)	150.9(L)	6.4	8.2	

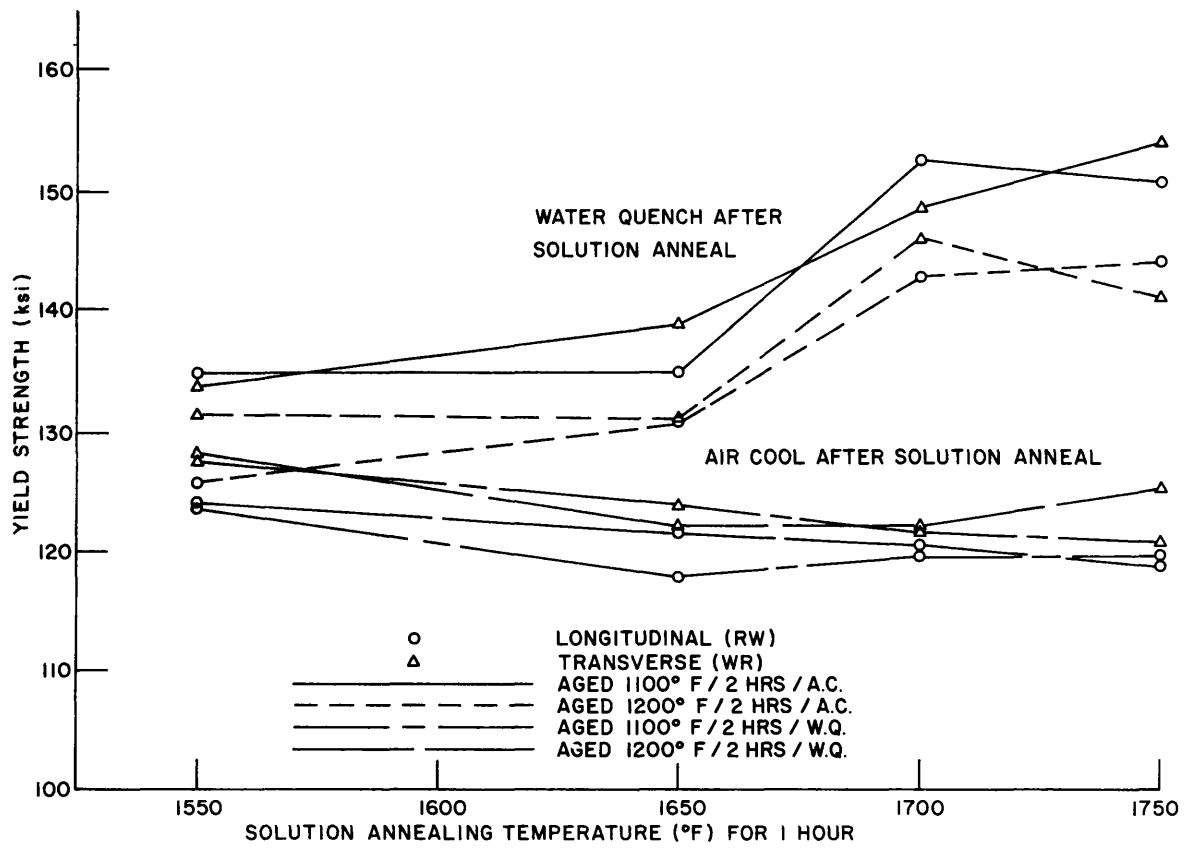


Fig. 2 - Effect of solution annealing temperature on the yield strength of the alloy Ti-6Al-4V-2Sn (T-67) with aging treatment

The alloy Ti-7Al-2.5Mo (T-71) shows the capability of developing an excellent combination of high strength and good fracture toughness. Some excellent combinations have already been obtained as can be seen from Table 3. One of the best treatments obtained to date is a solution anneal at 1700°F for one hour and water quenching followed by an 1100°F age for two hours with an air cool. (Both treatments were conducted in an argon atmosphere and inconel muffle.) This treatment results in a combination of 138-ksi YS and approximately 40 ft-lb C<sub>v</sub> energy at 32°F. Figure 3 shows the effect of variations in solution annealing temperatures on the yield strength of the alloy Ti-7Al-2.5Mo (T-71) with aging treatment. The yield strength of the alloy is relatively insensitive to heat treatment if air cooled after the solution anneal. However, by water quenching after a solution anneal near the beta transus, yield strengths in excess of 150-ksi are obtained.

Figure 4 shows the effect of solution annealing temperature on the C<sub>v</sub> energy of the alloy Ti-7Al-2.5Mo (T-71) with aging treatment. It was intended that 1850°F be the highest annealing temperature to correspond with the 1850°F heat treatment on the tensile specimens, but due to an instrument malfunction, the specimens overheated to 1870°F for a short time. The much lower fracture toughness values for the 1870°F temperature excursion shows how sensitive the material is to heat treatment above the beta transus. It is very interesting to note the significant increase in C<sub>v</sub> values exhibited by specimens given a water quench after the solution anneal. The excellent combination of yield strength and fracture toughness obtained through the 1700°F/1 hr/WQ, 1100°F/2 hr/AC heat treatment might possibly be improved upon by a treatment at some lower solution annealing temperature. A further heat treatment to study, which is indicated by the trends established in the heat treatments shown in Figs. 3 and 4, would be a solution anneal at 1600°F-1650°F for one hour and water quench. A slightly lower aging temperature might also be used, such as 900°F or 1000°F for two to four hours and air cool.

The effect of heat treatment on the C<sub>v</sub> energy of several titanium alloys in the 120-145-ksi YS range is shown in Fig. 5. The bar graph illustrates that by

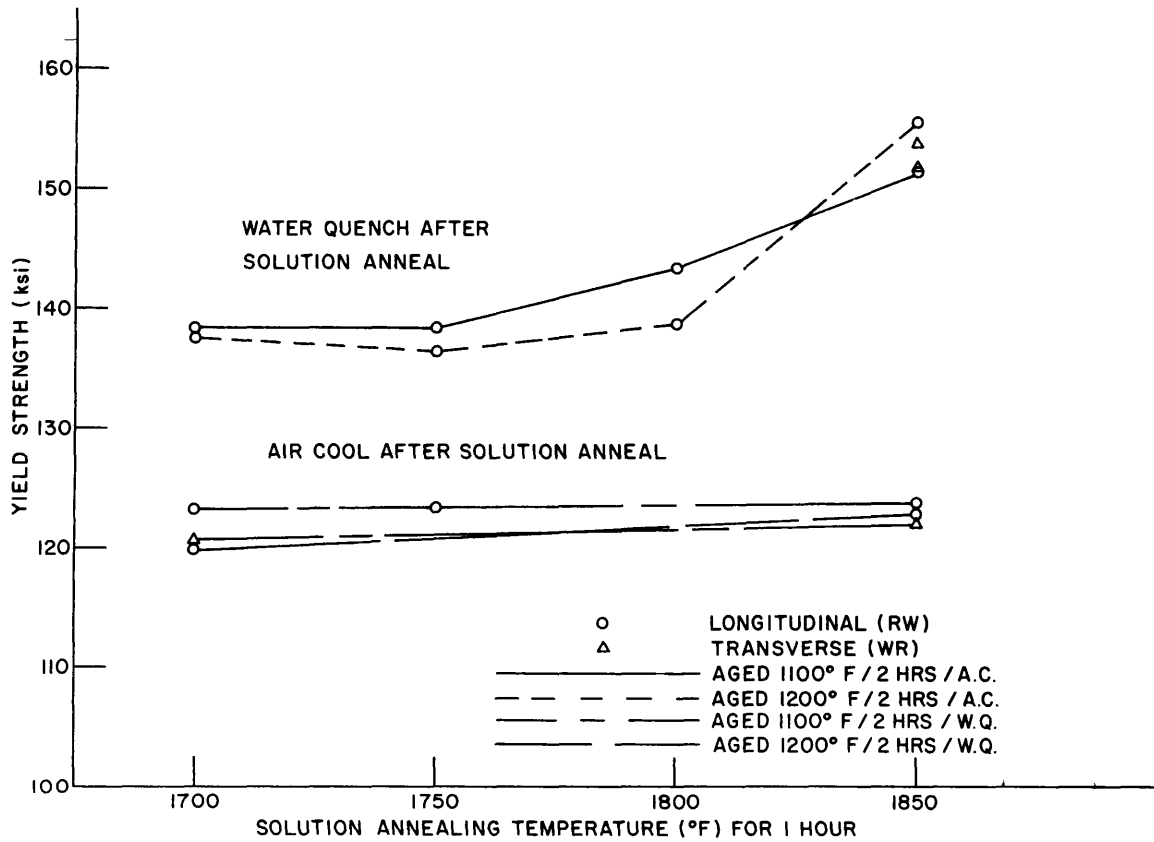


Fig. 3 - Effect of solution annealing temperature on the yield strength of the alloy Ti-7Al-2.5Mo (T-71) with aging treatment

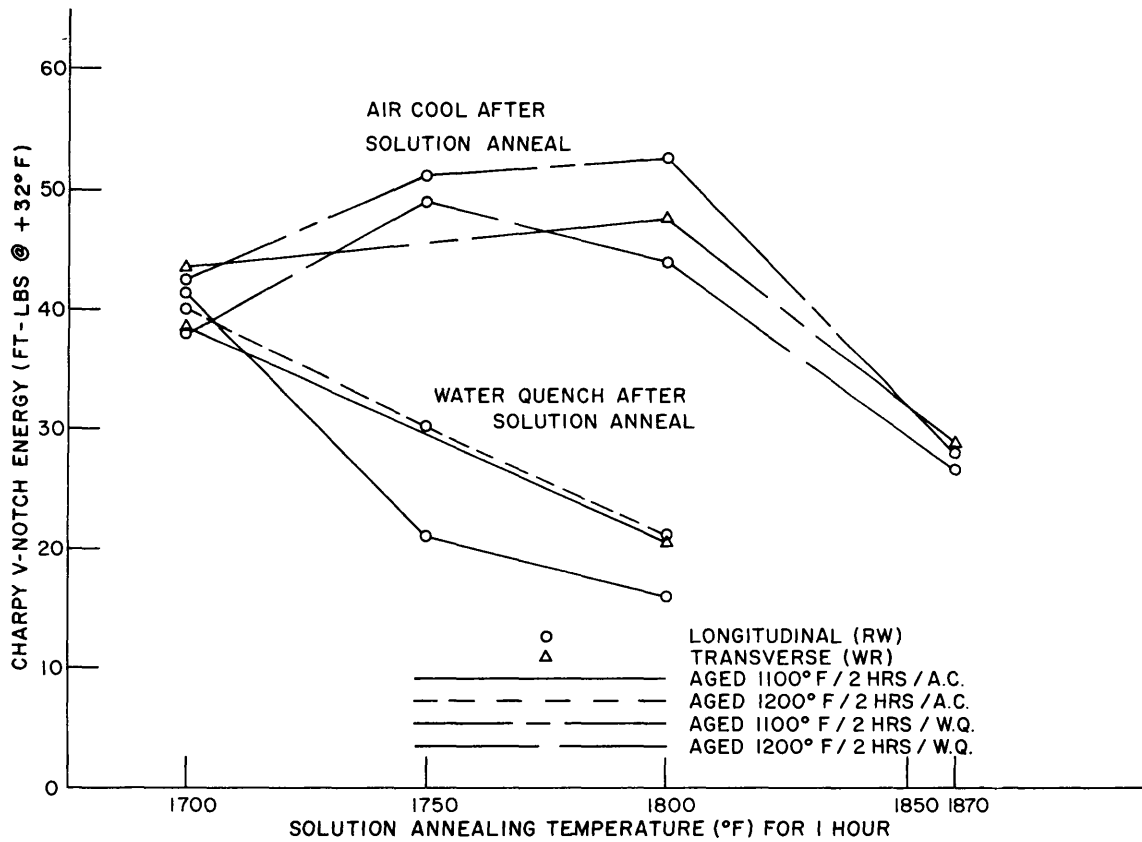


Fig. 4 - Effect of solution annealing temperatures on the Charpy V notch energy of the alloy Ti-7Al-2.5Mo (T-71) with aging treatment

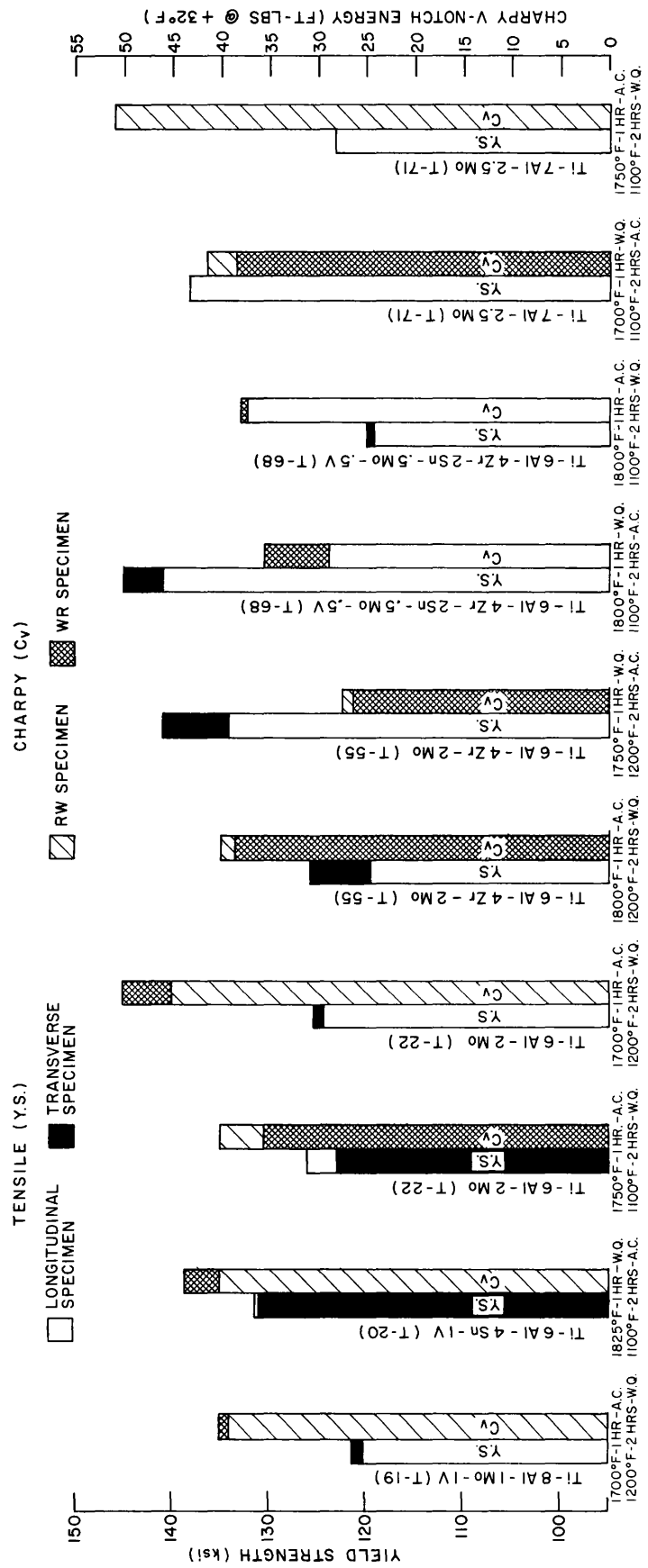


Fig. 5 - Effect of heat treatment on the Charpy V notch energy of several titanium alloys in the 120-145 ksi yield strength range

selective heat treatment it is possible to develop these alloys to a good fracture toughness level while still maintaining a yield strength of 120-ksi or more. The alloys Ti-6Al-4Sn-1V (T-20), Ti-6Al-2Mo (T-22), and Ti-7Al-2.5Mo (T-71) have shown the best combinations of strength and fracture toughness through selective heat treatment of all the alloys investigated to date.

The effects of heat-treatment environments and cooling conditions on the resistance of the alloy Ti-8Al-1Mo-1V (T-28 and T-19) to stress-corrosion-cracking were studied. The SCC test used was that developed by B.F. Brown (4). The bar-type specimens were notched, fatigued, and side-grooved prior to heat treatment with the exception of those of T-28 that were vacuum heat treated. For those, the machining was performed after heat treatment.

Due to a limited quantity of material available for stress-corrosion-cracking tests, it was not possible to use a separate specimen to determine the dry-break load value. Thus an attempt was made to utilize the specimens broken in the 3.5% salt water solution for this purpose. The specimens listed in Table 4 were all examined under the microscope and measurements were taken which included the mill-cut depth  $C_1$ , the fatigue-crack depth  $C_2$ , and the depth of the corrosion into the parent material  $C_3$ . This total measurement -  $C_1+C_2+C_3$  - was called  $C_\Delta$ , and was inserted into the stress intensity formula† in order to calculate a  $K_{I\Delta}$  which could be comparable to a dry-break load. This calculation was very dependent on the accurate determination of the depth at which stress-corrosion-cracking ended and the onset of fast fracture began. This depth was extremely difficult to pinpoint in most cases. Therefore, the validity of the  $K_{I\Delta}$  values are questionable. However, the difference between  $K_{I\Delta}$  and  $K_{Isc}$  does provide an indication of the degree of sensitivity.

---

† See section in this report on "Stress-Corrosion-Cracking of Titanium"

TABLE 4

EFFECTS OF SEVERAL HEAT TREATMENTS ON RESISTANCE OF Ti-8Al-1Mo-IV  
(T-28 AND T-19) TO STRESS-CORROSION-CRACKING IN A 3.5 PERCENT NaCl SOLUTION

Nominal Composition	Solution Heat Treatment	Aging Heat Treatment	K <sub>I</sub> (ksi/in.) No Break	Time (min.)	K <sub>Isc</sub> (ksi/in.)	Time To Break (min.)	K <sub>IA</sub> (ksi) Calcul. Dry Break Load	Specimen Type *
Ti-8Al-1Mo-IV † (T-28)	1950°F/Vacuum/2 hr/HeC	None	118.2	10	121.2	5	121.2	B
	1950°F/Vacuum/2 hr/HeC	None	110.1	450	117.4	2	117.4	B
	1700°F/Argon/1 hr/AC	1200°F/Argon/2 hr/WQ	94.6	10	96.3	2	162.0	B
	1950°F/Argon/1 hr/AC	1200°F/Argon/2 hr/WQ	40.3	10	43.7	5	134.5	B
Ti-8Al-1Mo-IV † (T-19)	1700°F/Argon/1 hr/AC	1200°F/Argon/2 hr/WQ	42.8	3	45.0	3-1/2	125.8	A
	1700°F/Argon/1 hr/AC	1200°F/Argon/2 hr/AC	32.3	6	38.0	3-2/3	117.1	A
	1700°F/Vacuum/1 hr/HeC	1200°F/Vacuum/2 hr/HeC	49.3	3	55.7	1-1/3	194.2	A
	1700°F/Vacuum/1 hr/HeC	1200°F/Argon/2 hr/AC	42.0	12	45.8	2	135.0	A
	1700°F/Vacuum/1 hr/HeC	1200°F/Argon/2 hr/WQ	47.1	3	50.2	1/2	140.2	A
	1950°F/Argon/1 hr/AC	1200°F/Argon/2 hr/AC	27.6	3	33.5	2	133.7	A
	1950°F/Argon/1 hr/AC	1200°F/Argon/2 hr/WQ	32.9	3	38.8	3-1/3	135.2	A
	1950°F/Vacuum/1 hr/HeC	1200°F/Vacuum/2 hr/HeC	36.8	5	39.1	5-3/4	143.7	A
1950°F/Vacuum/1 hr/HeC	1200°F/Argon/2 hr/AC	41.7	6	44.1	2-3/4	137.7	A	
1950°F/Vacuum/1 hr/HeC	1200°F/Argon/2 hr/WQ	40.3	3	44.0	2-1/2	154.3	A	

NOTE: T-28 specimens are all in the longitudinal (RW) direction.  
T-19 specimens are all in the transverse (WR) direction.

\* Specimen Type A is 3/8" x 1" x 5" (1/16" side notch depth).  
Specimen Type B is 1/2" x 1" x 5" (1/32" side notch depth).

† (Extra low interstitial) - Fine-grained structure in the as-received plate.

‡ (Low interstitial) - Coarse-grained structure in the as-received plate.

A drastic change is evident in the resistance to stress-corrosion-cracking of the extra low interstitial alloy Ti-8Al-1Mo-1V (T-28), which was made at NRL and INFAB processed (5). To a large part, the change seems dependent upon the environmental conditions associated with the heat treatment of the material. The heat treatment, consisting of a 1700°F/1 hr solution anneal in an argon atmosphere, followed by air cooling and aged at 1200°F/2 hr/WQ, results in a material which is only slightly susceptible to stress-corrosion-cracking. However, this same alloy is very susceptible to stress-corrosion-cracking when heat treated for one hour at 1950°F in an argon atmosphere, air cooled, then aged at 1200°F for two hours and water quenched. The 1700°F solution anneal was below the beta transus (1885°F ± 15°F) of the alloy while the 1950°F treatment was above the beta transus. This resulted in the 1700°F solution anneal still retaining its original fine grained microstructure. The 1950°F solution anneal produced a coarse beta grain microstructure. The large grain structure was retained on subsequent cooling. Under this type of treatment, it appears the large grain microstructure leaves a structure that has a well defined path of attack for stress-corrosion-cracking to occur. One might suspect this path to be along the network of large connecting grain boundaries which generally are high in impurity concentrations. However, the large prior beta grain structure with its well defined grain boundaries is not in itself conducive to lowering the alloy's resistance to stress-corrosion-cracking. This can be readily seen when looking at the two specimens which were heat treated at 1950°F for two hours in a "cold wall" vacuum furnace (1 × 10<sup>-5</sup>mm.Hg) and helium cooled (Table 4). No evidence of failure by stress-corrosion-cracking was observed in either specimen's fracture surface after breaking in a 3.5% NaCl solution. The  $K_{Isc}$  values, which were equal to those of dry-break loading for both of these specimens would confirm this (121.2 and 117.4-ksi/in., respectively, or an average for the two of 119.3-ksi/in.). The microstructure of these specimens appeared under the microscope to be very similar to that of the specimen given the 1950°F for one hour solution annealing treatment in an argon atmosphere, followed by an air cooling and aging treatment. If the large beta grain type structure by itself can be made insensitive to stress-corrosion-cracking in the extra low interstitial T-28 material by controlling environmental conditions during the heat treatment, the condition that

existed in the T-28 sample, heat treated in argon at 1950°F, which made it susceptible to stress-corrosion-cracking was either not precipitated or it was eliminated by the vacuum treatment. The removal of interstitial hydrogen contamination by the vacuum heat treatment is, of course, a prime possibility.

Further data from the extra low interstitial Ti-8Al-1Mo-1V alloy (T-28) was not possible due to a lack of material. The low interstitial alloy Ti-8Al-1Mo-1V (T-19) was used as a substitute to see if the same trends would develop if heat treatments similar to those used on T-28 were employed. The microstructure of the T-19 plate in the "as-received" condition was quite different from that of the T-28 plate. The T-28 alloy had a fine grained type microstructure in the "as-received" condition, whereas the T-19 material had a large grained beta structure resulting from a final processing temperature above its beta transus. The interstitial contents were higher in most instances, as can be seen from Table 5.

It can be seen from the data presented in Table 4 that the T-19 specimens that were solution annealed in vacuum were slightly more resistant to attack by stress-corrosion-cracking than those solution annealed in an argon atmosphere and air cooled for similar heat treatments.

The T-19 and T-28 data also show that the 1700°F solution anneal in all instances (both solution annealing in an argon atmosphere with air cooling and solution annealing in vacuum with helium cooling) with duplicate aging treatments were more resistant to attack by stress-corrosion-cracking than those with 1950°F solution annealing treatments. Even though the "as-received" T-19 alloy material had a large grain structure, the heat treatment at 1950°F contributed to an additional beta grain growth. As indicated by the T-19 data this large prior beta grain structure could still have a detrimental effect on the stress-corrosion-cracking resistance of the material if the solution annealing treatment in vacuum was not sufficiently long enough to remove nearly all the hydrogen. This is not to say that interstitial hydrogen, in the amounts we are concerned with in T-19 and T-28, is responsible for the stress-corrosion-cracking behavior of these materials. The best interpretation of the data at present is that

TABLE 5

CHEMICAL COMPOSITION OF Ti-8Al-1Mo-1V PLATES T-19 AND T-28

Alloy No.	(Weight - Percent)								
	Al	Sn	V	Fe	Mo	O <sub>2</sub>	N <sub>2</sub>	C	H <sub>2</sub>
T-19	7.96	.15	1.0	.12	.90	.07	.013	.049	.006
T-28	7.8	--	1.1	.02	.92	.054	.003	.009	.013

the hydrogen may be involved in one of several possible competing mechanisms that can cause the material to be environmental sensitive and that the combination of fine grain size and vacuum annealing decreases or eliminates the additive effect of hydrogen in that one mechanism.

Further work is in progress to determine through chemical analysis how the interstitial contents of T-19 and T-28 were changed by the heat treatments indicated in Table 4. Additional work is also in progress on a low interstitial Ti-7Al-1Mo-1V alloy (T-88). This alloy in the "as-received" condition has a more desirable fine grained structure. Duplicate heat treatments to those investigated in the T-19 and T-28 alloys will be used to determine if the same trends are reproducible in this alloy. Confirmation of this would then indicate one means of improving to some degree the aqueous stress-corrosion-cracking sensitivity of commercially produced plates of this alloy.

STRESS-CORROSION-CRACKING  
OF TITANIUM ALLOYS

(R.W. Judy, Jr., and R.J. Goode)

Tests have been initiated to determine the degree of stress-corrosion-cracking sensitivity of a wide variety of titanium alloy plates and welds. The test procedures and equipment used are those developed by B.F. Brown (4). Briefly, the specimen used is a bar of rectangular cross-section containing a fatigue crack flaw. Shallow side grooves are cut into the specimen to insure plane strain loading conditions. The specimen is loaded in cantilever fashion in air or in the presence of a 3.5% salt water solution. Time to failure at a given load is recorded with the primary objective of the test being to find a threshold value which denotes the lowest stress intensity factor which will cause crack extension and failure due to the environmental effects.

Loading conditions are expressed in terms of the stress intensity factor:

$$K_I = \frac{4.12M \sqrt{(1/\alpha^3) - \alpha^3}}{BD^{1.5}} \quad (4)$$

where  $M$  = moment applied at the test section,  
     $B$  = specimen width,  
     $D$  = specimen depth, and  
     $\alpha = 1-a/D$  ( $a$  = flaw depth).

A specimen broken in the normal air environment serves as a baseline value which is denoted as  $K_{IX}$ . The threshold value, above which stress-corrosion-cracking is certain to occur, is denoted as  $K_{ISCC}$ . Thus,  $K_{ISCC}/K_{IX}$  is an indicator of the relative sensitivity of a material to the aqueous environment.

## RESULTS

The alloys studied are listed in Table 6 along with some of the mechanical properties, and the stress-corrosion-cracking data. The Ti-5Al-2.5Sn (T-7) and Ti-13V-11Cr-3Al (T-9) alloys were obtained from the Department of Defense sheet rolling program and had high interstitial contents. The remainder of the alloys were of low interstitial content (0.08 oxygen maximum).

The results of the tests are shown for the various alloys as stress intensity - time curves in Figures 6 through 13. The limits shown on the points in these charts indicate a non-uniform fatigue crack front and the limit values were obtained using the shallowest and the deepest portions of the fatigue crack depth.

The test results show the alloys Ti-5Al-2.5Sn, Ti-8Al-2Cb-1Ta, Ti-6Al-4Zr-2Mo, and Ti-6Al-4Zr-2Sn-.5Mo-.5V to be sensitive to the 3.5% salt water solution in the condition tested. This is indicated by the low  $K_{ISCC}/K_{IX}$  ratios (Table 6). The other alloys had  $K_{ISCC}/K_{IX}$  ratios from .79 to .92 indicating a relative insensitivity to the aqueous environment.

An important point to note in all these charts is that when the specimens are stressed even slightly above the threshold value, stress-corrosion-cracking occurs and failure results in a matter of only a few minutes. At stresses slightly below  $K_{ISCC}$ , there is no indication of stress-corrosion-cracking and subsequent failure even after very long times. For purposes of screening titanium materials, it would appear that in this test 60-minutes would be a sufficient amount of time to determine reasonably accurate  $K_{ISCC}$  values.

TABLE 6

PROPERTIES OF TITANIUM ALLOYS

Nominal Composition	Alloy No.	YS (ksi)	UTS (ksi)	C <sub>y</sub> at 32°F (ft-lb)	C <sub>v</sub> at -80°F (ft-lb)	DWTT (ft-lb)	K <sub>1x</sub> (ksi/in.)	K <sub>1scc</sub> (ksi/in.)	$\frac{K_{1scc}}{K_{1x}}$
Ti-5Al-2½Sn	T-7	125.5	130.5	15	13	2000	118	50	.42
Ti-13V-11Cr-3Al	T-9	128.5	135.5	7	6	1000	98		
Ti-8Al-2Cb-1Ta	T-23	113.0	123.2	32	20	1750	102	31	.30
Ti-6Al-2Sn-1Mo-1V	T-37	121.5	132.5	30	25	1660	112	90	.80
Ti-6Al-4Zr-2Mo	T-55	121.4	125.0	--	--	1478	118	46	.39
Ti-6Al-4V-2Sn	T-67	115.8	127.6	21	--	1173	98	85-90	~.92
Ti-6Al-4Zr-2Sn-½Mo-½V	T-68	113.5	121.1	26.5	--	1784	124	35-40	~.32
Ti-7Al-2½Mo	T-71	113.5	127.5	40.5	34	1751	111	88	.79

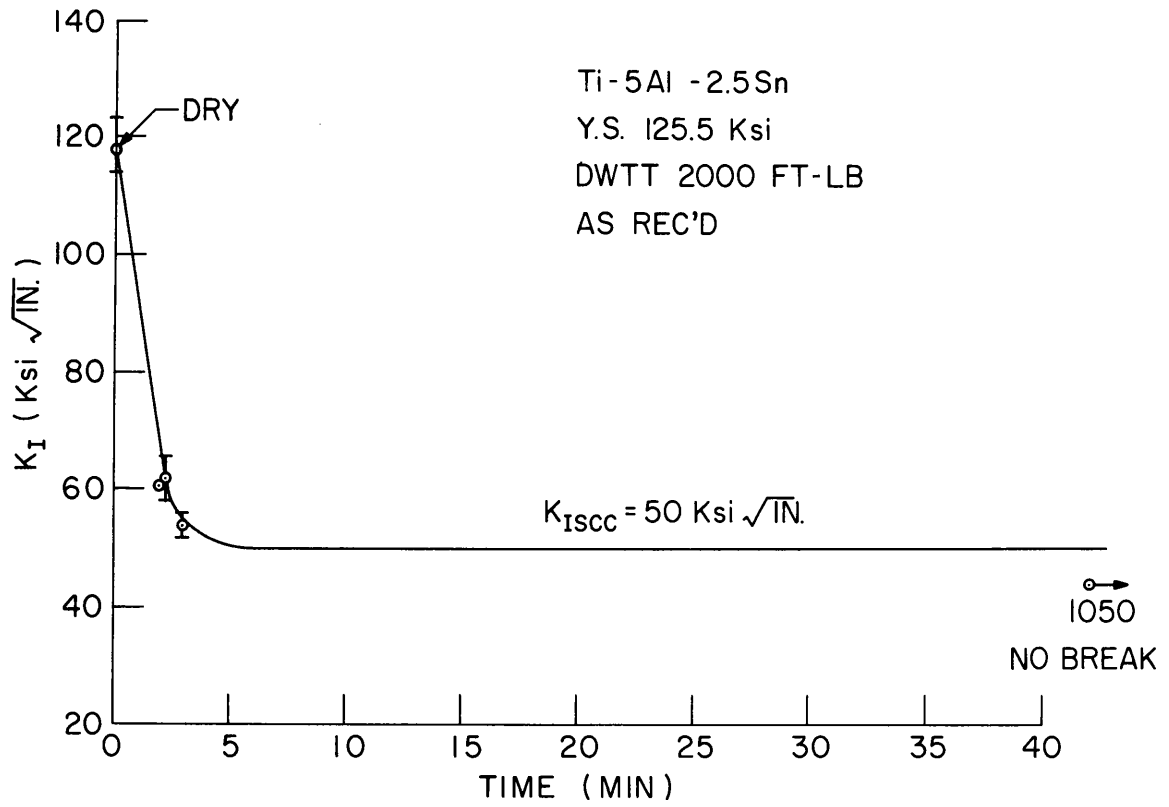


Fig. 6 - Environmental cracking characteristics of T-7 alloy  
 in 3.5% salt water solution

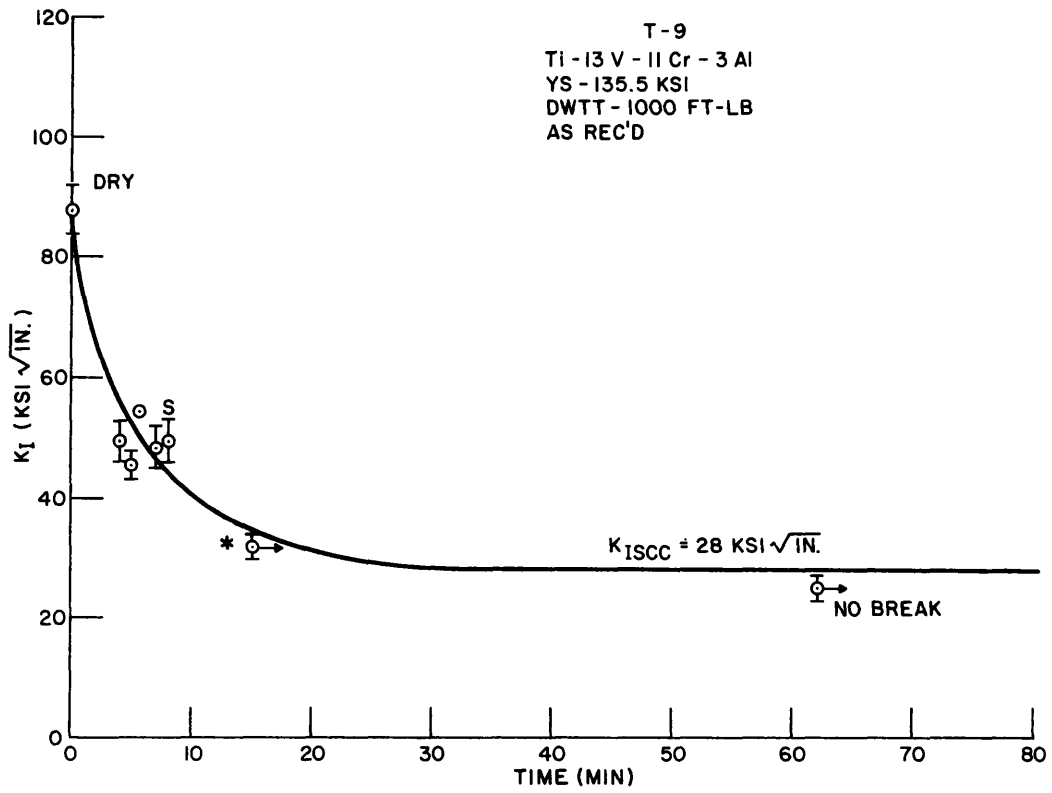


Fig. 7 - Environmental cracking characteristics of T-9 alloy in 3.5% salt water solution

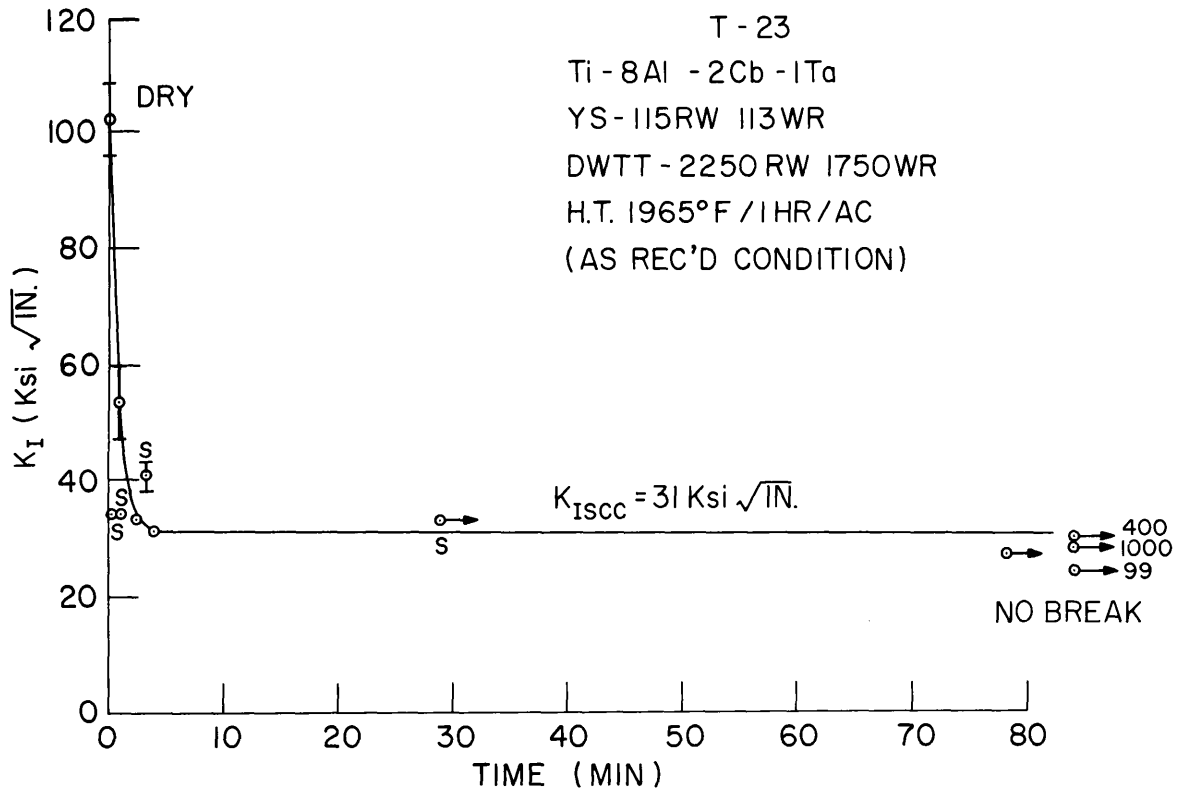


Fig. 8 - Environmental cracking characteristics of T-23 alloy in 3.5% salt water solution

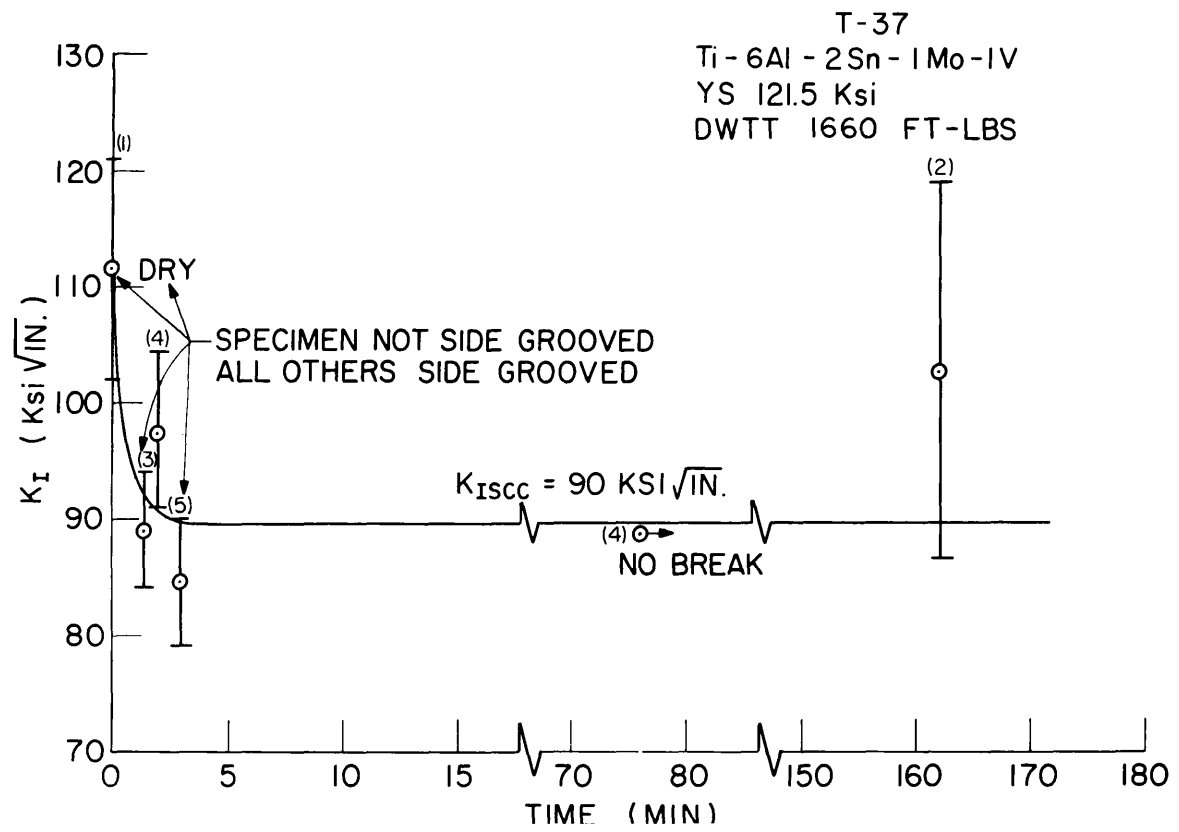


Fig. 9 - Environmental cracking characteristics of T-37 alloy in 3.5% salt water solution

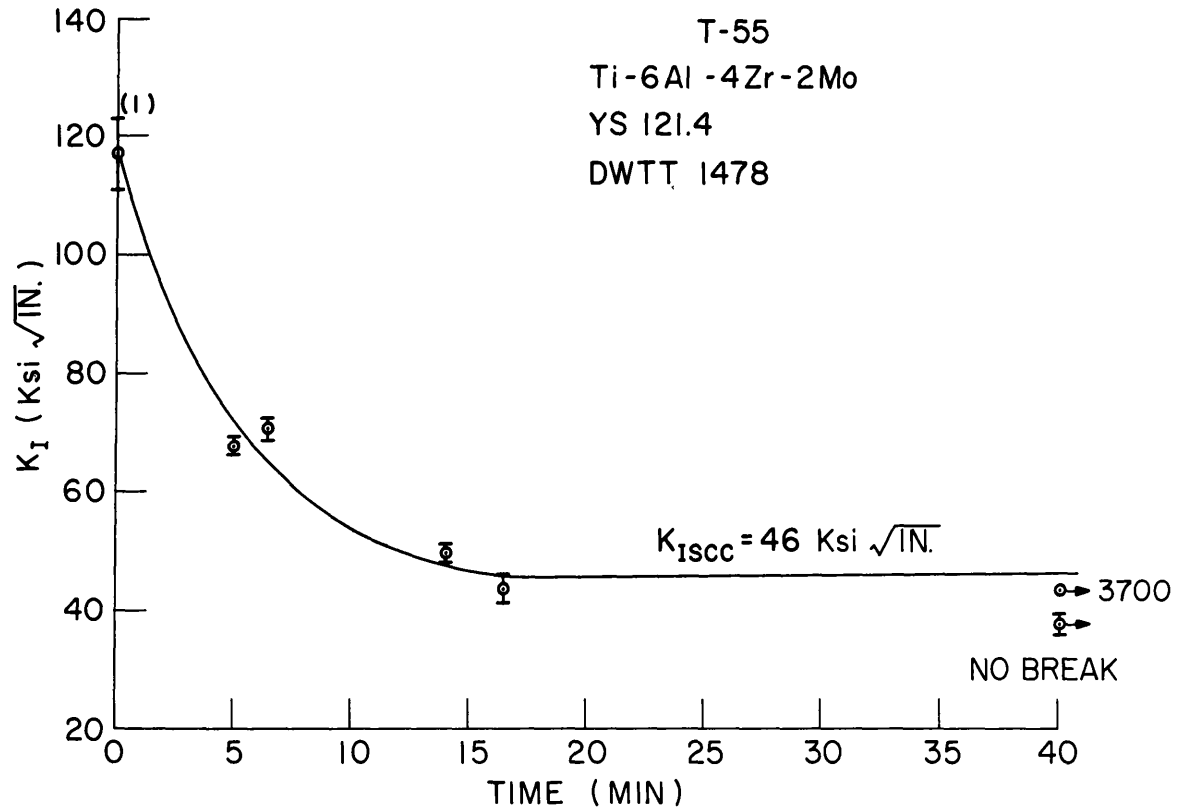


Fig. 10 - Environmental cracking characteristics of T-55 alloy in 3.5% salt water solution

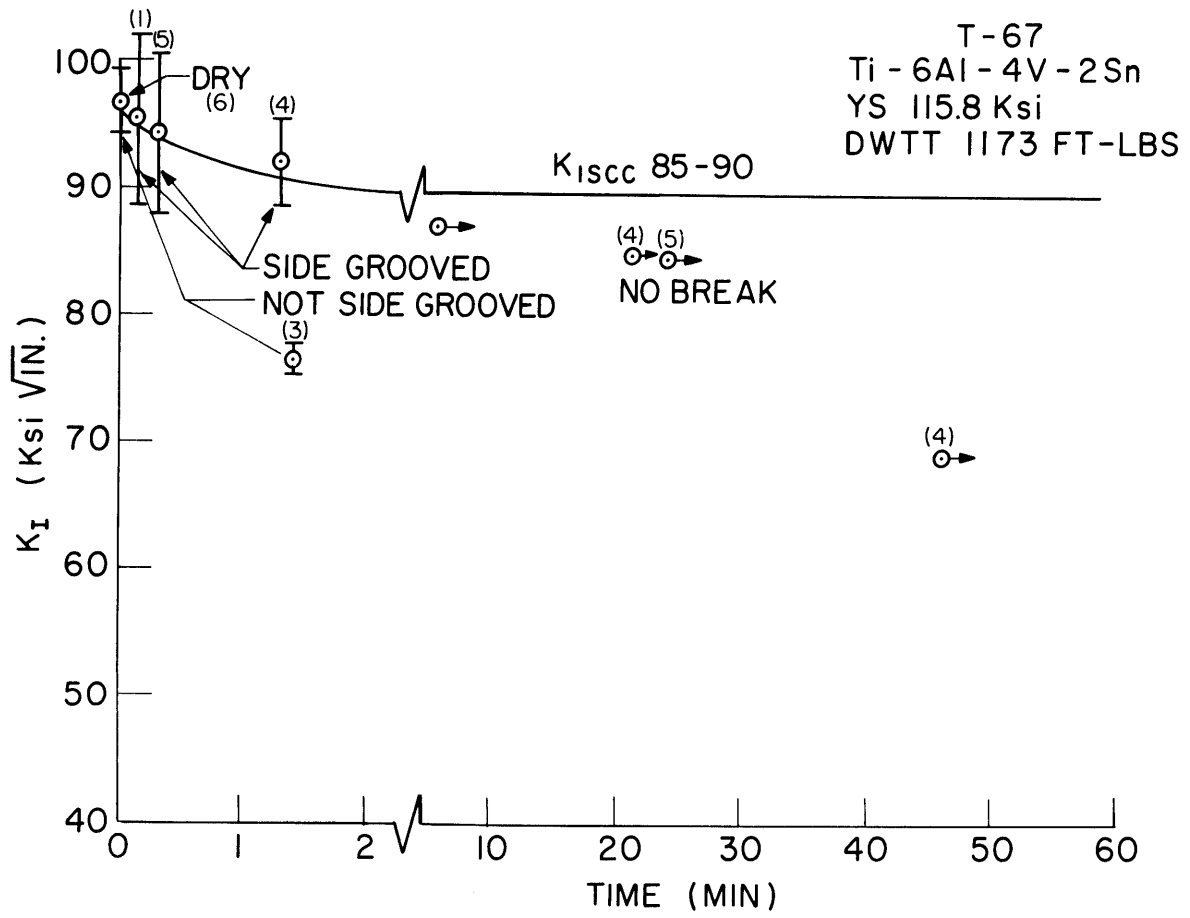


Fig. 11 - Environmental cracking characteristics of T-67 alloy in 3.5% salt water solution

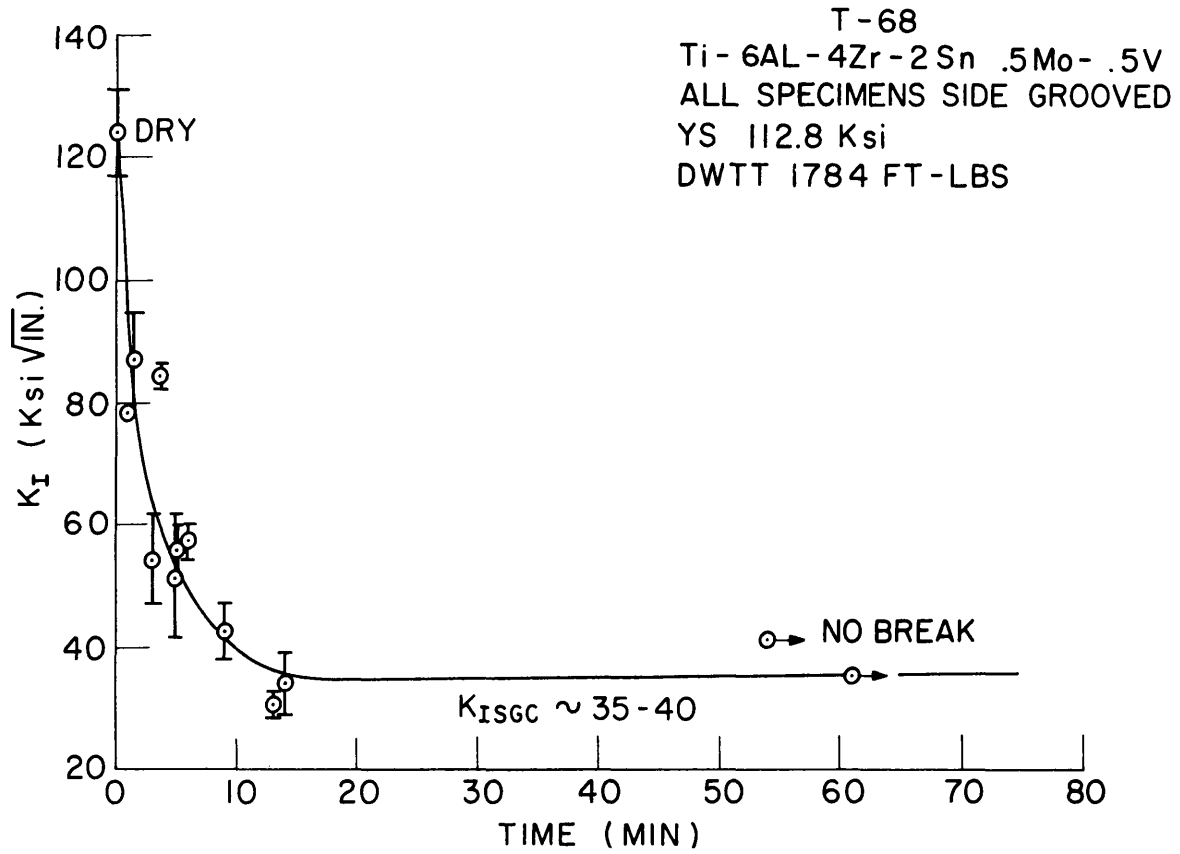


Fig. 12 - Environmental cracking characteristics of T-68 alloy in 3.5% salt water solution

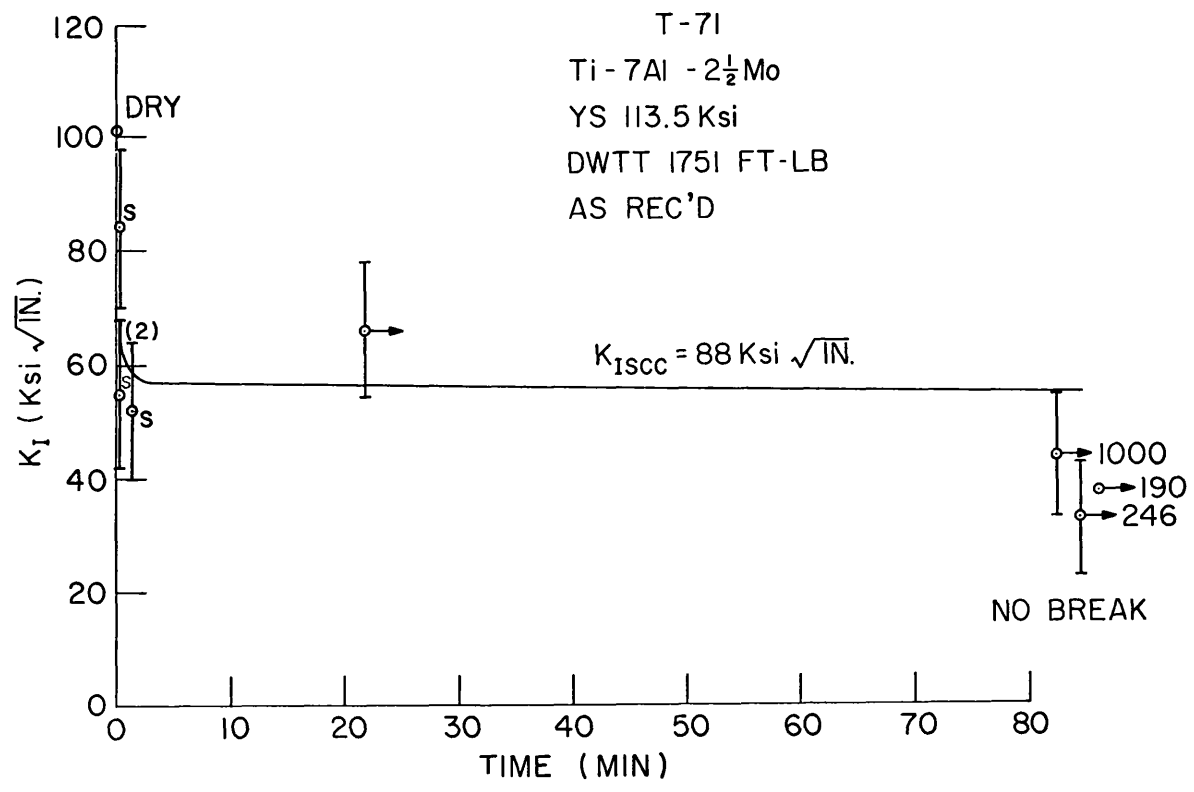


Fig. 13 - Environmental cracking characteristics of T-71 alloy in 3.5% salt water solution

## HIGH STRENGTH STEELS

(P.P. Puzak and K.B. Lloyd)

The present broad scope investigation of steels in thick sections has continued to develop new information relative to the fracture toughness characterization of the high strength steels and welds. The principle fracture toughness test employed in these studies has been the drop-weight tear test (DWTT) as correlated with results obtained in the large structural prototype element explosion tear test (ETT). These tests and the correlation procedure have previously been described in detail (6). From these studies, a simplified Fracture Toughness Index Diagram (FTID) which indexes the DWTT fracture toughness characteristics of the steel in terms of ETT performance of the material has been developed. Interpretation of the FTID data is aimed at providing more definitive information relative to the fracture-safe design utilization of the high strength steels in thick sections of complex welded structures.

Work completed during this reporting period has primarily been concerned with special melt practice HY-80 steels that were procured to develop more detailed data on the effects of process variables for the various types of steels. The fracture toughness characteristics of conventional melt and special melt SAE 4340 and 4140 steels were also evaluated by drop-weight tear tests.

### DROP-WEIGHT TEAR TESTS OF SPECIAL MELT PRACTICE HY-80 STEELS

One of the major contributions of these studies for steels has been the development of a better understanding of the significant role that mill processing variables perform in developing toughness properties of the alloy steels. It is now clear that the relative fracture toughness quality for a particular steel composition cannot be fully characterized unless the test directions with respect to rolling direction and the processing history are simultaneously defined (7). It is not possible to "index" the quality of a particular steel with respect to other steels without the above information. This is because the fracture toughness of steels at a given strength level varies not only

with compositions and process history, but also with the relative amounts of certain critical residual elements that must be maintained at very low levels to obtain the optimum strength-toughness properties in the steels.

NRL investigations of the brittle (cleavage) fracture problem encountered with conventional structural steels were particularly concerned with the evaluation of the significance of laboratory test specimen data as related to service performance correlations (8-12). Generally, these studies showed that the transition-temperature range, as indicated by the Charpy V ( $C_v$ ) curve, was always found to characterize the temperatures at which brittle fractures could initiate or propagate in the structural grade steels. Brittle fractures could not develop in the structural steels at temperatures corresponding to the maximum-energy, upper-shelf positions on the  $C_v$  curve. Ruptures could be developed under high overload conditions in the structural steels at the  $C_v$  shelf temperatures, but generally these ruptures were expected to be stable, 100% shear fractures which would propagate slowly. The possibility of developing unstable, "low-energy tear" shear ruptures in some plate metals or similar catastrophic ruptures via unique fracture paths in a weldment was recognized and predicted for some high strength steels (11). This possibility was subsequently corroborated by analysis of catastrophic service failures of heavy steel forgings at elevated temperatures in structures of normal design involving high stresses with materials that displayed unusually low (20 to 25 ft-lb) $C_v$  shelf values (13). Thus, it has been documented that the height of the maximum shelf-energy, shear-toughness level also must be considered to provide fracture safety even for structures of normal design.

From the beginning of the high strength steel studies, careful attention has been directed to the identification and separation of the processing and composition variables which affect fracture toughness. The transition-range problem of decreased toughness with decreased temperature was eliminated from consideration as the tests employed for evaluation of fracture toughness were limited to temperatures involving full-shear fractures in the steels being studied. NRL investigations showed the deleterious effects of increased carbon content on

maximum-shear-energy absorption values in SAE 4300 type steels containing five levels of carbon content ranging from 0.22 to 0.56% (14). Other studies (15) completed in the Bureau of Ships - United States Steel Corporation contract investigations showed a decrease in the maximum-shear-energy absorption of the HY-130/150 (5Ni-Cr-Mo-V) steel of approximately 3 ft-lb  $C_v$  per 0.01% increase in carbon content over the range of 0.05 to 0.25% carbon. These data coupled with the relatively high  $C_v$  shelf values generally noted for Armco ingot iron (nominally 0.01% C) and the recent experience developed with the essentially "carbon-free" maraging steels indicate that significant increases in maximum-energy-shelf values can be expected for additional decreases in carbon content below 0.05%. Because the strength level of quenched and tempered (Q&T) steels depends upon carbon content, the recommended level to maintain high toughness in Q&T steels appears to be the minimum carbon content necessary to develop the desired yield strength.

The effects of sulphur content on maximum-energy-shelf values were studied by other investigators with the SAE 4330 type steels which ranged from 0.005 to 0.179% sulphur (16). It was shown that with increasing sulphur content, the maximum  $C_v$  energy shelf values decrease; however, the transition-range temperatures of the  $C_v$  curve are not markedly affected by the sulphur content. Other studies on the effects of sulphur content on the maximum-energy-shelf values of the 5Ni-Cr-Mo-V steel, when it was systematically varied from 0.003 to 0.027% sulphur, showed an improved toughness at an increasing rate as sulphur is lowered within the range investigated (17). The improvement developed at the low end of the sulphur range investigated was shown to be about 10 ft-lb for each 0.001% decrease in sulphur.

Because the transition temperature problem had been eliminated from consideration in these studies, it was apparent that the attainment of optimum strength-toughness relationships in steels required consideration of the factors controlling the amount of the critical elements which affected the maximum-energy-shelf level toughness of steels. Since control of the carbon and sulphur contents in steel resides in the melt-shop, melting practice was the first processing variable

considered in these studies to separate the steels into characteristic groups that might be expected to exhibit different levels of fracture toughness. To date, this separation has involved "conventional melt" practice steels (defined as open-hearth or electric furnace, single oxidizing slag process with final deoxidation and alloy additions in the ladle) and "special melt" practice steels (all other practices including multiple-slag air-melt, and the various vacuum processes -- degassing, melting, or remelting). The general category of "special melt" practices was established because it was not possible to estimate the degree to which the various special processes would affect the level of carbon or sulphur contents, the concomitant residual gas content (oxygen, nitrogen, and hydrogen), or the cleanliness (inclusions), which might also affect the overall toughness performance of the steel.

Because of availability and Navy interest, most of the early studies of high strength steels were conducted with conventionally produced HY-80 steels. These were also studied in reheat-treated conditions to develop a spectrum of strength levels. A special heat of HY-80 steel produced with various degrees of prescribed cross-rolling ratios was procured to develop the data reported for anisotropy effects as a function of rolling variables (6, 18). Additional steel plates of the high chemistry (thick section) HY-80 composition, similar to that used for the cross-rolling variable studies, have been procured to develop more detailed data on the effects of special melt practices on fracture toughness properties of the HY-80 steel. The 1-in.-thick steel plates were rolled from material produced in a 20-ton, multiple-slag (one oxidizing plus one reducing) electric furnace, air-melt heat that was split to provide electrode ingots for vacuum remelting and the rolling of additional plates representing consumable-electrode-vacuum melt (CEVM) practice. The various plates were furnished with different degrees of cross-rolling ranging from straightaway-rolled to 1 to 1 cross-rolled, and in the mill quenched and tempered (Q&T) condition involving tempering temperatures of 950°, 1000°, 1060°, and 1125°F. Sections of the various plates were additionally retempered at 1160° and 1200°F by NRL. A comparison of the average chemical compositions of the steel heats used in these studies is given in Table 7.

TABLE 7  
AVERAGE CHEMICAL COMPOSITIONS OF HY-80 STEELS

Practice	C %	Mn %	Si %	P %	S %	Ni %	Cr %	Mo %	Studies
1-slag elec- tric furnace	0.20	0.35	0.32	0.008	0.013	3.20	1.62	0.72	Cross-rolling
2-slag elec- tric furnace	0.20	0.43	0.21	0.006	0.007	3.28	1.66	0.75	Special-melt
CEVM	0.19	0.32	0.20	0.007	0.004	3.20	1.62	0.72	Special-melt

Tension,  $C_v$ , and DWT tests on these special melt practice steels were conducted with the specimens in the "weak" (WR) fracture direction (3). The data are given in Table 8, and a graphical summary of the DWTT-YS relationships for these steels is presented in Fig. 14. The DWTT were conducted with the 5000 ft-lb capacity pendulum-type impact machine described in a previous report (19). For three of the steels which exceeded the 5000 ft-lb capacity of the machine, the tip of the vertical arrow in Fig. 14 indicates the estimated DWTT energy value as determined by the correlation data developed to date for DWTT-C results for steels (to be described). Relatively low DWTT toughness values were obtained for the tests at 30°F for all steels involving heat-treatment conditions with tempering at 950°F, because the transition temperature range had been raised to higher temperatures by this heat treatment, i.e., 30°F fracture surfaces involved mixed fracture modes. The data for the steels tempered at 950°F are not included in the summary of data given for steels in the FTID charts (to be described) which relate to optimum, maximum-energy-shelf level toughness data.

The bottom curve illustrated in Fig. 14 for conventional melt (one slag, electric furnace) straightaway-rolled HY-80 steels was established in previous studies of anisotropy effects (18). The sharp drop in toughness illustrated by the dashed portions of the various curves for the special melt HY-80 steels reflects the embrittlement (at 30°F) involving the transition-temperature range problem that is developed by tempering treatments of these steels at 950°F, as described above. Comparison of the various curves in Fig. 14 for straightaway-rolled materials provides an approximate evaluation of the improvements in toughness over that of conventional melt practice that may be developed by the use of the "special melt" practices. However, the double slag, air-melt practice plate steels differed in carbon and sulphur contents from those of the CEVM practice plate steels from this heat. The pronounced effect established (17) of a marked increase in the maximum-energy-shelf level toughness of the 5Ni-Cr-Mo-V steel by decreasing the sulphur content below approximately 0.010% was discussed earlier. Because of their different chemical compositions, a direct quantitative evaluation of the merits of the double-slag, air-melt and CEVM

TABLE 9

TEST DATA\* FOR SPECIAL MELT AND ROLL PRACTICE AND HEAT TREATED HY-80 STEELS

Specimen No.	Melt Practice	Roll	Temper- ature (°F)	0.505-in. Dia. Tension Test Data			Charpy V at 30°F (ft-lb)	Drop-Weight Tear at 30°F (ft-lb)
				0.2% YS (ksi)	UTS (ksi)	EL. in 2" (%)		
J43	2 slag E.F.	Str.	950	161.0	182.9	12.0	44.6	592
J44	2 slag E.F.	Str.	1000	159.7	182.7	14.0	45.4	870
J45	2 slag E.F.	Str.	1060	152.6	170.1	15.0	48.4	811
J46	2 slag E.F.	Str.	1125	134.5	149.6	16.8	53.7	1784
J43	2 slag E.F.	Str.	1160	113.2	130.1	19.0	58.9	3281
J43	2 slag E.F.	Str.	1200	104.3	121.0	20.5	57.8	3333
J51	CEVM	Str.	950	160.7	183.1	14.0	48.2	1723
J52	CEVM	Str.	1000	160.0	182.4	16.0	52.0	2236
J53	CEVM	Str.	1060	156.6	177.0	16.0	53.6	2902
J54	CEVM	Str.	1125	128.6	145.4	18.5	62.6	3747
J51	CEVM	Str.	1160	112.8	129.4	20.0	61.5	4651
J51	CEVM	Str.	1200	105.7	123.2	21.0	63.1	>5000
J39	2 slag E.F.	2-1	950	161.6	185.0	14.5	47.7	1173
J40	2 slag E.F.	2-1	1000	157.9	179.3	15.0	50.2	1570
J41	2 slag E.F.	2-1	1060	152.4	170.1	15.5	54.5	1631
J42	2 slag E.F.	2-1	1125	125.0	141.1	19.3	61.2	--
J39	2 slag E.F.	2-1	1160	110.0	127.8	20.0	61.1	3820
J40	2 slag E.F.	2-1	1200	107.5	124.2	21.0	65.9	3910
J47	CEVM	1-1	950	160.2	182.2	16.3	59.8	2266
J48	CEVM	1-1	1000	157.5	177.6	17.0	64.2	--
J49	CEVM	1-1	1060	155.6	175.2	18.5	64.3	3486
J50	CEVM	1-1	1125	143.7	159.4	18.0	61.8	--
J47	CEVM	1-1	1160	116.7	133.0	20.8	71.8	127
J48	CEVM	1-1	1200	107.5	124.6	23.0	72.4	>5000

\* NOTE: All specimens were tested in the "weak" (WR orientation) fracture direction.

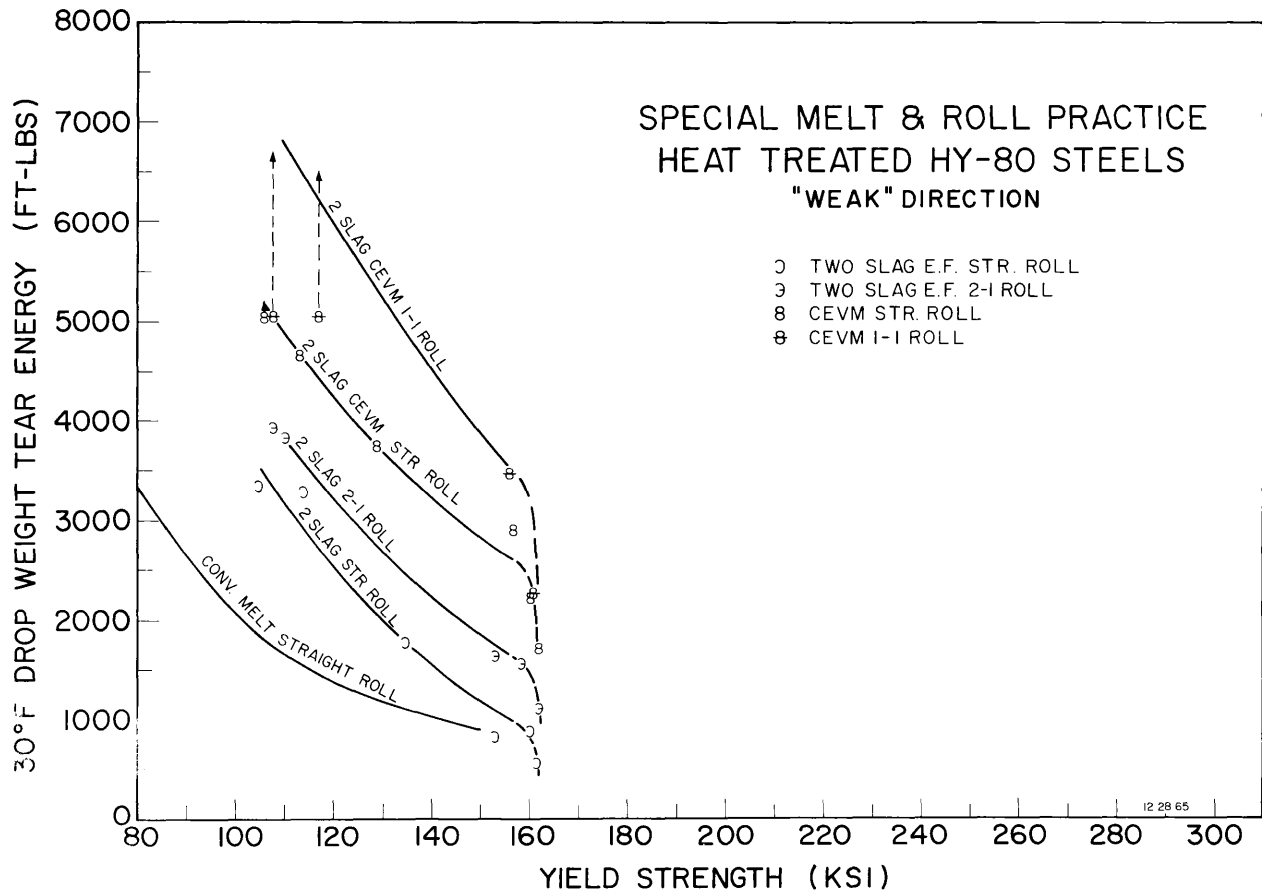


Fig. 14 - Drop-weight tear test (DWTT) energy absorption as a function of yield strength for 1-in. plates of specially melted and heat treated HY-80 type steels

practices for the illustrated HY-80 steels cannot be deduced from the data given in Fig. 14.

A graphical summary of the  $C_v$ -YS relationships for these special melt HY-80 steels is presented in Fig. 15. The lowest curve, shown in this chart for comparison purposes, is based upon previously developed data for conventional melt practice HY-80 steels. The other curves in Fig. 15 have been drawn to separate the data into characteristic groups relating to the special melting and rolling practice variables as described for the DWTT data given in Fig. 14. Generally, the observations, comments, and deductions given for the data in Fig. 14 are found to be closely similar to those developed by analysis of the  $C_v$  data given in Fig. 15.

In addition to the special melt HY-80 steels described herein, a considerable number of previously tested maraging and Q&T steels have involved CEVM practices. A review and analysis of the DWTT-YS data for all CEVM steels tested to date was made in order to establish the apparent limiting position of an OMTL for the CEVM steels. Generally, these steels were all found to be highly cross-rolled (essentially 1 to 1), and in the case of the 12% Ni and 18% Ni maraging steels, several different producers were involved. A summary of the DWTT-YS data for CEVM steels tested to date is presented in Fig. 16 in relation to the basic curves and correlation index features of the FTID chart. Several of the previously tested CEVM steels which are plotted above the CEVM curve illustrated in Fig. 16 represent materials which were tested early in this program when the "high" DWTT values were based upon "bracketing" the DWTT values within an increment of 250 (sometimes 500) ft-lb. In the 110 to 160-ksi YS range, the illustrated OMTL curve for all CEVM, 1 to 1 roll-practice steels is noted to agree quite closely with the solid portion of the curve given in Fig. 14 for the CEVM, 1 to 1 rolled HY-80 steels.

#### DROP-WEIGHT TEAR TESTS OF "OLD" ALLOY HIGH STRENGTH STEELS

The pronounced effects of processing variables on fracture toughness properties for some "old" and "new" high strength steel alloys in the 100+ ksi YS range have been described in an earlier quarterly progress

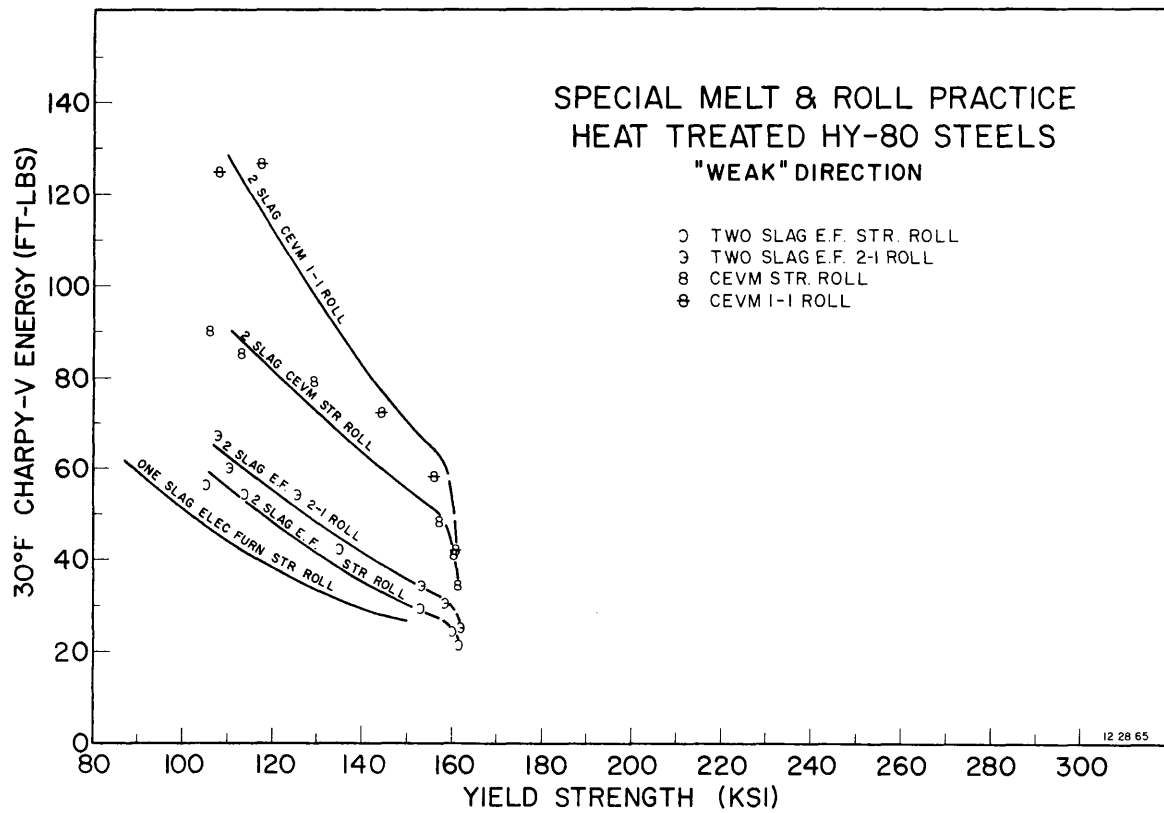


Fig. 15 - Charpy V ( $C_v$ ) energy absorption-yield strength relationship for specially melted and heat treated HY-80 type steels, as in Fig. 14

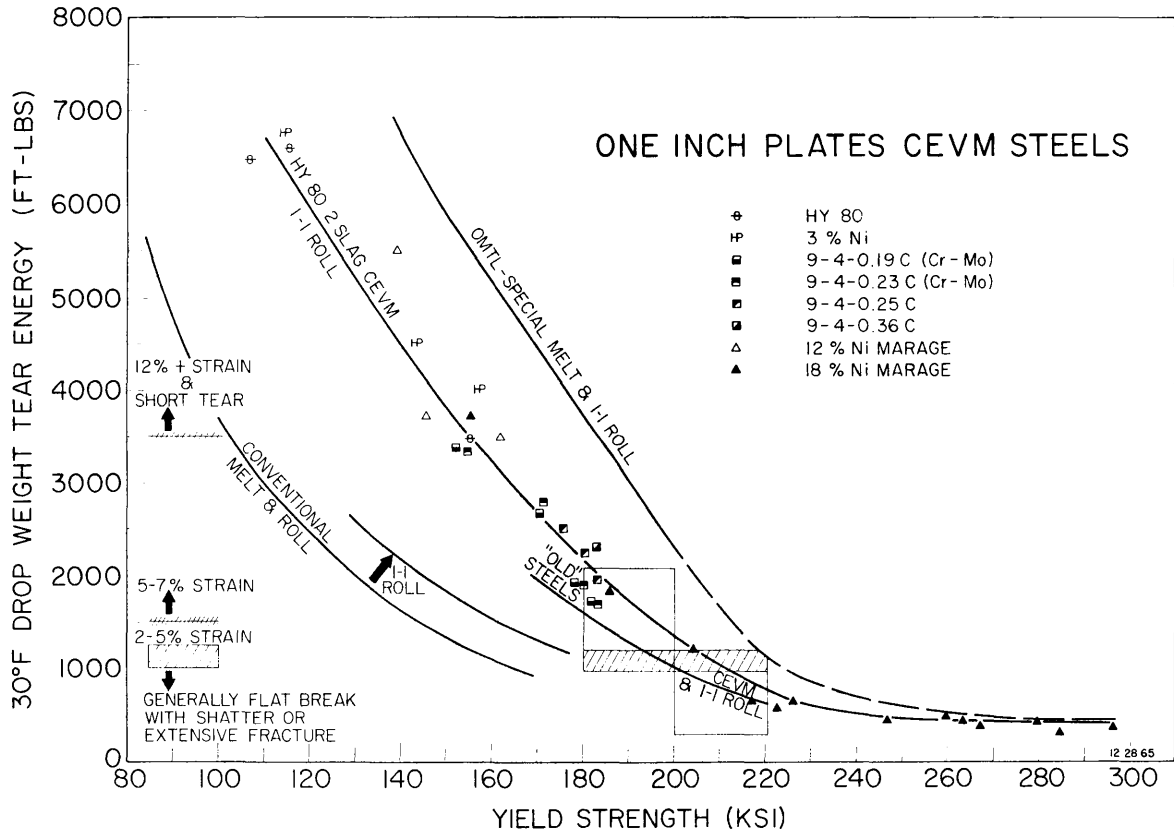


Fig. 16 - Summary of DWTT-yield strength relationships of all consumable-electrode-vacuum-melt (CEVM) steels tested. The "2-slag CEVM 1-1 roll" OMTL derived is shown in addition to the OMTL of the FTID.

report (7). The "old" steel types that have already been evaluated are generally characterized as the HY-80 compositions, heat-treated to a range of high strength levels, and the various 4330-4340, H-11, D-6, etc., steels. The "new" steel types are characterized by the "family" of 12% Ni and 18% Ni maraging, the 9Ni-4Co, and the 5% Ni-Cr-Mo-V varieties. During the past reporting period, additional "old" alloy steels of the SAE 4340 and 4140 types were evaluated to develop more detailed data on the effects of processing variables for the various types of steels. These steels represent conventionally-processed material, an open-hearth furnace heat of 4140 steel (No. H-56), an electric furnace heat of 4340 steel (No. H-59), and a special melt practice (CEVM) heat of 4340 steel (No. G-84). Both the conventional and the special melt practice 4340 steels were highly cross-rolled; however, the 4140 steel was spread-rolled to a 9 to 1 rolling ratio. The steels were received in the hot-rolled condition and evaluated at a spectrum of strength levels developed by Q&T heat treatments conducted by NRL. All of the steels contained vanadium which was used to deoxidize the steels instead of aluminum. The chemical compositions of these steels are given in Table 9.

Tension, C<sub>10</sub>, and DWT tests were conducted on these steels with specimens in the "weak" (WR) fracture direction. The data are given in Tables 10-12, and a graphical summary of the DWTT and YS values for these steels is presented in Fig. 17 in relation to the basic curves and correlation index features of the FTID chart. As expected for the conventional melt (open-hearth) practice, poorly cross-rolled 4140 steel, very low DWTT fracture toughness values are developed in all heat-treatment conditions studied. The slightly better DWTT values noted for the conventional melt (electric furnace) practice 4340 steel are considered to result from the high degree of cross-rolling applied to this steel. The moderately better toughness values generally noted for the cross-rolled CEVM 4340 steel, over that of the cross-rolled electric furnace steel, are considered to reflect the improvement resulting from the melting practice (double slag plus vacuum-consumable remelt) which was used to develop lower levels of residual elements (sulphur and phosphorus).

TABLE 9  
CHEMICAL COMPOSITIONS OF "OLD" ALLOY HIGH STRENGTH STEELS

NRL NO.	Type	C %	Mn %	Si %	P %	S %	Ni %	Cr %	Mo %	V %
H-56	Open-hearth furnace 4140	0.43	0.98	0.19	0.013	0.030	0.01	1.04	0.21	0.08
H-59	Electric furnace 4340	0.38	0.68	0.21	0.008	0.012	1.69	0.83	0.28	0.06
G-84	CEVM 4340	0.42	0.77	0.23	0.005	0.006	1.72	0.92	0.26	0.07

TABLE 10

TEST DATA\* FOR OPEN-HEARTH PRACTICE 4140 STEEL (NO. H-56)

(Austenitized 1550°F 1 hr, oil quenched; tempered 2+2 hr)

Tempering Temperature (°F)	0.505-in. Dia. Tension Test Data				Charpy V at +30°F (ft-lb)	Drop-Weight Tear at +30°F (ft-lb)
	0.2% YS (ksi)	UTS (ksi)	EL. in 2" (%)	R.A. (%)		
400	226.7	290.1	8.5	25.6	6	455
500	231.1	270.9	8.0	27.5	4	339
600	225.5	259.1	8.0	27.4	5	339
700	212.0	239.2	8.6	27.6	6	339
800	198.3	219.3	9.0	31.0	9	367
900	176.0	193.5	10.3	32.5	13	--
1000	165.2	178.3	12.0	39.6	15	573
1100	153.8	167.3	13.0	40.2	21	991

\*NOTE - All specimens were tested in the "weak" (WR orientation) fracture direction.

TABLE 11  
TEST DATA\* FOR ELECTRIC FURNACE PRACTICE 4340 STEEL (NO. H-59)

(Austenitized 1550°F 1 hr, oil-quenched; tempered 2+2 hr)

Tempering Temperature (°F)	0.505-in. Dia. Tension Test Data					Charpy V at +30°F (ft-lb)	Drop-Weight Tear at +30°F (ft-lb)
	0.2% YS (ksi)	UTS (ksi)	EL. in 2" (%)	R.A. (%)			
400	211.2	279.9	11.0	33.1	10	425	
500	213.8	252.3	8.5	34.4	8	425	
600	207.0	240.1	9.0	38.0	7	573	
700	198.7	223.1	9.0	37.2	8	455	
800	184.7	200.9	10.0	38.6	13	681	
900	173.4	187.8	12.0	40.6	17	750	
1000	163.7	177.1	14.0	46.5	21	1052	
1100	156.0	167.7	15.0	48.1	24	1418	
1200	122.2	135.0	18.5	55.7	37	2780	

\*NOTE: All specimens tested in the "weak" (WR orientation) fracture direction.

TABLE 12

TEST DATA\* FOR SPECIAL MELT CEVM PRACTICE 4340 STEEL (NO. G-84)

(Austenitized 1550° F 1 hr, oil-quenched; tempered 2+2 hr)

Tempering Temperature (° F)	0.505-in. Dia. Tension Test Data				Charpy V at +30° F (ft-lb)	Drop-Weight Tear at +30° F (ft-lb)
	0.2% YS (ksi)	UTS (ksi)	EL. in 2w (%)	R.A. (%)		
400	223.2	270.1	11.5	43.3	13	573
500	220.1	261.6	10.5	42.5	13	612
600	213.1	246.1	11.8	43.4	14	750
700	206.3	230.7	11.0	43.6	14	811
800	192.6	209.7	12.0	45.3	17	514
900	176.0	189.6	14.0	48.4	26	1356

\*NOTE: All specimens tested in the "weak" (WR orientation) fracture direction.

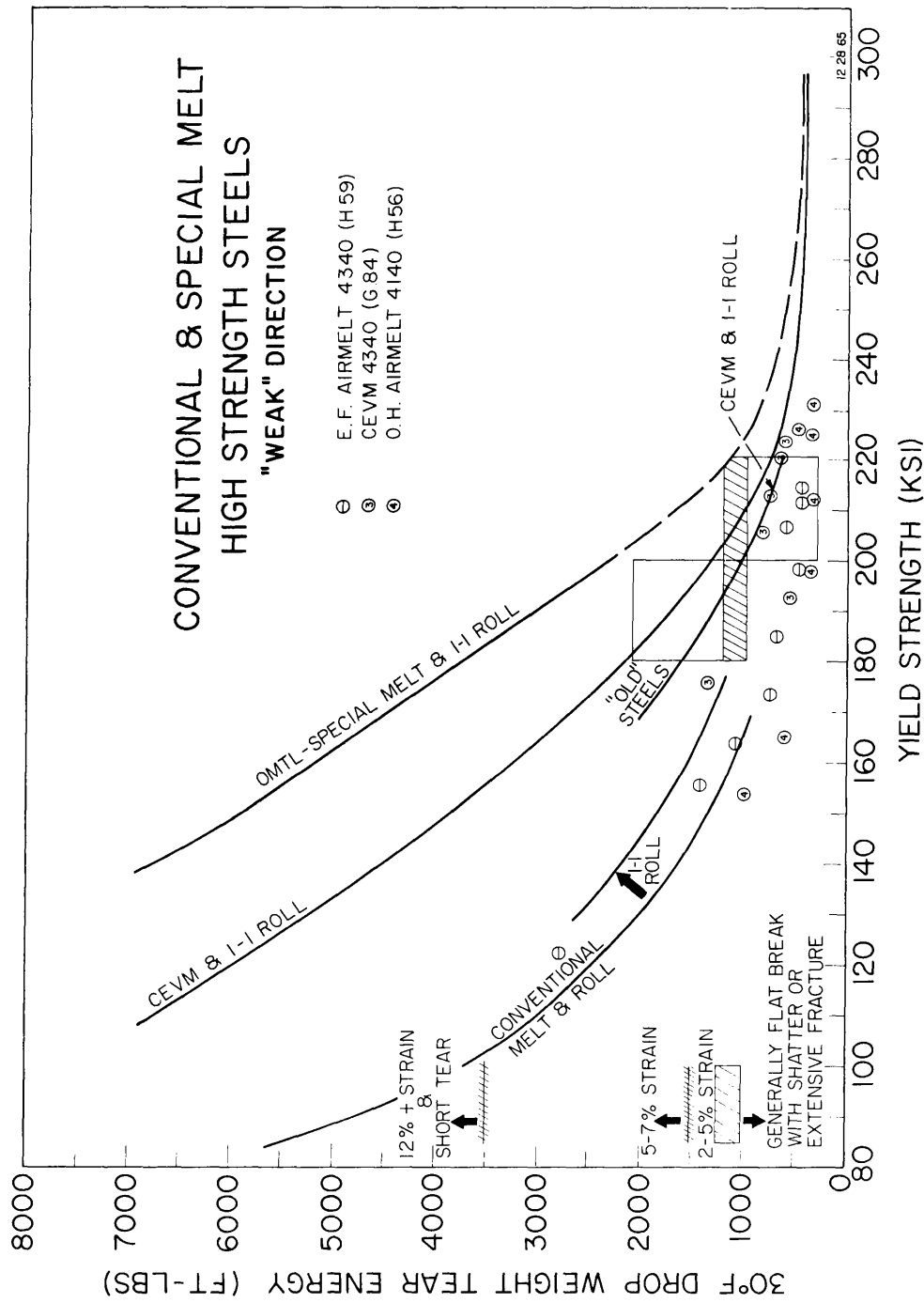


Fig. 17 - The DWTT energy absorption as a function of yield strength for three high strength steel series. The OMTL of the FTID is included for comparison

## FRACTURE TOUGHNESS INDEX DIAGRAM FOR STEELS

The FTID chart relating specifically to all 1-in.-thick steel plates evaluated to date is presented in Fig. 18. Each of the curves in this figure is designated an "optimum materials trend line" (OMTL) which separates the data into characteristic groups relating to the mill processing variables (melting practice and/or cross-rolling) of the steels. The OMTL illustrated for 1 to 1 cross-rolled consumable-electrode-vacuum melt (CEVM) practice represents a new addition to previously published FTID charts for the steels. All maraging steel data relating to the limiting ceiling OMTL curve for special melt practice steels have involved vacuum-induction-melt practices as contrasted to the electric furnace air-melt heats which were poured into electrode configurations suitable for consumable-vacuum-remelt practices that have characterized the CEVM practice steels. Evaluation of additional vacuum-induction-melt practice steels capable of developing yield strength levels in excess of 200-ksi are required for better definition of the dashed portion of the presently depicted limiting ceiling OMTL curve.

It should be emphasized that the spectrum of DWTT data given in Fig. 18 relates to tests of the steels that exhibited "upper-shelf" (i.e., fully-ductile mode fractures) properties at 30°F in the "weak" (WR) fracture direction providing such a direction existed. The effects of testing temperature (within the transition range) and cross-rolling have previously been described in detail (14, 19). The horizontal cross-hatched lines and shaded region indicated on the left side of the FTID depict the significance of the DWTT energy values presently established by indexing them to the ETT performance of the steels. Materials having DWTT energy values below the 1000-1250 ft-lb range shown by the shaded region have been characterized by the "flat breaks" and shattering in the ETT and thus would be expected to propagate fractures at high levels of elastic stress. Above the 1000-1250 ft-lb DWTT energy range, the relative level of DWTT energy is proportional to the expected level of plastic strain overload required to propagate fracture in the ETT as shown by the strain level values indicated above, between, or below the horizontal cross-hatched lines given on the left side of the FTID.

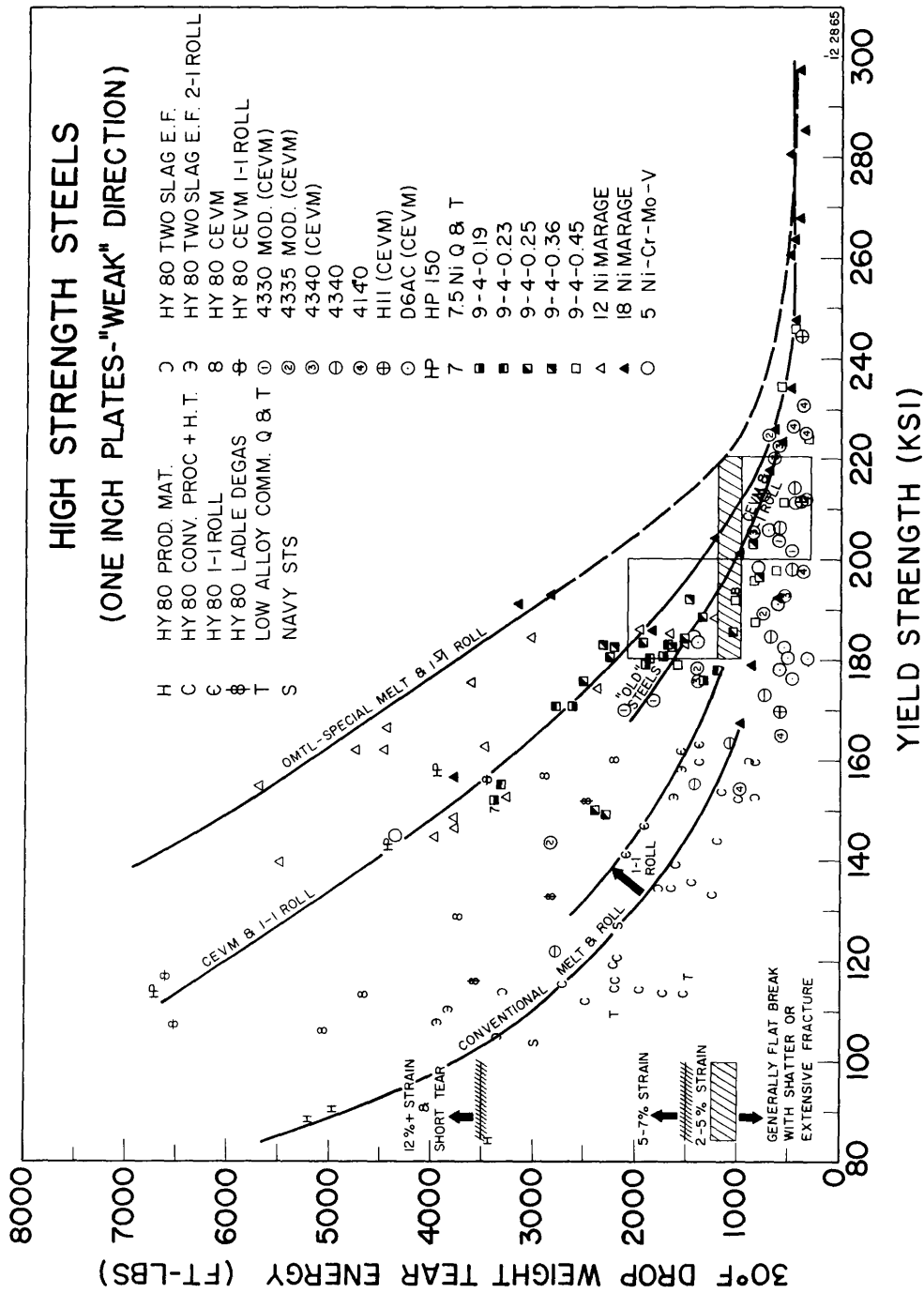


Fig. 18 - Fracture Toughness Index Diagram (FTID) derived from all high strength steels tested. The ETT correlation and the OMTL for various mill practices are included.

The various OMTL curves given in Fig. 18 indicate a general decrease in fracture toughness with increasing strength level for all characteristic groups of steel. Reheat-treatment studies of any given alloy steel have consistently shown a decrease in toughness concomitant with increased strength. This generally accepted phenomenon does not conflict with the more recently developed realization that improvements in fracture toughness can be obtained in a steel alloy at a given strength level by the use of special processing (melting and/or cross-rolling) practices. These studies have shown that the development of optimum strength-toughness relationships in steels requires the use of maximum (1 to 1) cross-rolling to eliminate directionality effects and the use of special melting practices that result in significantly lowering the levels of critical elements (particularly carbon and sulphur) that affect fracture toughness in steel.

The DWTT-ETT correlation index level of change from plastic to elastic loading requirements for fracture propagation (shaded region in Fig. 18) is the primary evaluation criterion for suitability of materials in complex welded structures at this stage of development of the FTID charts. Consideration of new alloys, or special processing, would be required to improve the fracture toughness of a characteristic group of steels at strengths higher than the maximum yield strength level at which the various OMTL curves cross-over this elastic-to-plastic performance transition band. For example, current HY-80 (80-ksi minimum YS) "conventional" production material does not require special processing considerations because even poorly cross-rolled HY-80 is highly resistant to fracture propagation. The "weak" direction for fracture in conventional HY-80 that is straightaway-rolled becomes potentially susceptible to fracture propagation at elastic stress levels for heat-treated conditions of approximately 120-130 ksi YS (OMTL for straightaway-rolled conventional melt practice steels not shown in Fig. 18). In heat-treatment conditions ranging from 120-130 ksi to approximately 150-160 ksi YS, special cross-rolling or melting practices with the conventional HY-80 steel would be required to develop "weak" direction fracture toughness properties equivalent to that of conventional production HY-80 material at lower yield strength levels. The tempering temperatures required to develop yield strength levels exceeding 150-160 ksi YS in HY-80 steels result in

embrittlement (at 30°F) due to the transition temperature range increase, and thus, new alloy compositions and special processing techniques are required to develop fracture tough steels exceeding approximately 160-170 ksi YS. Similarly, the cross-over of the plastic to elastic performance band for the "best" presently defined alloy steels indicates that all materials above about 200-210 ksi YS for CEVM practice and about 220-230 ksi YS for special melt vacuum-induction practice should be expected to propagate fractures through elastic stress regions.

The standard industry "small specimen" test for evaluating fracture toughness has been the  $C_v$  test. The correlation of the DWTT and the  $C_v$  tests, Fig. 19, have been surprisingly good, providing only the steels involving 100% shear fractures in the  $C_v$  test are considered -- i.e., the illustrated correlation relates to tests at temperatures of maximum  $C_v$  upper-shelf energies. Previous investigations have emphasized the fact that the  $C_v$  test can be highly misleading for cases involving mixed<sup>v</sup> fractures that feature even small amounts of cleavage (values in the transition range). When this condition exists, apparently "high"  $C_v$  energy numbers (60-80 ft-lb) are meaningless when compared to fracture toughness values signified by moderately low (40-50 ft-lb) upper-shelf level temperature (100% shear)  $C_v$  values. Within the described limitations, the DWTT correlations and ETT index procedures have been used to evolve the FTID chart for  $C_v$  and yield strength data given in Fig. 20 for all 1-in.-thick steels tested to date. Generally, the OMTL curves in this figure separate these data into characteristic groups relating to the processing variables of the steels similar to those shown in Fig. 18. These data provide for useful application of the  $C_v$  test for fracture-safe design analysis for high strength steels in terms of the simple FTID reference.

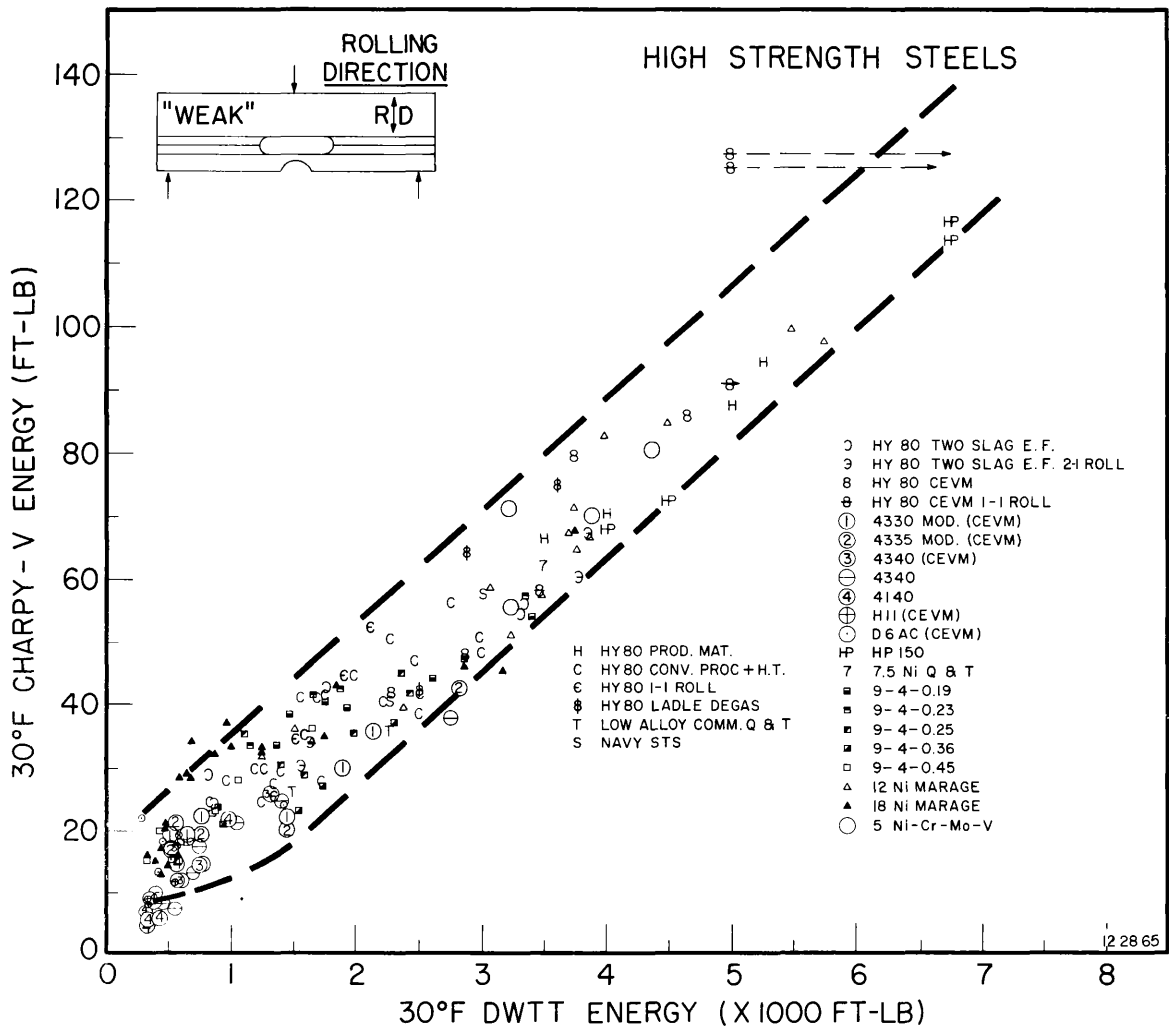


Fig. 19 - Correlation of DWTT and  $C_v$  data for all high strength steels tested. The data is for "shelf energies," i.e., at test temperatures where the fractures are fully ductile.

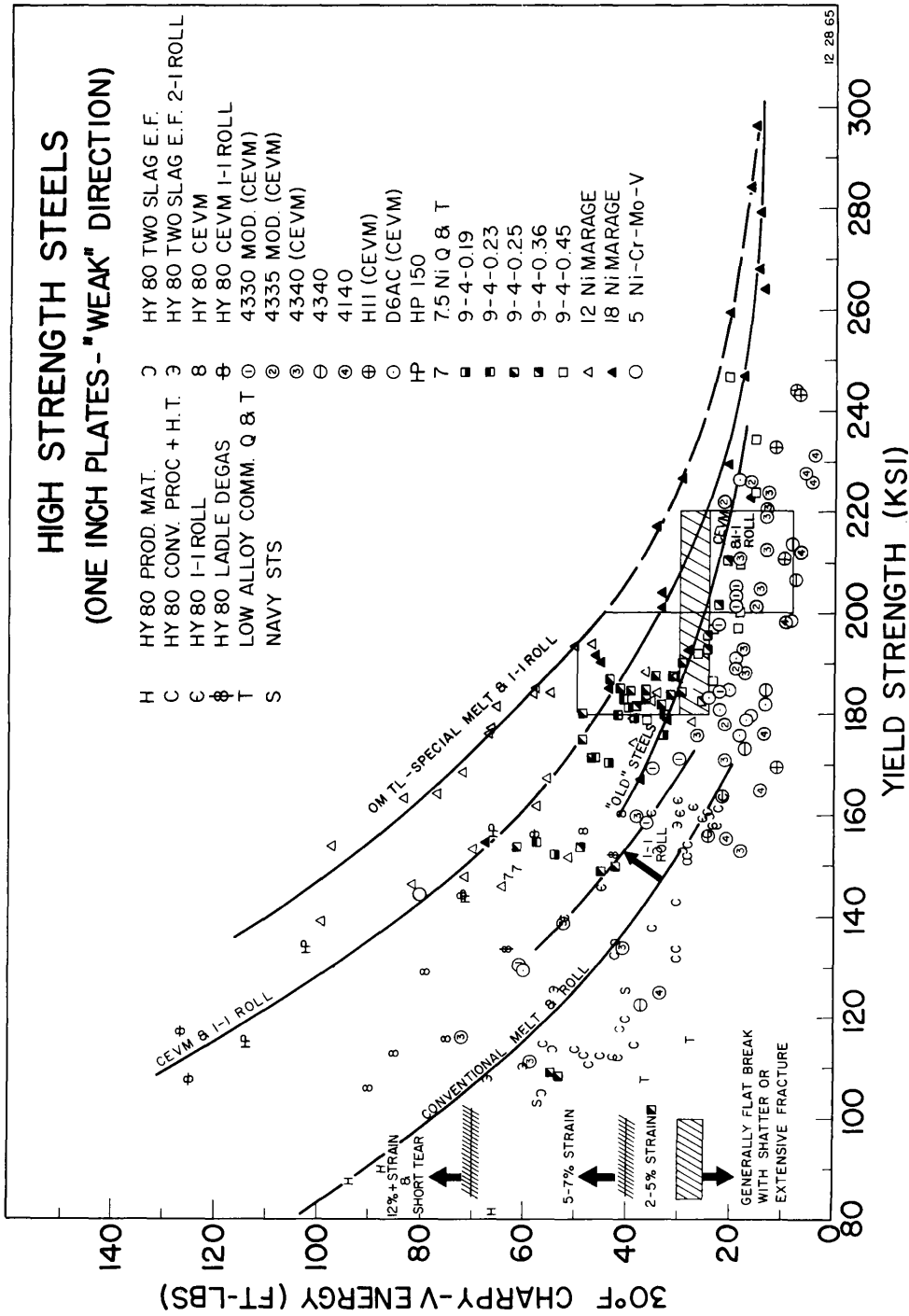


Fig. 20 - Summary of  $C_y$  data of Fig. 19 in relation to yield strengths. OMTL for various mill practices show same trends as Fig. 18.

## ALUMINUM ALLOYS

(R.W. Judy, Jr. and R.J. Goode)

Fracture toughness studies of aluminum alloys have been directed toward correlation of the explosion tear test (ETT), a large structural prototype test, with the smaller drop-weight tear test (DWTT), a laboratory test, over a wide yield strength (YS) range. From these studies a very preliminary Fracture Toughness Index Diagram (FTID) for aluminum has been developed. Modifications of the FTID have been made which incorporate early test results in some recently received plate material.

### SMALL LABORATORY TESTS

Four new aluminum alloy plates were furnished to NRL for the purpose of fracture toughness characterization and further FTID development. These materials were subjected to initial small laboratory tests, which included tensile, Charpy V ( $C_v$ ), and DWTT tests. The standard alloy designations and mechanical properties of these materials are shown in Table 13.

Two of the new plates represent different temper conditions of alloys previously tested. The yield strength (YS) of the 7075-T7351 alloy (A14) was about 65-ksi, approximately 13-ksi less than the 7075-T6 alloy (A5). A small increase in DWTT energy was also noted for the T7351 temper, compared to T6 temper for the 7075 alloy. The alloy 2219-T851 (A15) compared to 2219-T87 (A9), showed a small increase in yield strength and a disproportionately high increase in DWTT in the RW ("strong") fracture direction, while the WR ("weak") fracture direction (3) DWTT remained the same. The two remaining alloys -- 7005-T63 (A16) and 7106-T63 (A17) -- were in the 45-55 ksi YS range with "weak" direction DWTT energy values of 1022 and 573, respectively. Both of these alloys showed considerable directionality of fracture toughness properties.

Charpy V-notch tests, Fig. 21, of these four alloys did not yield much useful information. For the most part, the results showed very little change in  $C_v$  energy with changing temperature, and, as would be expected, the values were low.

TABLE 13  
MECHANICAL PROPERTIES OF ALUMINUM ALLOYS

Alloy	Alloy No.	YS		UTS		R.A.		Elong.		C <sub>v</sub> @32° F		DWTT RW (ft-lb)	
		L (ksi)	T (ksi)	L (ksi)	T (ksi)	L (%)	T (%)	L (%)	T (%)	RW (ft-lb)	WR (ft-lb)		
7075-T7351	A14	63.9	65.6	75.4	75.5	33.3	27	11.4	9.7	6	4	339	198
2219-T851	A15	59.3	58.4	73.4	74.3	22.7	19.6	10	9.4	5	5	514	281
7005-T63	A16	46.3	45.9	53.2	51.7	54.6	51.6	16.4	15.6	19	13	1905	1022
7106-T63	A17	52.1	52.5	61.2	60.8	45.7	40.0	13.6	13.9	10	8	1478	573

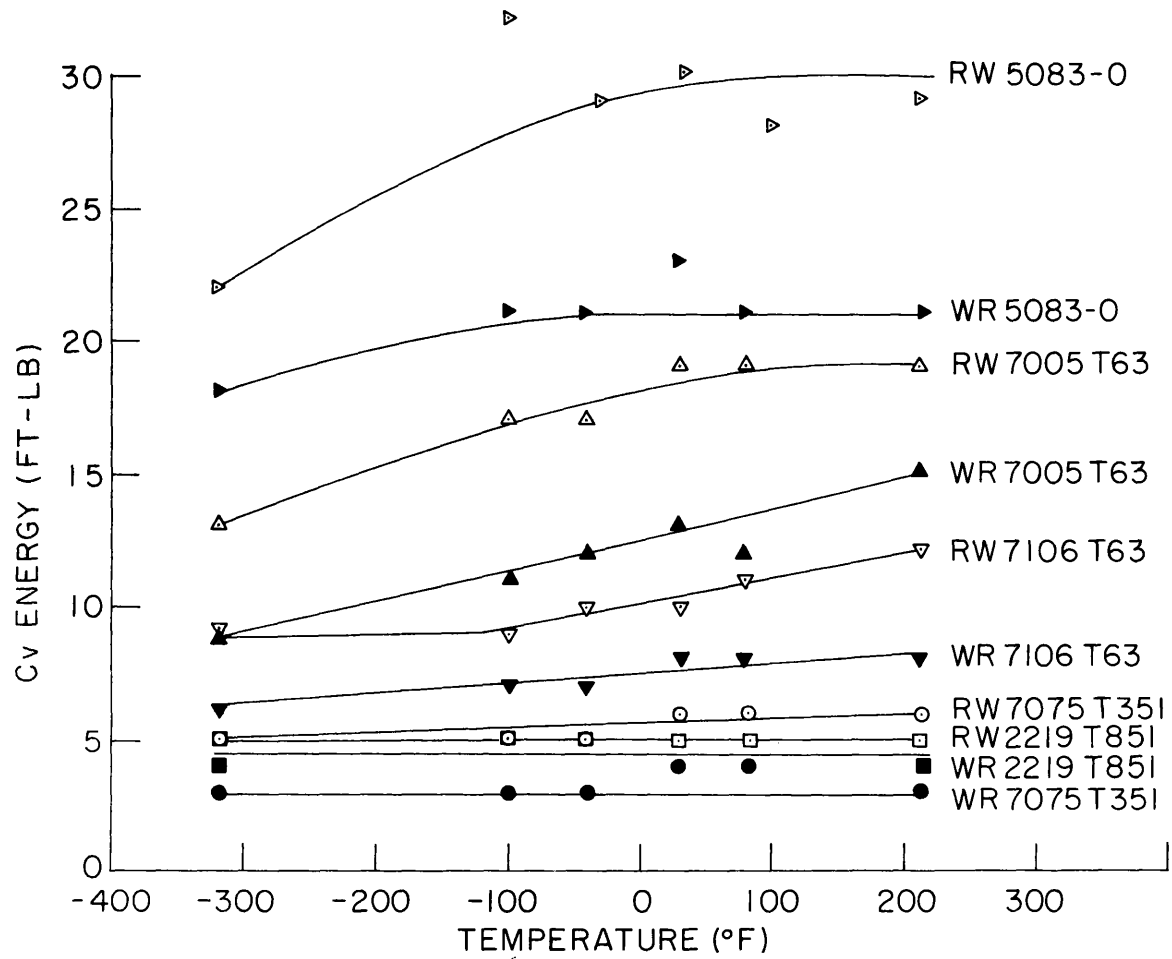


Fig. 21 - Charpy V notch curves of some aluminum alloys

## EXPLOSION TEAR TESTS

Sixteen ETT plates -- all with 2-in. through-thickness brittle electron beam weld flaws -- were tested. Specimens of 2219-T871 (A15) and 7075-T7351 (A14) fractured completely at or below yield strength loading (Fig. 22), indicating practically no resistance to ETT crack propagation. Specimens of 7106-T63 (A17) contained the moving crack to a short tear approximately 3-in. long at each end of the flaw at 3-5% permanent strain while fracturing completely at 7-9% strain (Fig. 23). This indicates the probable ETT capability of this alloy would be limited to 5-7% plastic strain overloads. Alloy 7005-T63 (A16) demonstrated a plastic overload capability in the presence of a flaw of approximately 7-9% strain. Specimens of this alloy fractured completely at 10-12% plastic strain while limiting the crack to a short tear at 5-7% plastic strain (Fig. 24).

In tests of other alloys, 5083-0 (A12), 5086-H112 (A7), and 5456-H321 (A3), (Fig 25) demonstrated an ability to withstand 15-20% plastic strain in the presence of a sharp flaw. In successive tests of four specimens of 5456-H321 (A3), crack extensions at each end of the flaw were 2-1/2-in. at 7-9% plastic strain, 3-in. at 10-15%, 4-1/2-in. at 12-15%, and 5-1/2-in. at 15-20% plastic strain (Fig. 25 top). Alloys 5083-0 (A12) and 5086-H112 (A7) had previously been tested to plastic strain levels in excess of 12% and 16%, respectively (20, 21). In this series of tests, specimens of each alloy were extended to plastic strain levels approaching 20%; none of the specimens fractured completely (Fig. 25, middle and bottom).

## FRACTURE TOUGHNESS INDEX DIAGRAM

The Fracture Toughness Index Diagram (FTID), (Fig. 26) reflects the correlation of the DWTT and ETT fracture toughness test with yield strength. The most important factor in these studies is the DWTT energy values, which are plotted against yield strength (YS). The optimum materials trend line (OMTL) shows the limiting or optimum values in the WR fracture orientation with respect to principal rolling direction seen in tests conducted to date on commercially-produced plate. Since the WR direction of fracture propagation is the "weak" fracture direction, the primary concern for users of the data is the properties in this direction.

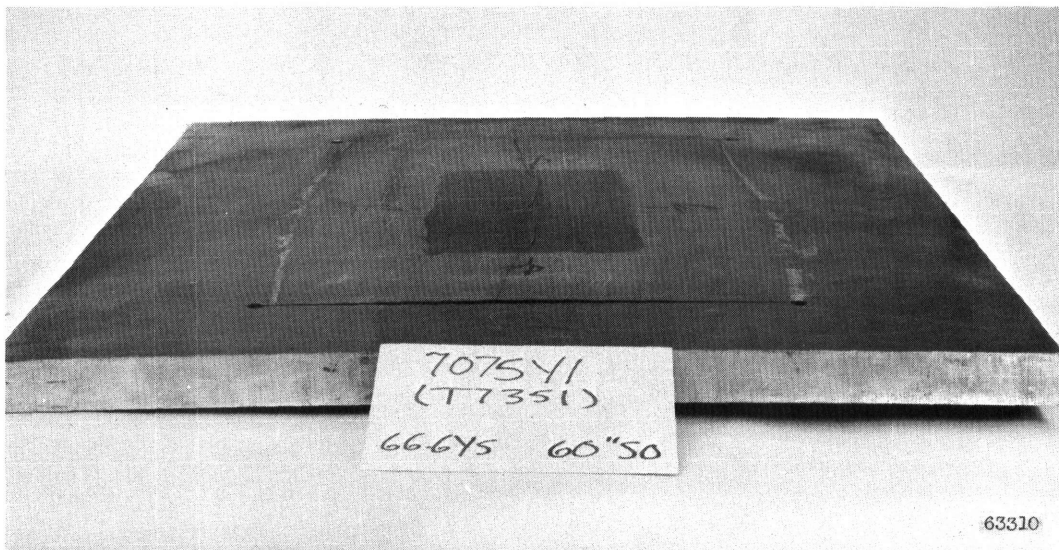
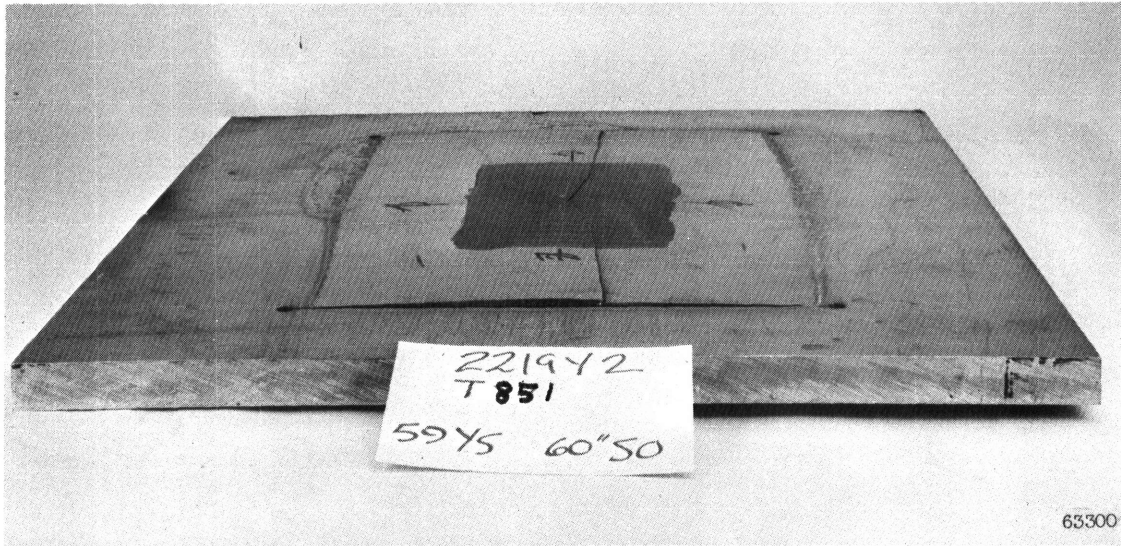


Fig. 22 - ETT specimens of 2219-T871 (top) and 7075-T7351 (bottom) which fractured at or below yield strength loading

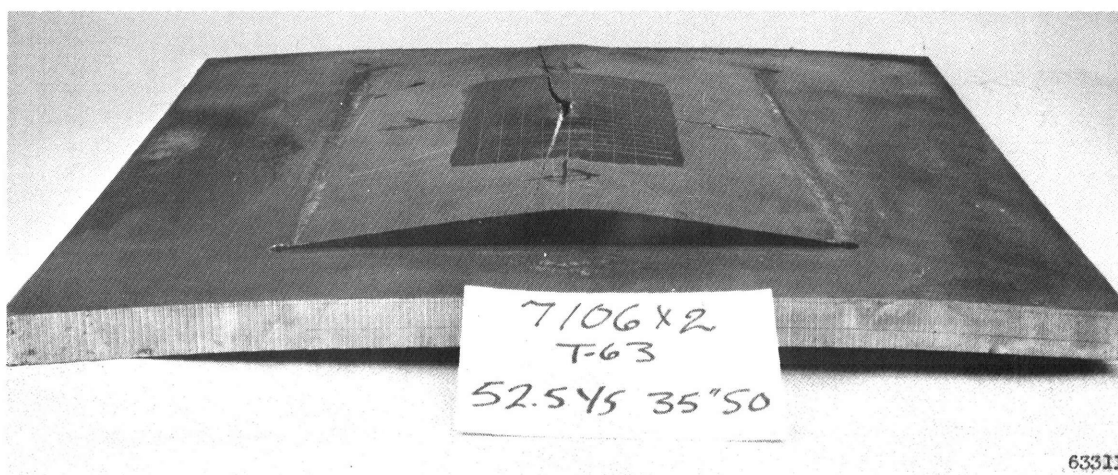
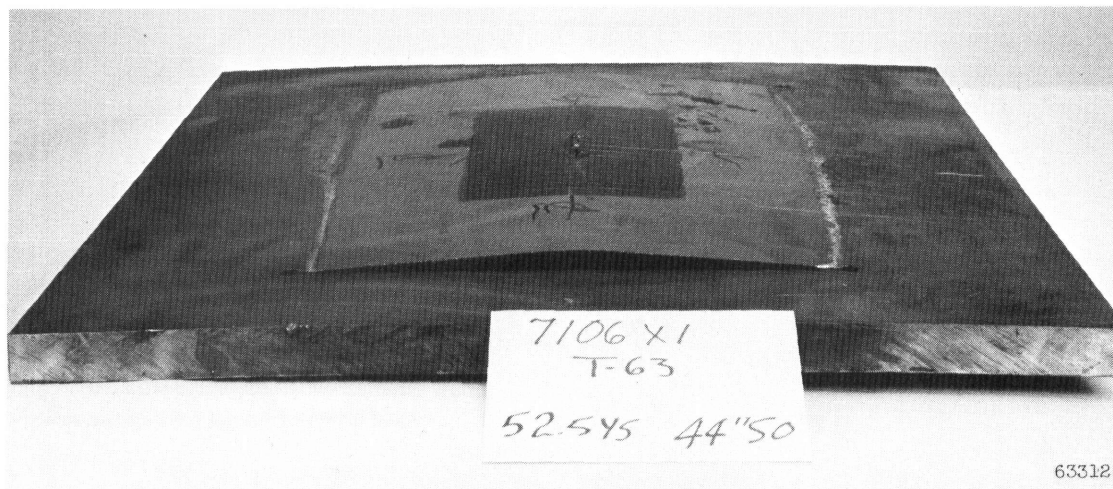
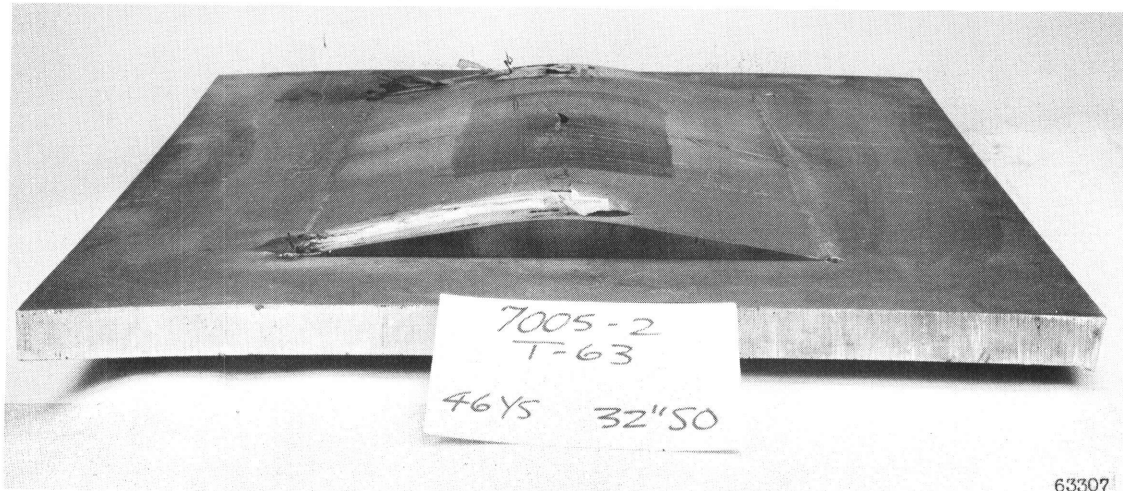


Fig. 23 - ETT specimens of 7106-T63. Top specimen loaded to 3-5% plastic strain; bottom specimen loaded to 7-9% plastic strain.



63307



63308

Fig. 24 - ETT specimens of 7005-T63. Top specimen loaded to 7-9% plastic strain; bottom specimen loaded to 10-12% plastic strain. Remnants of experimental strain gates can be seen on the plate surface adjacent to the cut slots.

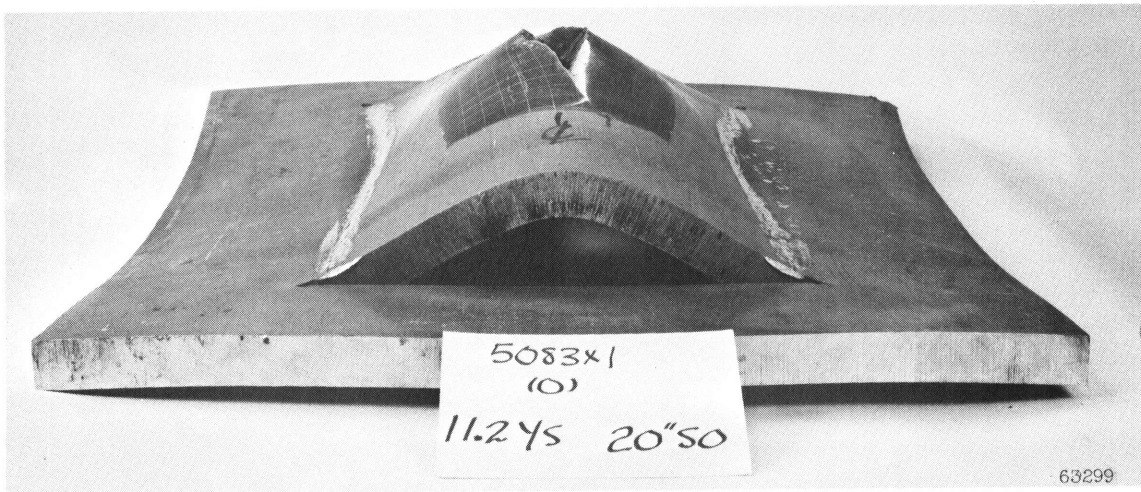
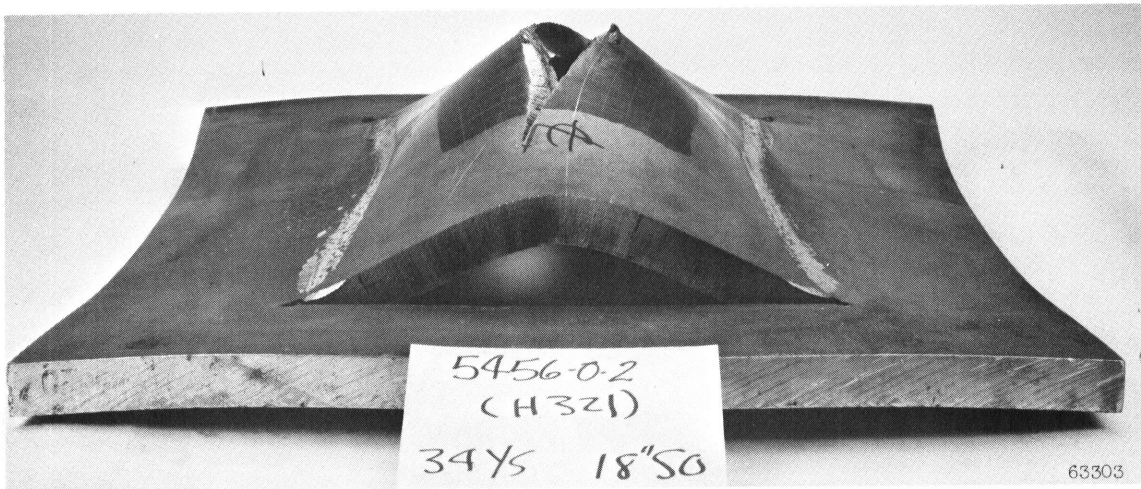


Fig. 25 - ETT specimens of 5456-H321 (top), 5083-0 (middle), and 5086-H112 (bottom) alloys. All specimens loaded to 15-20% plastic strain.

ALUMINUM ALLOYS  
ONE-INCH PLATE - 30°F

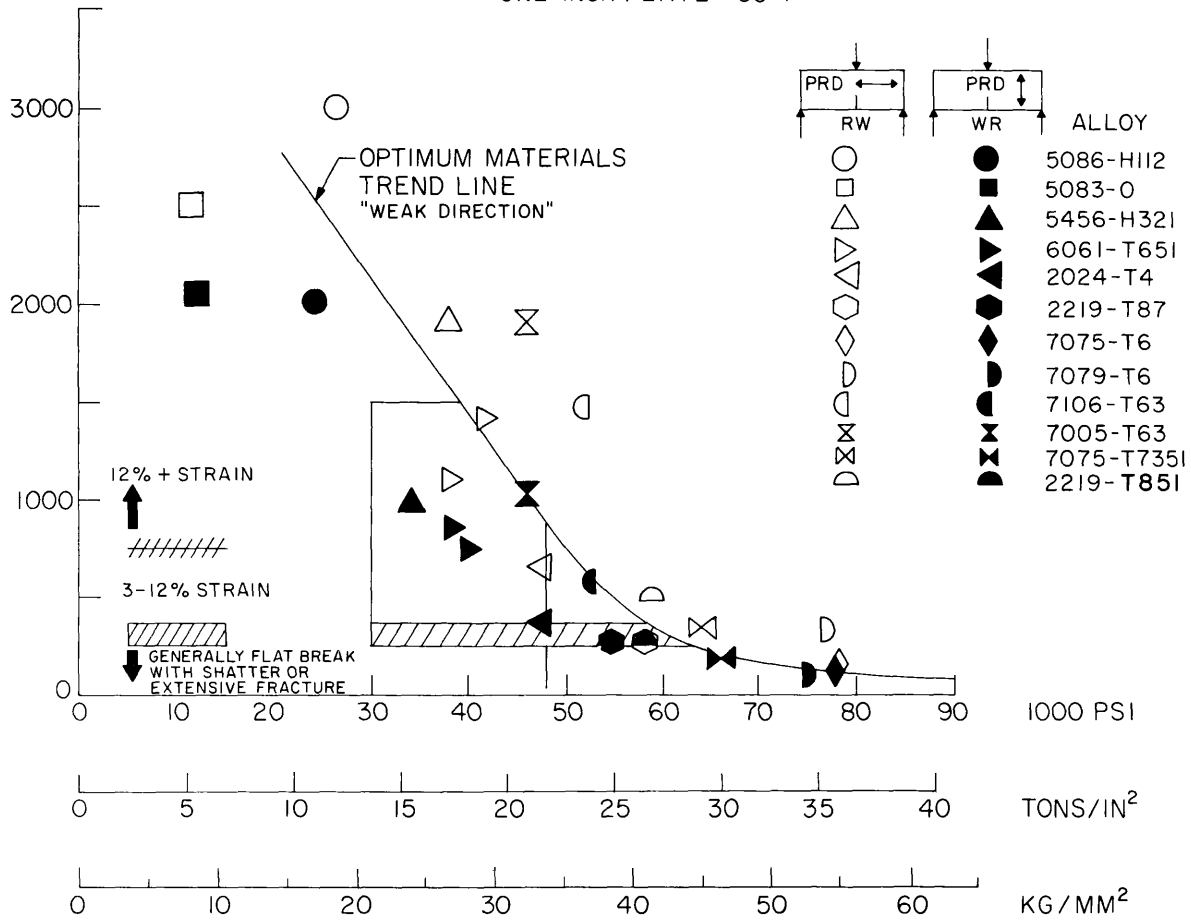


Fig. 26 - Fracture Toughness Index Diagram for 1-in.-thick aluminum alloy plates

Correlations of ETT performance with DWTT energy values are shown at the left of the diagram. High strength, low toughness alloys break flat and/or shatter at DWTT values in or below the cross-hatched band. The other ETT performance levels indicate the expected capabilities of the specific alloys in the ETT according to DWTT energies.

As in the diagrams for steel and titanium, the elastic-to-plastic transition band separates the brittle materials, where fracture toughness is best determined by fracture mechanics techniques, from those which can withstand high levels of plastic strain in the presence of a flaw. Above about 60-ksi YS all alloys would be expected to propagate fractures through elastic stress regions. Below 50-ksi YS, a wide variety of alloys should be available that would require high plastic overloads for fracture. In fact, all the alloys studied with yield strength below 50-ksi have demonstrated "weak" direction elastic overload capabilities in the ETT.

THE EFFECT OF MEAN STRAIN ON  
LOW-CYCLE FATIGUE CRACK PROPAGATION  
IN 5Ni-Cr-Mo-V STEEL AND 7079-T6 ALUMINUM

(T.W. Crooker, R.E. Morey, and E.A. Lange)

Current interest in higher performance materials for Naval structures has focused attention on a wide variety of potential metals and alloys. 5Ni-Cr-Mo-V quenched and tempered (Q&T) steel (134-ksi yield strength (YS)), and 7079-T6 aluminum alloy (77-ksi YS) are among the many materials presently under evaluation for future structural requirements. One vital characteristic of a structural material for many applications is the ability to resist the growth of crack-like flaws during cyclic loading. Small flaws invariably are formed during fabrication and manufacture of a large structure, despite the use of the best processing and inspection techniques. Since fabrication flaws are unavoidable, the only practice recourse is to provide fracture-safe design criteria for preventing the growth of flaws to a critical size from repeated service loads.

Previous reports have dealt with the role of cyclic strain as a parameter in determining the rate of fatigue crack growth in structural materials. However, cyclic strain alone is not sufficient to fully describe the loading which materials undergo in many structures when placed under actual service conditions. Static preload and/or residual stresses exist in most structures, creating a mean strain upon which cyclic strain is then superimposed.

This report describes a series of laboratory tests in which various mean strains, both tensile and compressive, were introduced under cyclic loading conditions to determine their influence on the rate of fatigue crack growth.

#### MATERIALS AND EMPERIMENTAL PROCEDURE

The two materials employed in this series of tests have been the subject of previous fatigue testing by the authors, as described in Reference 21 for the 5Ni-Cr-Mo-V steel and Reference 22 for the 7079-T6 aluminum alloy. The fatigue crack propagation characteristics for these two materials are shown in Fig. 27, which is a log-log plot of fatigue crack growth rate versus total strain range for each material under balanced cycle (zero mean strain) loading. The respective proportional limit for each material in the plate bend specimen is indicated in Fig. 27. A summary of the tensile properties of both materials is given in the upper left hand corner of Fig. 27 for reference in this report.

Lehigh-type plate bend fatigue test specimens were machined from 1-in.-thick rolled plate stock. Specimen orientation was chosen so that the measured fatigue crack propagation was perpendicular to the principal rolling direction.

Experimental data are based on the optically measured macroscopic growth of fatigue cracks across the surface of the center-notched Lehigh-type plate bend fatigue specimens cycled in cantilever loading. All tests described in this report were conducted in a room temperature air environment. Nominal surface strains across the test section were measured with an electrical resistance strain gage. Strain gage signals

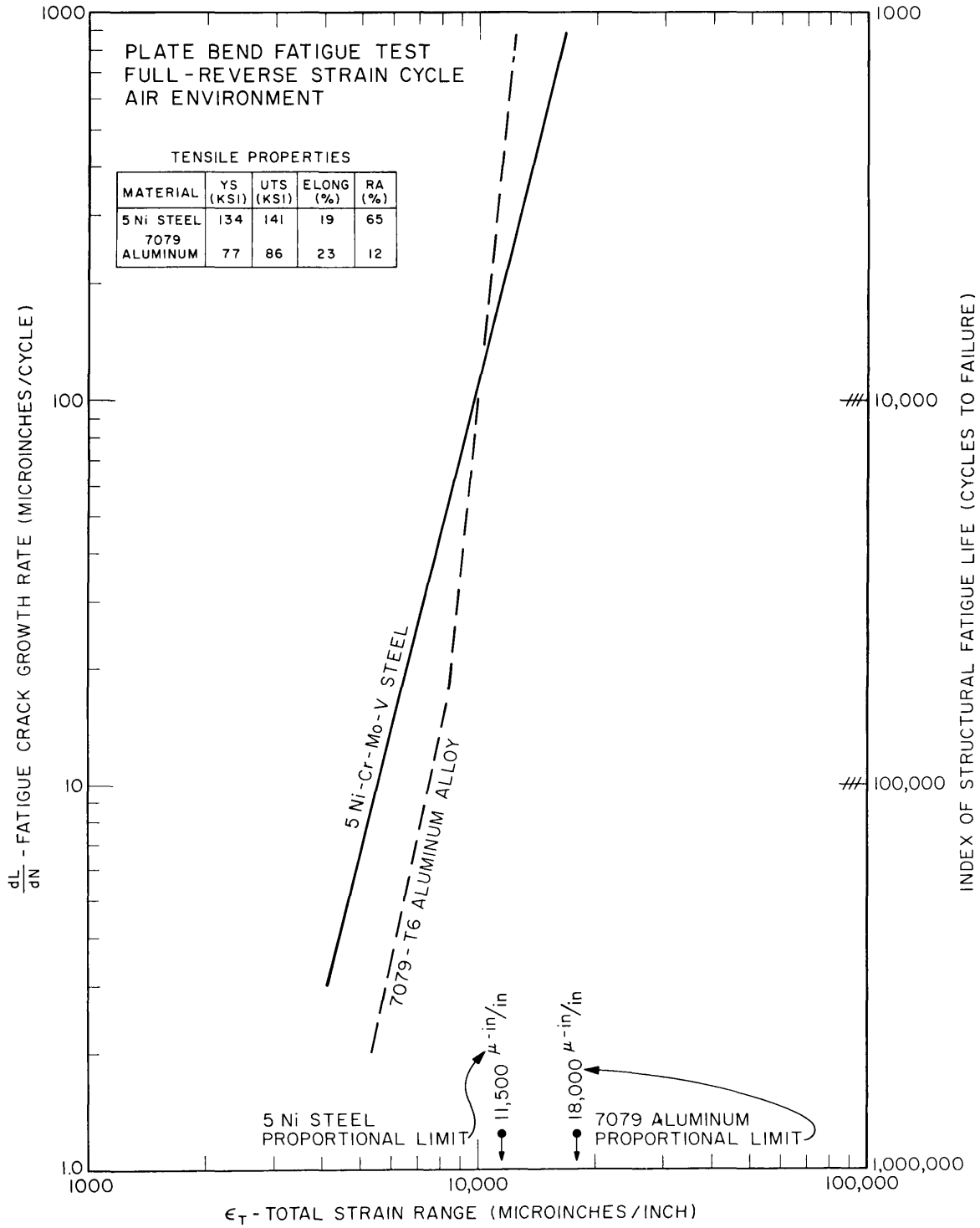


Fig. 27 - Log-log plot of fatigue crack growth rate versus total strain range for 5Ni-Cr-Mo-V steel and 7079-T6 aluminum alloy. The data are for a full-reversed strain cycle and the respective proportional limit of each material in the plate test specimen is indicated.

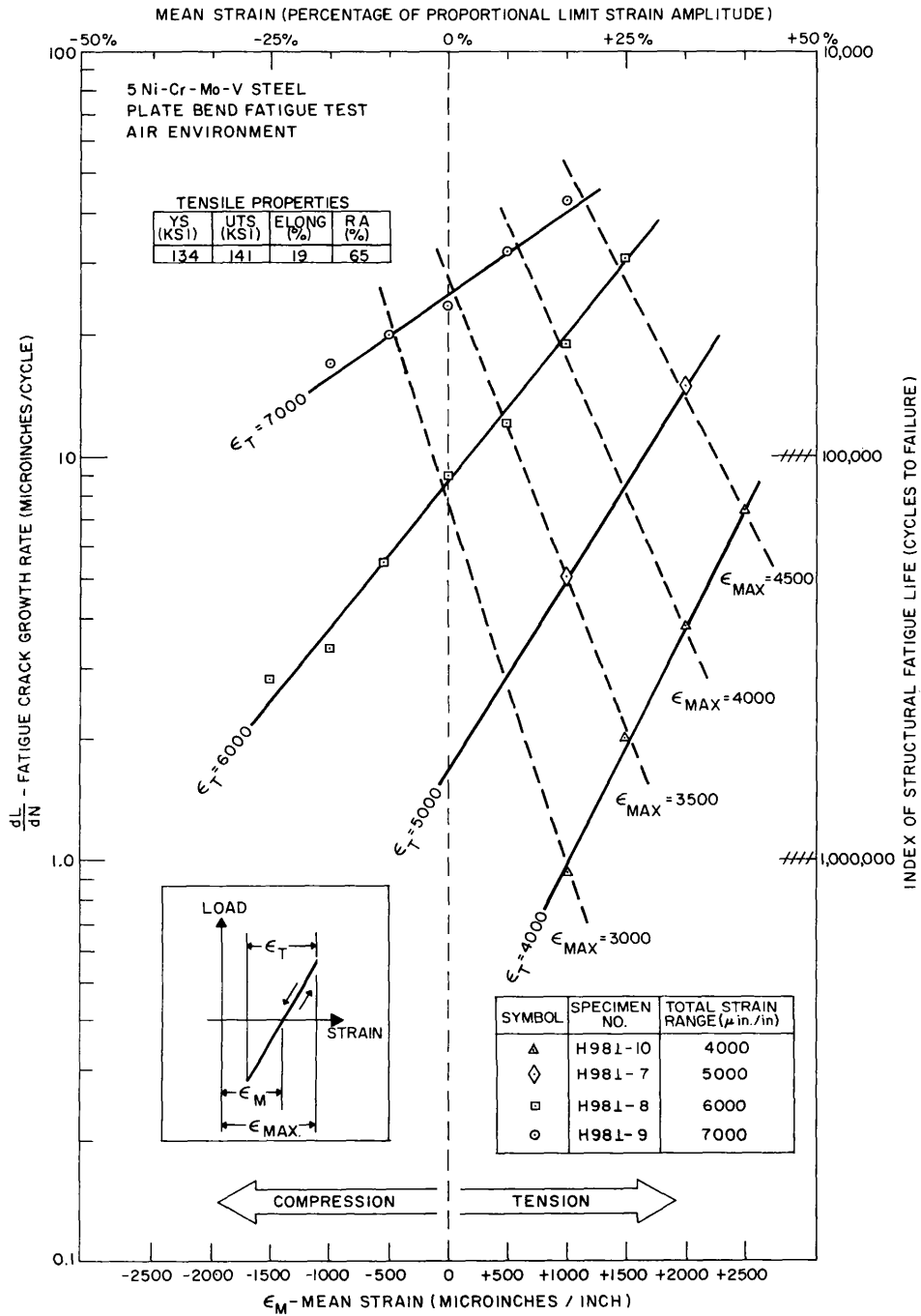


Fig. 28 - Semilogarithmic plot of fatigue crack growth rate versus mean strain for 5Ni-Cr-Mo-V steel plate bend fatigue specimens tested at four levels of cyclic strain range. Dashed lines represent values of constant maximum strain amplitude.

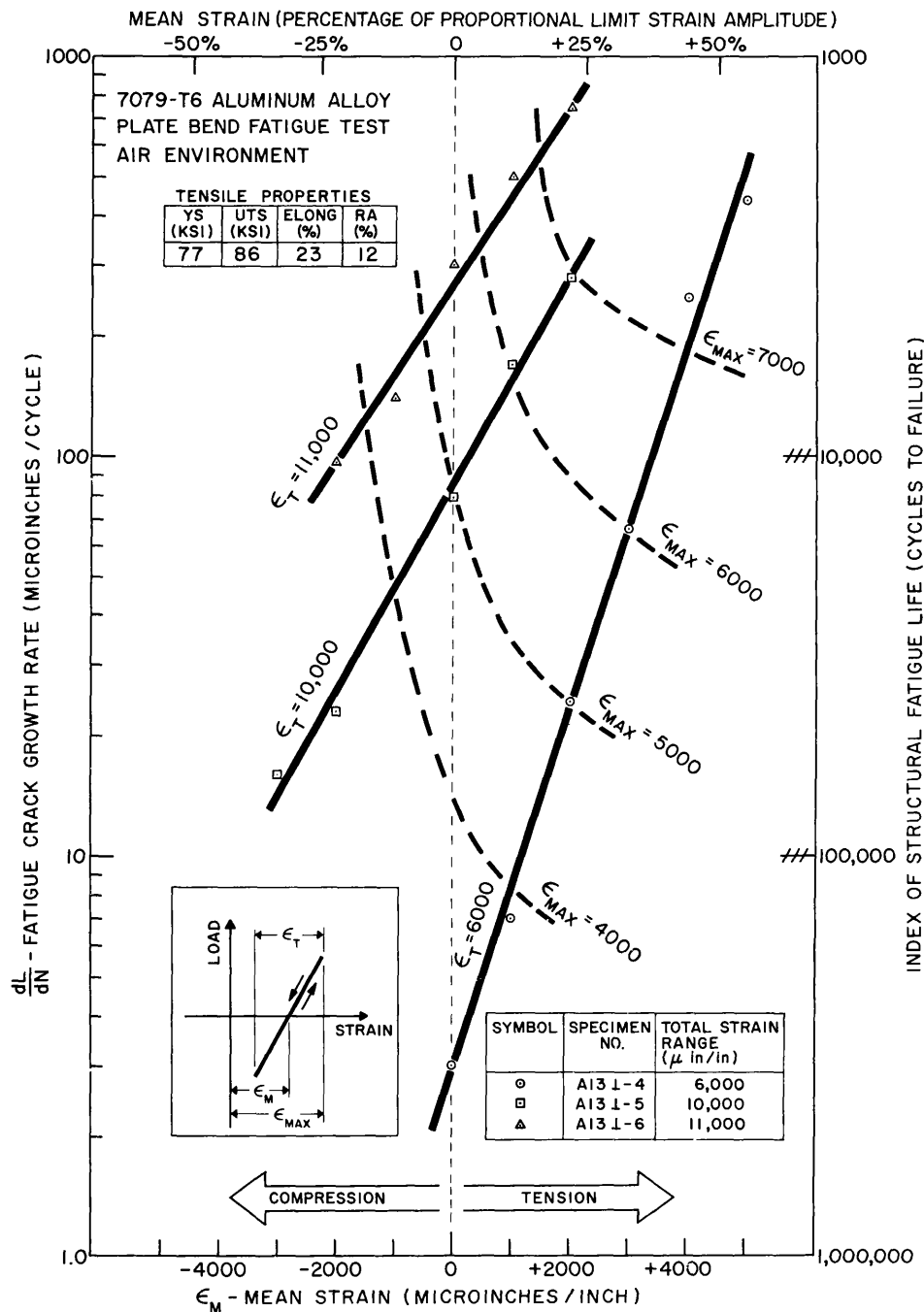


Fig. 29 - Semilogarithmic plot of fatigue crack growth rate versus mean strain for 7079-T6 aluminum alloy plate bend fatigue specimens tested at three levels of cyclic strain range. Dashed lines represent values of constant maximum strain amplitude.

were combined on an X-Y recorder with signals from a load cell placed in series with the actuating hydraulic cylinder to generate load-strain charts.

The loading cycle employed in the present series of tests, shown schematically in the lower left corners of Figs. 28 and 29, differs from that described in References 21 and 22 in that the full-reversed balanced (tension-compression) cycle is not used throughout. Instead, the loading cycle is unbalanced so as to provide a known mean strain for study. Each specimen was tested at a specific constant value of cyclic strain range, to which various known mean strains were added. Usually, the lowest desired value of mean strain was applied first and the specimen was cycled for an interval of several hundred to several thousand cycles until the crack growth rate could be established. Then, holding the cyclic strain range constant, mean strain was increased to the next highest desired value and cycling was resumed for another interval. In this manner, a series of fatigue crack growth rate versus mean strain data points for a constant cyclic strain were obtained from each specimen.

Care was taken to keep maximum strain amplitudes within the elastic limit of the material. This permitted relaxation of the bend specimen to the initial zero strain at zero load, and thus enabled accurate measurement of mean strains.

#### DISCUSSION OF TEST RESULTS

The experimental data are shown plotted in Fig. 28 for 5Ni-Cr-Mo-V steel and in Fig. 29 for 7079-T6 aluminum alloy. These figures are semilogarithmic plots of fatigue crack growth rate (log scale) versus mean strain (linear scale). The solid lines represent the response of the fatigue crack growth rate to the application of mean strain for a constant value of cyclic strain, indicated by the symbol  $\epsilon_T$  (total cyclic strain range). The dashed lines represent contours of constant maximum strain amplitude, as indicated by the symbol  $\epsilon_{MAX}$ .

These test results are an extension of the results from previous mean strain studies conducted by the authors on HY-80 composition Q&T steels (5). The former tests were conducted using a zero-tension

deflection cycle with loads extending into the plastic strain region. A variety of cyclic total strain range values were examined and at each value the mean strain was assumed to be 50% of the total strain range. Results from those tests indicated that the tensile mean strain caused an approximate threefold increase in fatigue crack growth rates at all levels of cyclic strain tested, compared to the crack growth rates obtained from a full-reverse, balanced cycle with a mean strain value of zero.

As thick plate sections of new, higher strength alloys became available, it was apparent that new information concerning the effect of mean strain was required for these materials. For the higher strength metals, such as HY-150 steel, cyclic loads in the elastic strain region are adequate to limit their structural lives to less than 10,000 cycles of loading. This is in contrast to HY-80 steel which requires plastic strain loading for fatigue lives in this range.

Qualitatively, it can be seen that tensile mean strain accelerates the growth of fatigue cracks and compressive mean strain retards the growth of fatigue cracks. The magnitude of the effect of mean strain on fatigue crack growth rate depends upon the level of the cyclic strain and the low-cycle fatigue characteristics of the material.

The threefold increase in fatigue crack growth rates observed in previous tests in HY-80 steels under zero-tension plastic strain loading appears to be a lower bound estimate. The data obtained in this study (Fig. 28 and 28) show that accelerations in fatigue crack growth under elastic loading conditions can approach an order of magnitude in 5Ni-Cr-Mo-V steel and two orders of magnitude in 7079-T6 aluminum from the combined effect of a relatively small cyclic strain range and a relatively large static tensile mean strain. In terms of structural life, this suggests that mean strains in high strength materials should not be ignored at elastic strain levels normally considered safe from danger of low-cycle fatigue failure. It is at these strain levels that tensile mean strain can reduce fatigue life by a factor of ten, and in some cases, by a factor of one hundred, below calculated estimates of life based only on cyclic strain. At higher cyclic strain levels, with tensile strain amplitudes in the plastic region, the maximum reduction in fatigue life due to

tensile mean strain appears to be approximately a factor of three for both of the new materials tested, as was determined in the previous tests with HY-80 steel.

These preliminary data appear to indicate that the sensitivity of the fatigue crack propagation characteristics of metals to mean strain corresponds with their sensitivity to cyclic strain. For example, fatigue crack propagation in 7079-T6 aluminum alloy was found to be highly sensitive to cyclic strain in previous tests (22), as indicated by the slope of its curve in Fig. 27, and this material also exhibits great sensitivity to mean strain in the current series of tests.

Whereas cyclic strain range provides a simple denominator for describing fatigue crack growth rates in the absence of mean strain (21, 22), no such single parameter exists in the presence of mean strain. Under this condition, crack growth rates become a more complex function involving both cyclic strain and mean strain. In the basic fatigue crack growth rate relationship for plate bend specimens,  $\frac{dL}{dN} = c(\epsilon_T)^m$

where  $\frac{dL}{dN}$  = growth rate in microinches/cycle,  
c = constant,  
 $\epsilon_T$  = total strain in range in microinches/inch,  
m = exponent,

mean strain acts similar to an additive in strain range at elastic strain amplitudes, i.e.,  $\frac{dL}{dN} = c(\epsilon_T + \epsilon_M)^m$   
-- but at plastic strain levels the effect is limited to a factor of approximately three, i.e.,  $\frac{dL}{dN} = 3c(\epsilon_T)^m$ .  
Thus, for a low strength material mean strain would appear to have a relatively limited effect on the growth rate of fatigue cracks in the low-cycle range, but in higher strength materials mean strain becomes a much more critical parameter.

#### SUMMARY

1. Mean strain acts as a complex parameter on the growth rate of low-cycle fatigue cracks, and its effect is dependent upon mean strain level and cyclic total strain range level.

2. When the strain amplitude remains in the elastic range, mean strain acts as an additive increase in strain range for tension mean strains and a similar decrease in strain range for compressive mean strains.

3. When maximum strain amplitude levels are in the plastic range, the effect of increasing mean strain is limited to an approximate threefold increase in fatigue crack growth rates.

4. The limiting effect of mean strain, when plastic strains are involved, results in a limited effect of mean strain on the low-cycle fatigue life of structures constructed of low strength materials.

5. For steels with yield strengths in the 135-ksi range and aluminum alloys with yield strengths in the 75-ksi range, mean strain can have a 10× and 100× effect, respectively, on the structural life of high performance structures constructed with these materials.

#### DEVELOPMENT OF A LOW-CYCLE

#### FATIGUE CRACK PROPAGATION TEST

#### EMPLOYING FRACTURE MECHANICS PARAMETERS

(T.W. Crooker, R.E. Morey, and E.A. Lange)

Development work is currently underway on specimen design and experimental procedure for a fatigue crack propagation test for high strength materials employing fracture mechanics parameters. Test methods have previously been developed for studying low-cycle fatigue crack propagation in Lehigh-type cantilever plate fatigue specimens. These previous test methods have been applied to a wide variety of structural materials and a considerable background of information has been established. However, a fracture mechanics analysis of the surface-cracked Lehigh specimen is beyond present capabilities. The work described in this report represents an extension of the Lehigh specimen studies in an attempt to broaden the significance of the fatigue data in terms of fracture mechanics parameters.

It has been shown that in many structural materials the rate of growth of a fatigue crack across the surface of a center-notched Lehigh fatigue specimen is proportional to the fourth power of the total strain range,  $\frac{d(2a)}{dn} = \text{constant } (\epsilon_T)^4$ , in full-reverse or zero-tension

cycling (5, 7, 18, 19, 20, 21, 23). Paris and Erdogan have shown that an empirical correlation exists between the rate of fatigue crack growth and the maximum stress intensity factor raised to the fourth power,  $\frac{da}{dn} = \text{constant } (K)^4$ , for many materials under zero-tension cycling (24). The similarity between these two relationships suggests that the Lehigh specimen fatigue crack propagation data could be interpreted in terms of fracture mechanics parameters, even though a rigorous analysis of the specimen is not available.

This experiment consists of testing several edge-notched cantilever specimens of materials which have previously undergone fatigue crack propagation tests in the Lehigh specimen. The geometry of the edge-notched cantilever specimen is one which can be analyzed by fracture mechanics procedures. The resulting data thereby establishes an empirical correlation between  $\epsilon_T$  and K for these materials in relation to rates of fatigue crack propagation.

#### TEST SPECIMEN DESIGN AND MATERIALS

The test specimen is basically a 2-1/2-in.-wide cantilever plate specimen placed on edge. The three specimens tested to date were machined to the edge-notched configuration from existing Lehigh specimens prepared from 1-in.-thick plates. Figure 30 is a dimensioned sketch of the resulting edge-notched cantilever specimen. Figures 31 and 32 are photos of the specimen and test set-up. These specimens were cycled in a fatigue machine designed for the Lehigh specimen with only minor modifications to the machine.

The first specimen was tested without side-grooves with the result that shear lip formation hampered optical observation of the fatigue crack along the surface. Consequently, the second and third specimens were side-grooved before fatigue testing. The dimensions of the side-grooves are as follows: depth 0.025 inches (5% of gross test section thickness), included groove angle 60°, and root radius of groove 0.010 inches. The remaining net section thickness was 0.45 inches. These dimensions were checked on an optical comparator for accuracy.

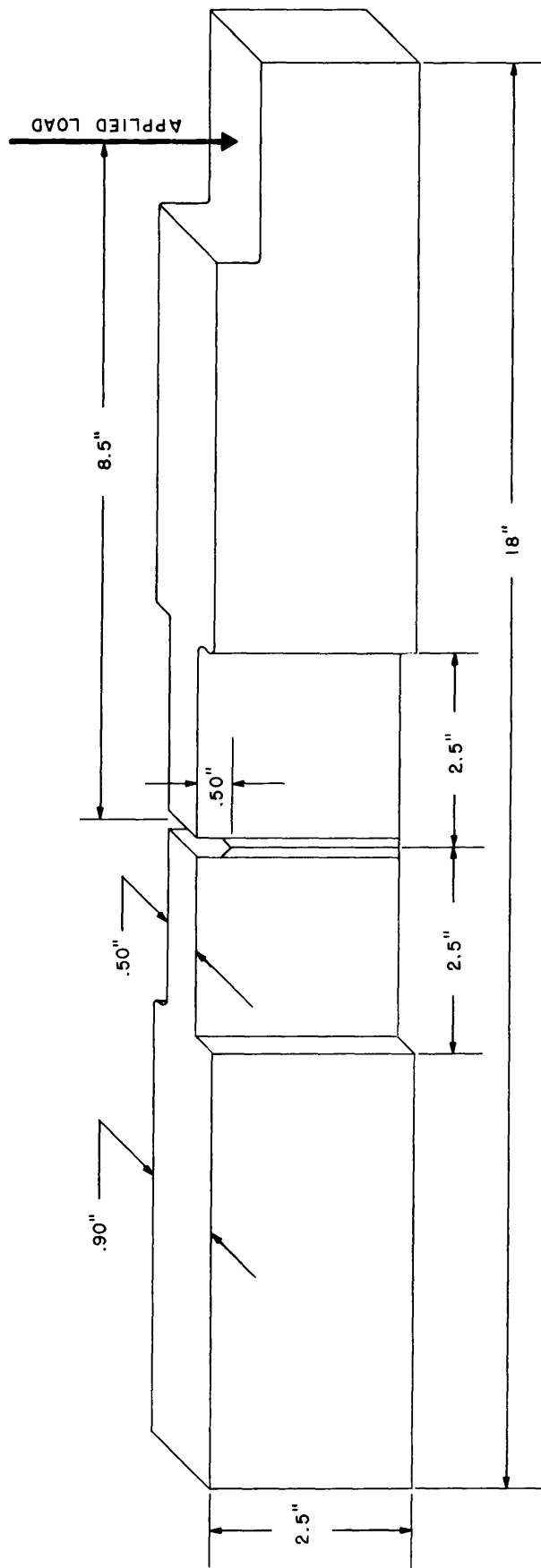


Fig. 30 - Sketch of edge-notched cantilever fatigue specimen showing principle dimensions

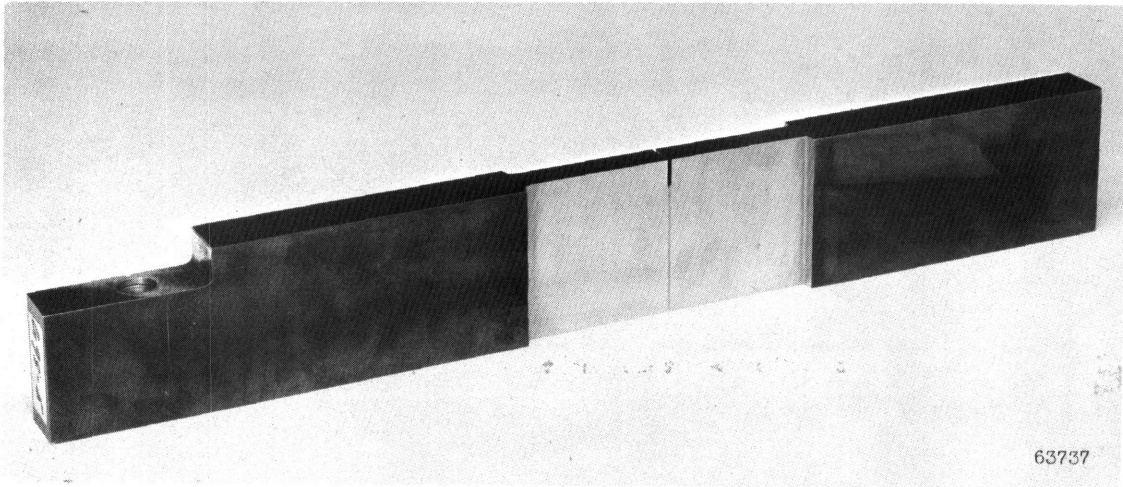


Fig. 31 - Photo of edge-notched cantilever fatigue specimen

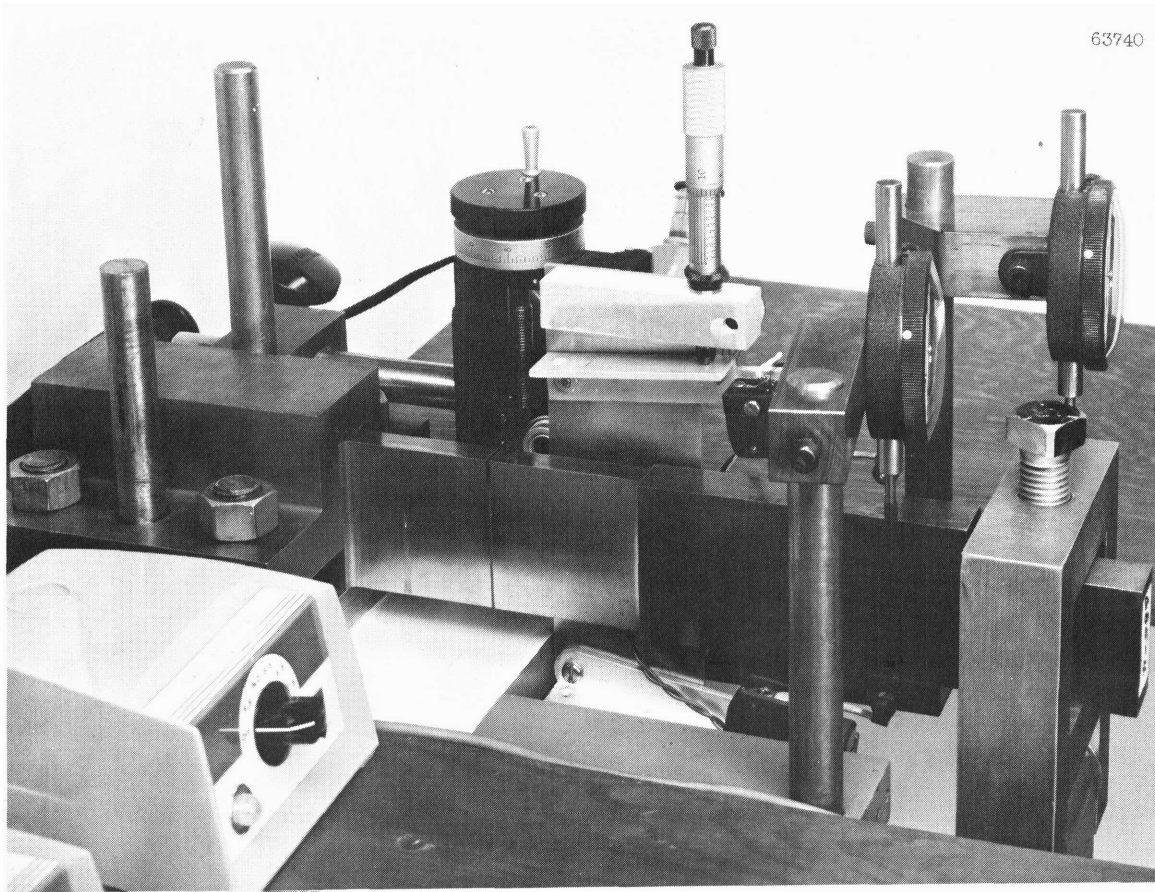


Fig. 32 - Photo of test set-up for cycling the edge-notched cantilever fatigue specimen

Materials chosen for this experiment were D6AC (G85) and 4335 (G98) steels which underwent previous testing described in Reference 20. The yield strengths of these two steels were 212 and 215-ksi, respectively, which qualifies them as "fracture mechanics materials", i.e., fracture can be self-propagating at elastic stress levels. The fracture toughness of these materials as measured by the drop-weight tear test was well under 1000 ft-lb of energy for the "weak" (WR) fracture direction.(3). Fatigue crack propagation measurements were in the "strong" (RW) fracture direction.

#### EXPERIMENTAL PROCEDURE

The experimental procedure applied to this series of tests is of interest due to its simplicity. Specimens were cycled zero-to-tension at constant load. Nominal stresses were kept well below the elastic limit of the materials, thus preventing any measurable hysteresis in the loading cycle. Fatigue crack length was measured optically at the surface at one side of the specimen. As the fatigue crack length increased under constant load, the intensity factor, K, increased and the rate of fatigue crack growth also increased, thus providing a spectrum of fatigue crack growth rates for examination.

Optical fatigue crack observations were made at 14x magnification. With the side-grooved specimens, it was found necessary to hand-polish grinding marks at the root of the groove. However, once this was accomplished, the fatigue crack could be observed without difficulty at the cycling rate of six cycles per minute.

The formula for calculating the stress intensity factors, after Kies, is as follows: (25)

$$K_I = \frac{4.12M \sqrt{\frac{1}{\alpha^3} - \alpha^3}}{BD^{1.5}}$$

$$\alpha = 1 - \frac{a}{D}$$

M = bending moment

B = net section thickness

D = section depth

a = total crack length (machined notch plus fatigue crack)

Previous low-cycle fatigue crack propagation studies on high strength steels using a fracture mechanics analysis have been made by Carman, et al. (26). These data provided a reference for the range of stress intensity values relevant to low-cycle fatigue crack propagation in this class of materials. With this information at hand, the tests were started at the lowest stress intensity value desired and cycled at constant load until the specimen failed in fracture or until the crack could no longer be observed with sufficient accuracy.

Experimental data were plotted on a chart of total crack length versus cycles of applied load, Fig. 33. From this chart of experimental data, the two parameters of interest,  $K$  and  $\frac{da}{dn}$ , can be calculated.

Under constant load cycling conditions,  $K$  is a function of the total crack length and  $\frac{da}{dn}$  is directly proportional to the slope of the curve.

#### PRELIMINARY TEST RESULTS

Three specimens were tested in the initial experiment. As previously mentioned, the first test involved a specimen without side-grooving (D6AC) and yielded no quantitative information because shear-lip formation prevented accurate observation of the crack front. The second test used a specimen (4335) that was side-grooved to eliminate this problem, but yielded only meager fatigue data. This was due to the failure of the specimen after only a few thousand cycles of repeated load because of the low fracture toughness of the material.

With these lessons in mind, the third specimen (D6AC) was somewhat more successful. This specimen was side-grooved and cycling was begun at a very conservative stress intensity level ( $K = 22,400 \text{ psi}\sqrt{\text{in.}}$ ). The data from this test are shown in Fig. 33, and are tabulated in detail in Table 14.

Like the second test, the third test was of limited duration as a result of the low fracture toughness of the material. The test was terminated short of terminal fracture due to an apparent change in fracture mode which made the crack extremely difficult to observe optically. This occurred at a stress intensity level of approximately  $33,000 \text{ psi}\sqrt{\text{in.}}$ , which corresponded to a nominal net section bending stress of  $39,000 \text{ psi}$ .

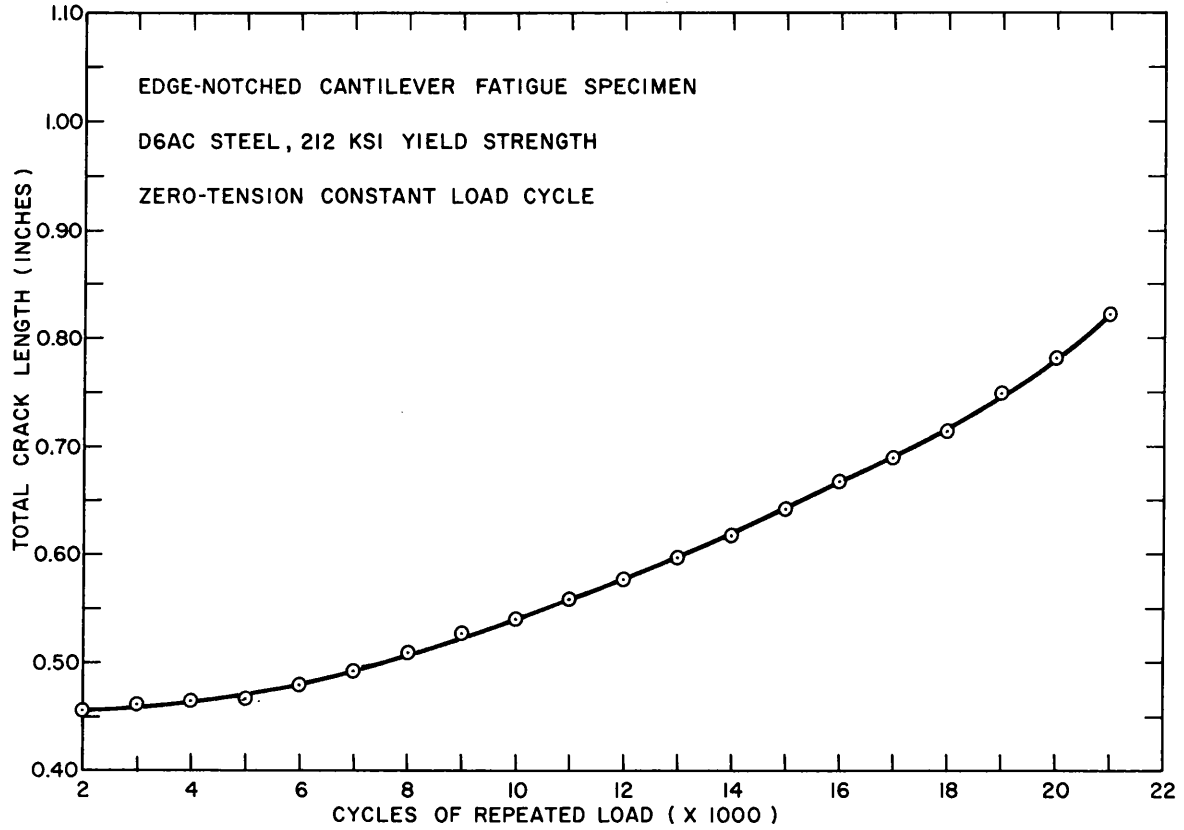


Fig. 33 - A plot of total crack length versus cycles of repeated load for D6AC steel edge-notched cantilever fatigue specimen

TABLE 14

FATIGUE CRACK GROWTH DATA FOR D6AC STEEL (G85)

Cycles	Total Crack Length (inches)	Cycles	Total Crack Length (inches)
2,000	0.4566	11,500	0.5681
2,500	0.4608	12,000	0.5781
3,000	0.4619	12,500	0.5876
3,500	0.4622	13,000	0.5982
4,000	0.4651	13,500	0.6081
4,500	0.4668	14,000	0.6188
5,000	0.4688	14,500	0.6291
5,500	0.4751	15,000	0.6428
6,000	0.4793	15,500	0.6521
6,500	0.4881	16,000	0.6673
7,000	0.4933	16,500	0.6793
7,500	0.5011	17,000	0.6893
8,000	0.5109	17,500	0.7040
8,500	0.5186	18,000	0.7159
9,000	0.5267	18,500	0.7348
9,500	0.5388	19,000	0.7507
10,000	0.5417	19,500	0.7663
10,500	0.5515	20,000	0.7836
11,000	0.5596	20,500	0.8032
		21,000	0.8221

At lower stress intensity levels, the fatigue crack appeared jagged and easily visible at 14× magnification. However, at the 33,000  $\text{psi}/\sqrt{\text{in.}}$  stress intensity level the fatigue crack changed to an extremely sharp hairline crack which could not be followed with accuracy. This specimen will be tested under static load to determine its critical stress intensity value.

Stress intensity and fatigue crack growth rate values calculated from the results of the third specimen are tabulated in Table 15 and are plotted on a log-log scale in Fig. 34. In addition, Fig. 34 also shows comparable data obtained from previous Lehigh specimen tests of this material.

## DISCUSSION

The results of this preliminary experimentation are limited but encouraging. Specimen design, adaption of existing fatigue machines, and experimental techniques have presented minimal difficulties. Preliminary data displayed in Fig. 5 parallel the data obtained from previous Lehigh specimen tests. These limited results suggest confirmation of the underlying assumption that for high strength materials and equivalence can be established between the two methods of analysis.

The results of these preliminary tests also point out the limitations of the cantilever edge-notched specimen for low-cycle fatigue crack propagation studies. The first limitation is the requirement for nominally elastic loading conditions in order that the fracture mechanics analysis be valid. The second limitation is the requirement for sufficient fracture toughness to permit fatigue crack propagation rates in the low-cycle range (10 to 1000 microinches/cycle). This requirement is illustrated by the brief span of the edge-notched specimen data in Fig. 5. Since relatively few materials presently possess both high strength and high fracture toughness, it is doubtful that this test has potential for widespread application. Further, even with the adaption of electronic sensing devices to follow the crack tip and elimination of the side-grooves, thus permitting shear-lip formation, the useful range of the specimen will remain limited.

TABLE 15

CRACK GROWTH RATE AND STRESS INTENSITY DATA FOR D6AC STEEL (G85)

Cycle Interval	Average Total Crack Length (inches)	Average Crack Growth Rate (microinches/cycle)	Average Stress Intensity Factor (psi/ $\sqrt{\text{in.}}$ )
2,500--4,500	0.4638	3.0	22,450
5,000--6,000	0.4740	10.5	22,800
6,500--9,500	0.5109	15.2	23,900
10,000-11,500	0.5549	17.6	25,300
12,500-14,500	0.6083	20.7	26,900
15,000-16,500	0.6610	24.3	28,600
17,500-19,000	0.7273	31.1	30,750
19,500-21,000	0.7942	37.2	33,000

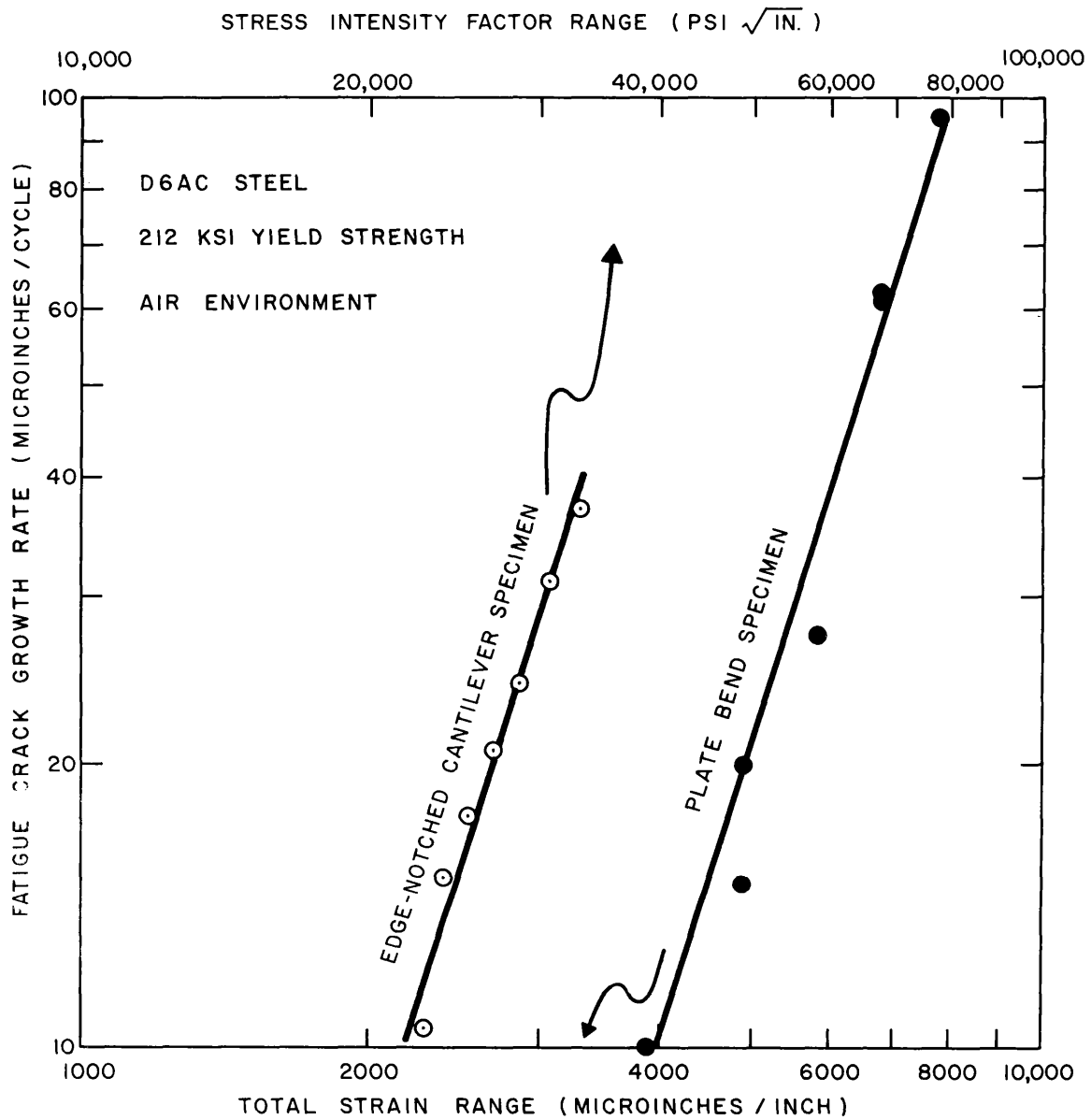


Fig. 34 - Comparative log-log plot of total strain range (lower scale) and stress intensity factor (upper scale) versus fatigue crack growth rate in D6AC steel for two specimen designs

Fortunately, many of the newest materials currently undergoing evaluation, such as steels with 160 to 180-ksi yield strength and titanium alloys with 100 to 120-ksi yield strength, do possess an excellent combination of strength and fracture toughness. Future experimentation on these materials with the cantilever edge-notched specimen is planned.

EFFECT OF SIDE-GROOVES ON  
PLANE-STRAIN FRACTURE TOUGHNESS MEASUREMENTS

(C.N. Freed)

Linear elastic fracture mechanics techniques are used to measure the resistance of a material to crack initiation and propagation under an applied load. This method of measuring fracture toughness is especially useful in determining the stress intensity required to initiate and propagate fractures from flaws in ultra-high strength materials of typically low fracture toughness. However, as the toughness of the material increases, the detection of initial crack instability with fracture mechanics methods becomes more difficult until, with sufficient toughness, the detection of crack instability is impossible. Thus for the higher toughness, low strength materials, valid fracture toughness measurements cannot be made using the presently accepted fracture mechanics techniques.

Experimenters have found that the modification of a single-edge-notch tensile specimen with side-grooves will sharpen the indication of crack instability (27). This permits the measurement of plane-strain fracture toughness,  $K_{Ic}$ , in cases which would not have been possible with a standard, smooth-sided specimen of the same thickness. The effect of side-grooves on the stress intensity factor,  $K$ , is dependent on the toughness anisotropy of the material--information that is not generally available. It has been proposed, however, that if shallow side-grooves are used, 5 or 10% deep on each flank, an accurate value of  $K_{Ic}$  may be obtained regardless of the toughness anisotropy relative to the fracture plane.

The plane-strain fracture toughness data reported here are preliminary results from an investigation to determine the maximum toughness of various 1-in.-thick materials for which  $K_{Ic}$  can be obtained. Since it is believed that side-grooved specimens will enable valid  $K_{Ic}$  values to be determined for materials of higher toughness than is possible for the smooth specimens, it is necessary to demonstrate that side-grooved specimens will produce valid  $K_{Ic}$  values.

#### EXPERIMENTAL DETAILS AND MATERIALS

Plane-strain fracture toughness values were determined with single-edge-notch (SEN) specimens; a detailed description of these specimens, both smooth and side-grooved, is presented in the Seventh Quarterly Report (20). Side-grooves were machined with an included angle of  $60^\circ$  and with a notch root radius of 0.010-in. The symmetrical grooves, which were machined across the width of the specimen parallel to the edge-notch, are described by the ratio of the unbroken thickness,  $B_N$ , to the thickness prior to grooving,  $B$ . The  $K_{Ic}$  for side-grooved specimens was determined by calculating  $K_{Nominal}$  ( $K_N$ ) as though no side-grooves were present and then correcting the result by multiplying it by  $(B/B_N)^{0.5}$  which is a thickness correction.

$$K_{Ic} = K_N(B/B_N)^{0.5}$$

A simple calculation will demonstrate that although the exponent may theoretically vary between 0.5 and 1.0, depending on the toughness anisotropy, the employment of shallow side-grooves will prevent  $K_{Ic}$  from being significantly affected by the use of the 0.5 exponent (27).

In Table 16, the mechanical properties of one titanium alloy, Ti-6Al-4V (T-27), and two aluminum alloys, 7075-T6 and 2219-T87, are presented. Mechanical property data for two other titanium alloys investigated, Ti-8Al-1Mo-1V (T-19) and Ti-6Al-4Zr-2Sn-0.5Mo-0.5V (T-68), are being obtained.

A number of specimens of Ti-6Al-4V (T-27) were solution annealed at  $1700^\circ\text{F}$  for one hour, water quenched, then aged at  $900^\circ\text{F}$  for two hours and air cooled. Many of the specimens were side-grooved so that  $B_N/B$  varied from 0.9 to 0.5 while others were left with "smooth" flanks.

TABLE 16

MECHANICAL PROPERTIES OF T-27, 7075 T-6, and 2219 T-87

Nominal Composition and Code No.	Fracture Direction	YS (ksi)	UTS (ksi)	Elong. (%)	RA (%)	DWTT (ft-lb)	C <sub>y</sub> at -80°F (ft-lb)	C <sub>y</sub> at 32°F (ft-lb)	Heat treatment
Ti-6Al-4V (T-27)	RW	132.5	150.5	10.6	25.2	1251	24.7	25.0	1700°F/1 hr/WQ then 900°F/2 hr/AC
	WR	140.1	155.9	10.6	23.1	930	17.7	19.8	
7075 T-6 (A-11)	RW	78.5	90.0			167		5.0	As received
	WR	77.8	88.2			83		4.0	
2219 T-87 (A-9)	RW	57.9	72.0			281		5.0	As received
	WR	55.2	72.0			281		5.0	

All specimens were fatigued (at a stress less than 0.5 yield strength) until an 0.1-in. crack was formed at the tip of the edge notch.

## RESULTS AND DISCUSSION

The results for the Ti-6Al-4V alloy are tabulated in Table 17. Two smooth specimens were tested in the RW (3) fracture direction and  $K_{Ic}$  values of 106,000 and 111,000  $\text{psi}/\sqrt{\text{in.}}$  were recorded at 132.5-ksi yield strength (YS). Six side-grooved RW specimens produced  $K_{Ic}$  values from 101,000 to 114,000  $\text{psi}/\sqrt{\text{in.}}$ , which is within 7% of the average value of the smooth RW specimens (108,500  $\text{psi}/\sqrt{\text{in.}}$ ). One RW side-grooved specimen gave a  $K_{Ic}$  of 123,000  $\text{psi}/\sqrt{\text{in.}}$ .

Two smooth WR specimens indicated  $K_{Ic}$  values of 104,000 and 105,000  $\text{psi}/\sqrt{\text{in.}}$  at 140-ksi YS. Two other WR specimens were side-grooved so that  $B_N/B$  equaled 0.7 and 0.6. The  $K_{Ic}$  numbers obtained were 108,000 and 114,000  $\text{psi}/\sqrt{\text{in.}}$ , respectively. The bar graph in Fig. 35 gives a graphic portrayal of the  $K_{Ic}$  values for smooth and side-grooved specimens.

The fracture toughness results on T-27 indicate that both shallow and deep ( $B_N/B = 0.5$ ) side-grooves resulted in  $K_{Ic}$  values equivalent to those determined with specimens which were not side-grooved. However, it should be restated that the use of deep side-grooves may cause invalid values in other instances and is not recommended. Of additional interest is the fact that the nominal stress to yield stress ratio as high as 1.1 gave valid  $K_{Ic}$  results.

Plane-strain fracture toughness data for the two aluminum alloys are reported in Table 18. Six specimens of 7075-T6 were prepared so that the fracture would propagate in the RW direction (78.5-ksi YS). Three specimens were not side-grooved while three were grooved 5% on each flank ( $B_N/B = 0.9$ ). The smooth specimens produced  $K_{Ic}$  values of 32,000, 33,000, and 34,000  $\text{psi}/\sqrt{\text{in.}}$ , while all of the side-grooved specimens recorded a  $K_{Ic}$  of 32,000  $\text{psi}/\sqrt{\text{in.}}$ . One smooth WR specimen (77.8-ksi YS) indicates a  $K_{Ic}$  of 24,000  $\text{psi}/\sqrt{\text{in.}}$ .

Four specimens of 2219-T87 were tested. Two RW specimens (57.9-ksi YS) produced  $K_{Ic}$  values of 32,000 and 34,000  $\text{psi}/\sqrt{\text{in.}}$ , while two WR specimens (55.2-ksi YS) indicated

TABLE 17

PLANE STRAIN FRACTURE TOUGHNESS TEST DATA FOR Ti-6Al-4V † (T-27)

Fracture Direction	Thickness Between Side Grooves (in.)	Total Thickness B (in.)	$\frac{B_n}{B} \times 100\%$ (%)	Width W (in.)	Crack Length $a_c$ (in.)	$a_c/W$	Load P (lbs.)	$K_{Ic}$ (psi/in.)	Nominal Stress to Yield Stress $\sigma_n/\sigma_{YS}$	Percent Shear $\perp$
WR	No side grooves	0.95	--	5.00	1.53	0.31	129,000	105,000	0.64	46
WR	No side grooves	0.95	--	5.00	1.52	0.30	128,000	104,000	0.64	38
WR	0.64	0.95	67	4.50	1.43	0.32	98,800	108,000	0.87	--
WR	0.57	0.95	60	4.50	1.45	0.32	96,700	114,000	1.00	--
RW	No side grooves	0.96	--	4.50	1.50	0.33	113,000	106,000	0.75	39
RW	No side grooves	0.96	--	5.00	1.68	0.34	123,000	111,000	0.73	39
RW	0.86	0.96	90	4.99	1.59	0.32	120,000	107,000	0.75	--
RW	0.85	0.96	89	4.99	1.63	0.33	121,000	114,000	0.76	--
RW	0.77	0.96	80	5.00	1.62	0.33	104,000	102,000	0.73	--
RW	0.65	0.96	68	5.51	1.77	0.32	126,000	123,000	0.95	--
RW	0.56	0.96	58	5.50	1.79	0.33	93,000	101,000	0.84	--
RW	0.49	0.95	51	4.51	1.42	0.31	88,000	108,000	1.05	--
RW	0.48	0.96	50	4.50	1.41	0.31	91,000	112,000	1.11	--

† Heat treatment: Solution anneal - 1700°F/1 hr/WQ, Age - 900°F/1 hr/WQ

$\beta$  transus : 1820 ± 25°F

1 Shear lips did not form on side-grooved specimens

TABLE 18  
 PLANE STRAIN FRACTURE TOUGHNESS TEST DATA FOR 7075 T-6 AND 2219 T-87 ALUMINUM

Alloy	Fracture Direction	Thickness between Side Grooves B <sub>n</sub> (in.)	Total Thickness B (in.)	B <sub>n</sub> x100% B (%)	Width W (in.)	Crack Length a <sub>c</sub> (in.)	a <sub>c</sub> /W	Load at K <sub>IC</sub> P (lbs)	K <sub>IC</sub> (psi/in.)	Nominal Stress to Yield Stress (σ <sub>n</sub> /σ <sub>YS</sub> )	Percent Shear $\perp$
7075-T6	RW	No side grooves	1.00	--	5.00	1.65	0.33	39,000	33,000	0.38	15
7075-T6	RW	No side grooves	1.01	--	5.00	1.64	0.33	40,000	34,000	0.36	15
7075-T6	RW	No side grooves	1.00	--	5.00	1.69	0.34	37,000	32,000	0.36	16
7075-T6	RW	0.90	1.00	90	5.00	1.62	0.32	36,000	32,000	0.37	--
7075-T6	RW	0.91	1.01	90	5.00	1.60	0.32	38,000	32,000	0.37	--
7075-T6	RW	0.90	1.00	90	5.00	1.62	0.32	37,000	32,000	0.38	--
7075-T6	WR	No side grooves	1.02	--	4.51	1.62	0.36	24,000	24,000	0.28	7
2219-T87	RW	No side grooves	1.04	--	5.50	1.60	0.29	51,000	34,000	0.49	38
2219-T87	RW	No side grooves	1.04	--	5.50	1.57	0.29	48,000	32,000	0.45	41
2219-T87	WR	No side grooves	1.03	--	5.50	1.55	0.28	45,000	29,300	0.45	41
2219-T87	WR	No side grooves	1.03	--	5.50	1.57	0.29	46,000	30,000	0.45	39

$\perp$  Shear lips did not form on side-grooved specimens

Aluminum specimens were tested in the "as-received" condition

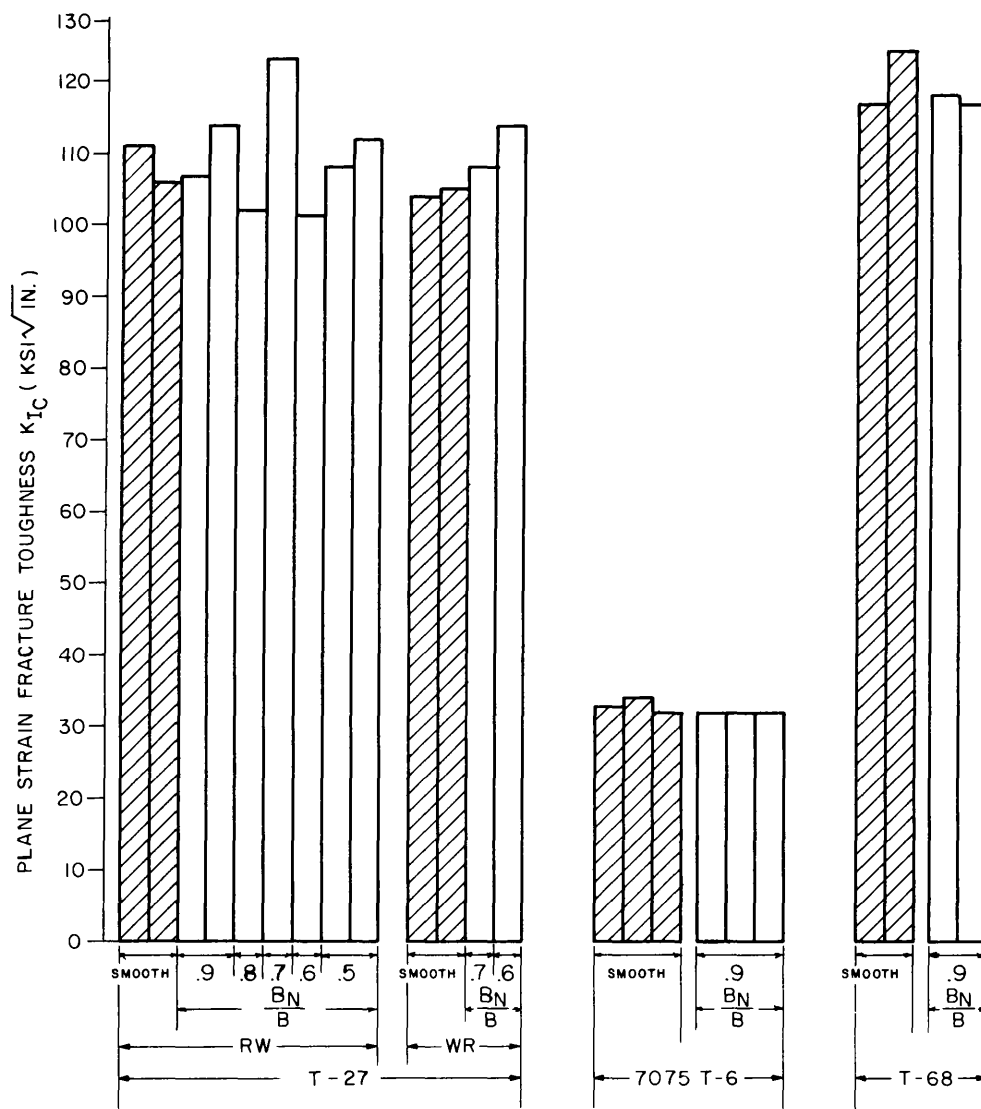


Fig. 35 -  $K_{Ic}$  values for smooth and side-grooved single-edge notch specimens

$K_{Ic}$  numbers of 29,000 and 30,000  $\text{psi}\sqrt{\text{in.}}$ . Both the 7075-T6 and the 2219-T87 were tested in the "as-received" condition.

Table 19 is a tabulation of the plane-strain fracture toughness data determined to date for the Ti-8Al-1Mo-1V (T-19) and Ti-6Al-4Zr-2Sn-0.5Mo-0.5V (T-68) alloys. The four smooth T-19 specimens were solution annealed at 1800°F for one hour, water quenched, then aged at 1100°F for two hours and air cooled. Two specimens were given a second aging treatment of 1100°F for two hours and air cooled. No significant difference was found in the  $K_{Ic}$  values between the two heat treatments.

Four RW specimens of T-68 were solution annealed at 1800°F for one hour, water quenched, then aged at 1100°F for two hours and air cooled. Two specimens were tested without side-grooves while two were grooved so that  $B_N/B = 0.9$ . The smooth specimens resulted in  $K_{Ic}$  values of 117,000 and 124,000  $\text{psi}\sqrt{\text{in.}}$ , while the side-grooved specimens produced  $K_{Ic}$  values of 118,000 and 117,000  $\text{psi}\sqrt{\text{in.}}$ .

For the toughness levels of T-27, T-68, and 7075-T6, side-grooving appears to provide valid  $K_{Ic}$  data. The validity of the  $K_{Ic}$  determinations for T-19 and T-68 will depend upon the tensile properties presently being determined. This will be reported in a future report.

Further experiments are being conducted to assess the value of shallow side-grooving at higher toughness levels on a variety of materials. Additional information will also be obtained regarding the relationship between the nominal-to-yield stress ratio and valid  $K_{Ic}$  values for smooth and side-grooved SEN specimens.

TABLE 19

## PLANE STRAIN FRACTURE TOUGHNESS TEST DATA

FOR Ti-8Al-1Mo-1V (T-19), Ti-6Al-4Zr-2Sn-0.5Mo-0.5V (T-68)

Alloy	Fracture Direction	Thickness Between Side Grooves B <sub>n</sub> (in.)	Total Thickness B (in.)	$\frac{B_n}{B}$ ×100% (%)	Width W (in.)	Crack Length a <sub>c</sub> (in.)	a <sub>c</sub> /W	Load at K <sub>Ic</sub> P (lbs)	K <sub>Ic</sub> (psi/in.)	Percent Shear (%)
T-19 A	RW	No side grooves	0.89	--	5.00	1.62	0.32	73,000	68,000	38
T-19 A	RW	No side grooves	0.87	--	5.00	1.73	0.35	68,000	70,000	27
T-19 A	RW	No side grooves	0.88	--	4.99	1.75	0.35	62,000	64,000	25
T-19 A	RW	No side grooves	0.88	--	5.00	1.71	0.34	67,000	67,000	30
T-68	RW	No side grooves	1.00	--	5.00	1.65	0.33	138,000	117,000	
T-68	RW	No side grooves	1.05	--	5.00	1.61	0.32	159,000	124,000	
T-68	RW	0.883	1.00	0.89	5.00	1.65	0.33	132,000	118,000	
T-68	RW	0.843	0.95	0.89	5.00	1.60	0.32	128,000	117,000	

Heat treatments: T-19 A - 1800°F/1 hr/WQ solution anneal followed by 1100°F/2 hr/AC age  
T-19 B - 1800°F/1 hr/WQ solution anneal followed by two consecutive aging treatments of 1100°F/2 hr/AC  
T-68 - 1800°F/1 hr/WQ solution anneal followed by 1100°F/2 hr/AC age

## REFERENCES

1. Huber, R.W., and Goode, R.J., "Fracture-Toughness Tests for Titanium Alloy Plate and Forgings," NRL Report 6228, April 21, 1965
2. Goode, R.J., and Huber, R.W., "Fracture Toughness Characteristics of Some Titanium Alloys for Deep-Diving Vehicles," Journal of Metals, Vol. 17, No. 8, August 1965, pp. 841-846
3. ASTM Materials Research & Standards, Vol. 1, No. 5, May 1961
4. Brown, B.F., "A New Stress-Corrosion Cracking Test Procedure for High-Strength Alloys," ASTM Materials Research and Standards (in press)
5. Goode, R.J., et al., "Metallurgical Characteristics of High Strength Structural Materials (Fourth Quarterly Report)," NRL Report 6137, June 1964
6. Pellini, W.S., et al., "Review of Concepts and Status of Procedures for Fracture-Safe Design of Complex Welded Structures Involving Metals of Low to Ultra-High Strength Levels," NRL Report 6300, June 1965
7. Pellini, W.S., et al., "Metallurgical Characteristics of High Strength Structural Materials (Sixth Quarterly Report)," NRL Report 6258, December 1964
8. Puzak, P.P., and Pellini, W.S., "Evaluation of Notch Bend Specimens," The Welding Journal, April 1954, p. 187s
9. Puzak, P.P., Schuster, M.E., and Pellini, W.S., "Applicability of Charpy Test Data," The Welding Journal, September 1954, p. 433s
10. Puzak, P.P., Schuster, M.E., and Pellini, W.S., "Crack-Starter Tests of Ship Fracture and Project Steels," The Welding Journal, Vol. 33, No. 10, pp. 481s-508s, October 1954
11. Puzak, P.P., and Pellini, W.S., "Evaluation of the Significance of Charpy Tests for Quenched and Tempered Steels," The Welding Journal, June 1956, p. 275s

12. Puzak, P.P., Babecki, A.J., and Pellini, W.S., "Correlations of Brittle Fracture Service Failures in Laboratory Notch Ductility Tests," The Welding Journal, September 1958, p. 391-s
13. Babecki, A.J., Puzak, P.P., and Pellini, W.S., "Report of Anomalous 'Brittle' Failures of Heavy Steel Forgings at Elevated Temperatures," ASME Paper No. 59-MET-6, May 1959
14. Puzak, P.P., "Effect of Carbon Content and Tempering Temperature on the Fracture Toughness of High-Strength Quenched and Tempered Steels," PhD. Thesis, University of Maryland, College Park, Md., 1961; Advance Distribution, BuShips Code 634B, November 1960
15. Manganello, S.J., and Porter, L.F., "Effect of Carbon on the Hardenability and Mechanical Properties of 5Ni-Cr-Mo-V Steel," Project No. 40.018-001(25) Contract No. 88540, July 1964
16. Hodge, J.M., Frazier, R.H., and Boulger, F.W., "The Effects of Sulphur on the Notch Toughness of Heat Treated Steels," TRANS of the AIME, Vol. 215, p. 745, October 1959
17. Manganello, S.J., Porter, L.F., and Sitko, R.J., "Effect of Sulphur on the Mechanical Properties of 5Ni-Cr-Mo-V Steel," Project No. 39.018-001(45) Contract No. 88540, July 1965
18. Crooker, T.W., et al., "Metallurgical Characteristics of High Strength Structural Materials (Fifth Quarterly Report)," NRL Report 6196, September 1964
19. Puzak, P.P., et al., "Metallurgical Characteristics of High Strength Structural Materials (Third Quarterly Report)," NRL Report 6086, January 1964
20. Goode, R.J., et al., "Metallurgical Characteristics of High Strength Structural Materials (Seventh Quarterly Report)," NRL Report 6327, May 1965
21. Puzak, P.P., et al., "Metallurgical Characteristics of High Strength Structural Materials (Eighth Quarterly Report)," NRL Report 6364, August 1965

22. Crooker, T.W., Morey, R.E., and Lange, E.A., "Low Cycle Fatigue Crack Propagation," Report of NRL Progress, June 1965, pp. 37-40
23. Crooker, T.W., Morey, R.E., and Lange, E.A., "Low Cycle Fatigue Crack Propagation Characteristics of Monel 400 and Monel K-500 Alloys," NRL Report 6218, March 10, 1965
24. Paris, P.C., and Erdogan, F., "A Critical Analysis of Crack Propagation Laws," ASME Journal of Basic Engineering, December 1963
25. Kies, J.A., Smith, H.L., Romine, H.E., and Bernstein, H., "Fracture Testing of Weldments," in "Fracture Toughness Testing and Its Applications," a Symposium of the ASTM, June 1964; Philadelphia 1965, pp. 328-351
26. Carman, C.M., Katlin, J.M., and Paris, P.C., "Low Cycle Fatigue Properties of High Strength Solid Propellant Rocket Motor Materials," Fourth Maraging Steel Project Review, Air Force Materials Laboratory, Dayton, Ohio, June 1964
27. Krafft, J.M., and Freed, C.N., "Effect of Side Grooving on Measurements of Plane Strain Fracture Toughness," Report of NRL Progress, June 1965, pp. 23-24

**This page intentionally blank.**

DOCUMENT CONTROL DATA - R&D		
<i>(Security classification of title, body of abstract and indexing annotation must be entered when the overall report is classified)</i>		
1. ORIGINATING ACTIVITY (Corporate author) U.S. Naval Research Laboratory Washington, D.C. 20390		2 a. REPORT SECURITY CLASSIFICATION <b>Unclassified</b>
		2 b. GROUP
3. REPORT TITLE METALLURGICAL CHARACTERISTICS OF HIGH STRENGTH STRUCTURAL MATERIALS (Ninth Quarterly Report)		
4. DESCRIPTIVE NOTES (Type of report and inclusive dates) A progress report on various problems		
5. AUTHOR(S) (Last name, first name, initial) Goode, R. J., Huber, R. W., Howe, D. G., Judy, R. W. Jr., Puzak, P. P., Lloyd, K. B., Crooker, T.W., Morey, R. E., Lange, E. A., and Freed, C. N.		
6. REPORT DATE November 1965	7 a. TOTAL NO. OF PAGES 104	7 b. NO. OF REFS 27
8 a. CONTRACT OR GRANT NO. NRL Problems F01-17, M01-05, M01-18, M03-01, b. PROJECT NO. Sp-01426; SF-020-01-01- 0724, 0850; RR-007-01-46-5405, 5420, c-5414; SF-020-01-05-0731; MIPR-ENG- NAV 66-2 d.		9 a. ORIGINATOR'S REPORT NUMBER(S) NRL Report 6405
		9 b. OTHER REPORT NO(S) (Any other numbers that may be assigned this report) None
10. AVAILABILITY/LIMITATION NOTICES Distribution of this document is unlimited.		
11. SUPPLEMENTARY NOTES None		12. SPONSORING MILITARY ACTIVITY Dept of the Navy (Office of Naval Research) BuShips, and Special Projects Office, and Dept of the Army (Office of Chief of Engineers)
13. ABSTRACT A progress report covering research studies in high strength structural materials, conducted in the period August 1965 to November 1965, is presented. This report includes fracture toughness studies on high strength steels, titanium alloys, and aluminum alloys. Fracture Toughness Index Diagrams, modified to include the latest information, are presented for these materials; the effects of melting practice and processing variables are reflected in the Fracture Toughness Index Diagram for steels by the addition of a new optimum materials trend line for consumable-electrode-vacuum melting of steels. Results are presented for studies concerning (1) the use of side-grooved plane-strain fracture mechanics specimens for valid determinations of fracture toughness, (2) heat-treatment effects on fracture toughness of several titanium alloys, (3) the effect of vacuum heat treatment on stress-corrosion-cracking sensitivity of titanium, and (4) the screening of a variety of titanium alloy plates for sensitivity to stress-corrosion-cracking. The effects of mean strain on low-cycle fatigue crack propagation in 5Ni-Cr-Mo-V steel and 7079-T6 aluminum are presented. Also described in a newly-developed low-cycle fatigue crack propagation test employing fracture mechanics parameters. Results are given for D6AC steels studied in this new test.		

**Security Classification**

14. KEY WORDS	LINK A		LINK B		LINK C	
	ROLE	WT	ROLE	WT	ROLE	WT
Engineering principles						
Titanium Alloys						
Aluminum Alloys						
High strength steels						
Fracture toughness						
Low-cycle fractures						
Corrosion fatigues						
Mechanical properties						
Explosion tear test						
Explosion bulge test						
Drop-weight tear test						
Processing variables						
Heat treatment						
High strength steel welds						
Maraging steel welds						
Weld testing						

**INSTRUCTIONS**

1. **ORIGINATING ACTIVITY:** Enter the name and address of the contractor, subcontractor, grantee, Department of Defense activity or other organization (*corporate author*) issuing the report.

2a. **REPORT SECURITY CLASSIFICATION:** Enter the overall security classification of the report. Indicate whether "Restricted Data" is included. Marking is to be in accordance with appropriate security regulations.

2b. **GROUP:** Automatic downgrading is specified in DoD Directive 5200.10 and Armed Forces Industrial Manual. Enter the group number. Also, when applicable, show that optional markings have been used for Group 3 and Group 4 as authorized.

3. **REPORT TITLE:** Enter the complete report title in all capital letters. Titles in all cases should be unclassified. If a meaningful title cannot be selected without classification, show title classification in all capitals in parenthesis immediately following the title.

4. **DESCRIPTIVE NOTES:** If appropriate, enter the type of report, e.g., interim, progress, summary, annual, or final. Give the inclusive dates when a specific reporting period is covered.

5. **AUTHOR(S):** Enter the name(s) of author(s) as shown on or in the report. Enter last name, first name, middle initial. If military, show rank and branch of service. The name of the principal author is an absolute minimum requirement.

6. **REPORT DATE:** Enter the date of the report as day, month, year; or month, year. If more than one date appears on the report, use date of publication.

7a. **TOTAL NUMBER OF PAGES:** The total page count should follow normal pagination procedures, i.e., enter the number of pages containing information.

7b. **NUMBER OF REFERENCES:** Enter the total number of references cited in the report.

8a. **CONTRACT OR GRANT NUMBER:** If appropriate, enter the applicable number of the contract or grant under which the report was written.

8b, 8c, & 8d. **PROJECT NUMBER:** Enter the appropriate military department identification, such as project number, subproject number, system numbers, task number, etc.

9a. **ORIGINATOR'S REPORT NUMBER(S):** Enter the official report number by which the document will be identified and controlled by the originating activity. This number must be unique to this report.

9b. **OTHER REPORT NUMBER(S):** If the report has been assigned any other report numbers (*either by the originator or by the sponsor*), also enter this number(s).

10. **AVAILABILITY/LIMITATION NOTICES:** Enter any limitations on further dissemination of the report, other than those

imposed by security classification, using standard statements such as:

- (1) "Qualified requesters may obtain copies of this report from DDC."
- (2) "Foreign announcement and dissemination of this report by DDC is not authorized."
- (3) "U. S. Government agencies may obtain copies of this report directly from DDC. Other qualified DDC users shall request through \_\_\_\_\_."
- (4) "U. S. military agencies may obtain copies of this report directly from DDC. Other qualified users shall request through \_\_\_\_\_."
- (5) "All distribution of this report is controlled. Qualified DDC users shall request through \_\_\_\_\_."

If the report has been furnished to the Office of Technical Services, Department of Commerce, for sale to the public, indicate this fact and enter the price, if known.

11. **SUPPLEMENTARY NOTES:** Use for additional explanatory notes.

12. **SPONSORING MILITARY ACTIVITY:** Enter the name of the departmental project office or laboratory sponsoring (*paying for*) the research and development. Include address.

13. **ABSTRACT:** Enter an abstract giving a brief and factual summary of the document indicative of the report, even though it may also appear elsewhere in the body of the technical report. If additional space is required, a continuation sheet shall be attached.

It is highly desirable that the abstract of classified reports be unclassified. Each paragraph of the abstract shall end with an indication of the military security classification of the information in the paragraph, represented as (TS), (S), (C), or (U).

There is no limitation on the length of the abstract. However, the suggested length is from 150 to 225 words.

14. **KEY WORDS:** Key words are technically meaningful terms or short phrases that characterize a report and may be used as index entries for cataloging the report. Key words must be selected so that no security classification is required. Identifiers, such as equipment model designation, trade name, military project code name, geographic location, may be used as key words but will be followed by an indication of technical context. The assignment of links, roles, and weights is optional.